UNIVERSITÀ DEGLI STUDI DI PADOVA

Department of Civil, Environmental and Architectural Engineering

Water and Geological Risk Engineering

Master's Degree Thesis

Evaluation of surface soil moisture retrievals from microwave satellite sensors using ground observations.

George Phiri

[2045468]

Supervisor

Professor Marco Marani

Department of Civil, Environmental and Architectural Engineering

2023/2024

Dedication.

To Mum, Dad and family, your constant love and unwavering support have been a source of strength throughout my academic pursuit. Your guidance and encouragement have shaped me into the person I am today. This thesis is dedicated to you.

Acknowledgement.

I would like to extend my heartfelt gratitude to my supervisor, Professor Marco Marani for his unwavering support, and mentorship throughout the development of this dissertation. This work would not have been possible without his persistent direction and invaluable guidance.

Abstract.

The aim of this work is to evaluate the performance of surface soil moisture (SSM) measurements from microwave satellite sensors, specifically the Copernicus Sentinel-1 and SMAP (Soil Moisture Active Passive) missions, using ground-based observations. Soil moisture is a critical environmental variable that influences various hydrological and ecological processes. Accurate measurement of soil moisture is essential for applications such as agricultural monitoring, flood forecasting, and climate modeling.

This study focuses on two distinct regions: the Twente region in the Netherlands, known for its comprehensive soil moisture monitoring network, and the Italian basins affected by the severe flood event in May 2023. By comparing satellite-derived soil moisture estimates with in-situ measurements, the research assesses the temporal and spatial correlations between these data sources.

Key methodologies include the use of statistical metrics such as Root Mean Square Error (RMSE), the coefficient of determination (R^2), and correlation analyses to evaluate the accuracy of satellite data. Additionally, the study investigates how well the Sentinel-1 SSM1km product captures variations in soil moisture before, during, and after the flood event. This assessment aims to determine the capability of the SSM1km product in reflecting significant changes in soil moisture associated with flooding events, which is crucial for effective flood management and mitigation strategies.

The results indicate that while satellite-derived soil moisture data generally correlate well with ground-based measurements, there are notable discrepancies influenced by factors such as land cover and surface roughness. The study found that the RMSE values ranged from 0.1065 to 0.306, with correlation coefficients (R^2) varying across different stations. These findings highlight the strengths and limitations of current microwave remote sensing techniques for soil moisture retrieval and underscore the importance of continuous validation against ground observations.

Content

List of Figures

List of Tables

Chapter 1 Introduction.

1.1 Soil Moisture and its importance.

Soil moisture is generally defined as the water contained in the unsaturated zone of the soil, which lies between the soil surface and the groundwater table (Hillel, 2003; Moene & Dam, 2014). It is often divided into surface and root zone soil moisture, where surface soil moisture is the water content of the top part of a soil, often the top 5 cm, and root zone soil moisture is the water used for vegetation is available, which is sometimes viewed as the water content of the top 200 cm of a soil (Kerr, 2006).

The significance of soil moisture spans multiple disciplines and practical applications, leading to its recognition as an essential climate variable (ECV) by the Global Climate Observation System ((WMO), 2016).

It plays a vital role in natural disaster monitoring systems, such as those for floods, droughts, and forest fires (Dorigo et al., 2011), and is crucial for understanding biophysical processes related to energy and mass exchange between the hydrosphere, atmosphere, and biosphere (Zhang et al., 2015). As a key component of the water cycle, soil moisture regulates the division of precipitation into infiltration and runoff, thereby influencing stream flow, groundwater recharge, and precipitation patterns (Tuttle & Salvucci, 2014). It is also essential for predicting droughts and floods.

Soil moisture significantly affects processes across the soil-atmosphere interface, particularly in water and energy balance, where it drives the flow of water and heat between the soil and the atmosphere(Petropoulos et al., 2015; Seneviratne et al., 2010). Moreover, soil moisture plays a crucial role in soil formation processes (Van Breemen & Buurman, 2002).

Other elements that affect soil moisture content include vegetation cover and soil properties (Hillel, 2003). Water content soil varies greatly in space. According to Crow et al., (2012) and Vereecken et al., (2014), soil properties, topography, land use and precipitation are the main factors affecting the spatial variability of soil moisture. The main large-scale spatial determinants of soil moisture distribution are precipitation and other meteorological influences.

Pedogenic processes, including the movement of water and solutes, chemical weathering, and reduction and oxidation processes, all occur in the presence of water. In addition, soil moisture content influences a wide range of soil properties, including stability, compactibility and soil structure (Hillel, 2003). Plant growth is significantly influenced by soil moisture, which serves as an essential source of water for vegetation. When soil moisture levels fall below optimal conditions, plants experience water stress, inhibiting their growth and reducing productivity (Asbjornsen, et al., 2011; Wang, et al., 2019). In agricultural settings, monitoring soil moisture is crucial for determining the need for irrigation and optimizing its scheduling. Proper soil moisture management ensures that crops receive the right amount of water at the right time, maximizing yield and maintaining crop health. Effective monitoring helps prevent both over-irrigation and water stress, contributing to sustainable agricultural practices and efficient water resource management.

Moreover, soil moisture directly influences the availability of nutrients and the movement of pollutants within the soil. Nutrients and pollutants dissolved in soil moisture can reach plants, impacting their growth and development (Rodríguez-Iturbe & Porporato, 2005; Wang, et al., 2019). This process is critical because it determines the availability of essential nutrients required for healthy plant growth.

1.2 Problem statement and Research Questions

For numerous small-scale applications of soil moisture data, high temporal and spatial resolution is imperative. Field measurements, often considered as ground truth, are inadequate for such applications due to their limited spatial coverage, remote sensing methods offer a broader perspective, allowing for the estimation of soil moisture over large regions. By combining the accuracy of ground-based measurements with the extensive coverage of remote sensing, a more comprehensive understanding of soil moisture dynamics can be achieved.

This work aims to evaluate the performance of global soil moisture data retrieved from Microwave Remote Sensing methods, namely the Copernicus Sentinel-1 1km Soil Moisture (SSM1km) and SMAP/Sentinel-1 surface moisture products. The aim is to investigate how well these products capture soil moisture variations in time and space by comparing remote sensing estimates of soil moisture and ground-based observations in the Twente Soil Moisture Network. We will also analyze how well these products captured soil moisture variations before, during and after the May 2023 Emilia Romagna Flood event in Italy. The results of this analysis will provide information on the strengths and limitations of these products for a range of end-use applications such as agricultural monitoring and hydrological modeling. In addition, by comparing ground observations and remote sensing data, this study will shed light on the spatial variability of soil moisture and help identify systematic biases or patterns. The following main questions are the focus of the study.

1. How well does microwave soil moisture data correlate with ground-based measurements at different stations, and time periods?
2. How well did SSM1km capture soil moisture variations before, during and after the May Emilia Romagna flood event?
3. Should remote sensing estimates be compared with point ground-based observations or their spatial interpolation?

This work is structured as follows: Chapter 3 is dedicated to the theory and the methods used in the work, while Chapter 2 presents the study area and the data sets. The results are presented in Chapter 4 and a discussion of the results and agreements is covered in Chapter 5.

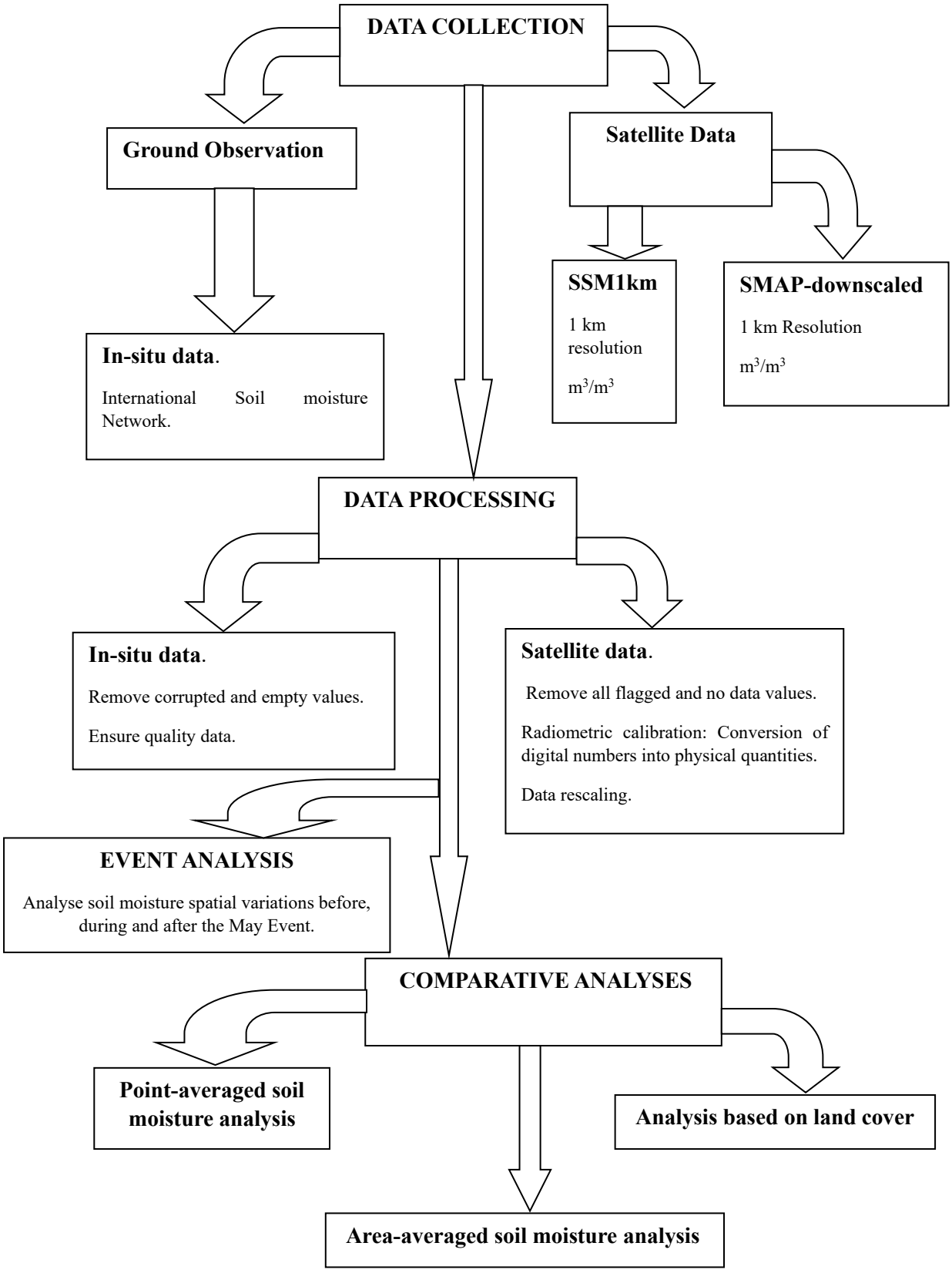

Figure 1 graphical representation of the tasks carried out in this study.

Chapter 2 Materials and Methods.

2.1 Methods

According to Hillel (2003), Moene and Dam (2014), soil moisture content can be expressed either as volumetric or gravimetric water content, which are related by the bulk density of the soil, or as relative water content, expressed as the percentage of saturation, which is determined by the porosity of the soil that can be converted into volumetric water content. Rainfall, Irrigation runoff, Drainage, Capillary rise and Evapotranspiration are some of the processes that affect the water content of a soil (Hillel, 2003; Moene & Dam, 2014).

Given the importance of soil moisture, a variety of methods have been developed to measure it across different spatial and temporal scales. These methods can be broadly categorized into two main approaches: ground-based observations or in-situ soil moisture and remote sensing estimates.

2.1.1 In-situ Soil Moisture Measurement Methods.

Ground-based observations consist of point measurements taken at specific locations and are often considered the gold standard, or "ground truth," for soil moisture estimation. These observations are critical for validating remote sensing data and for providing accurate, localized soil moisture information. Various methods are used to determine soil moisture content in the field, and the choice of method typically dictates the scale and application of these measurements in terms of both spatial and temporal resolution (Babaeian, et al., 2019; Dorigo W. A., et al., 2011; Hillel, 2003). Moisture content in the soil can be expressed as either gravimetric moisture content or volumetric moisture content.

1. Gravimetric Method

Gravimetric moisture content is the mass of water per mass of dry soil (Oommen & Philip, 2023). The gravimetric method is the most traditional and direct approach for measuring soil moisture content. This method involves collecting soil samples from the field, weighing them to obtain the wet weight (M_w), drying them in an oven at a standard temperature (usually around 105°C) for 24 hours period and then reweighing the samples to determine the dry weight(M_d). Gravimetric moisture content(GMC) is calculated as the difference in weight before and after drying, expressed as a percentage of the dry weight, is calculated using the formula below:

$$GMC = \frac{(M_w - M_d)}{M_d}\ 100 \qquad \textit{Equation (1)}$$

This method, while highly accurate, is labour-intensive, time-consuming, and destructive, as it requires physical removal of soil samples. Moreover, gravimetric measurements are point-specific, which can limit their ability to represent larger areas with high spatial variability (Hillel, 2003). Despite these limitations, the gravimetric method remains a benchmark for calibrating other soil moisture measurement techniques (Dorigo et al., 2011).

2. Capacitance Method

Capacitance sensors, also known as dielectric sensors, measure soil moisture by detecting changes in the soil's capacitance. These sensors work on the principle that the capacitance of a material depends on its dielectric properties, which change with moisture content. Capacitance sensors typically consist of two probes that generate an electromagnetic field. As the soil moisture changes, the dielectric constant of the soil changes, which in turn alters the capacitance detected by the sensor.
Capacitance sensors are widely used in agriculture due to their relatively low cost, ease of installation, and capability for continuous monitoring. However, they require calibration for different soil types, and their accuracy can be influenced by factors such as soil texture, temperature, and salinity (Decagon Devices, 2005).

In the Twente Soil Moisture Network, soil moisture measurements were conducted using the capacitance method, as described by Van der Velde et al. (2023). The network utilized ECH2O EC-TM and 5TM probes, both manufactured by METER Group (formerly Decagon Devices), which operate on the principle of capacitance measurement. These probes were installed laterally at depths of 5, 10, 20, 40, and 80 cm within the soil profile at each monitoring station. The installation process involved careful excavation to minimize soil disturbance, ensuring the accuracy and consistency of the measurements. After installation, the soil was backfilled and compacted to restore its original state, and the cables from the probes were routed to an EM50 data logger mounted on a nearby pole. Measurements were taken every minute, and the data was recorded at 15-minute intervals by the data loggers.

Given the diverse soil properties across the study area, soil-specific calibration was crucial to ensure that the sensor readings accurately reflected the true volumetric soil moisture (VSM). The calibration process began in the laboratory, where soil samples collected from various sites within the network were used to develop calibration functions. These functions were created by comparing the sensor outputs, such as voltage or frequency, with the gravimetrically determined soil moisture content. Linear regression models were employed to establish these relationships, tailoring the calibration functions to the specific characteristics of the soils at each site. This step was essential for adjusting the sensor readings to account for variables like soil texture and electrical conductivity, which can significantly influence the sensor's dielectric response.

To validate the calibration functions, cross-validation techniques were employed, testing the calibration equations against additional soil samples to ensure their accuracy and reliability. Further calibration was carried out during field campaigns using handheld ThetaProbes and HydraProbes, which were directly calibrated against gravimetric soil moisture values obtained in situ. This field calibration ensured that the handheld probe readings were consistent with the conditions in the specific study locations, allowing for precise soil moisture assessment in various field conditions.

Once validated, the calibration functions were applied to the raw sensor data collected by the network, ensuring that all soil moisture measurements reflected accurate and consistent values across the monitoring sites. This rigorous calibration process provided confidence in the reliability of the data, making it suitable for broader analyses, including the validation of satellite-based soil moisture observations.

3. Neutron Probes

Neutron probes are a sophisticated method of measuring soil moisture that involves emitting fast neutrons into the soil. When these neutrons collide with hydrogen atoms (found primarily in water molecules), they slow down. The probe records the number of returning slow neutrons, which is directly related to the hydrogen content in the soil and therefore soil moisture. Neutron probes are very accurate and can measure soil moisture at various depths, making them useful for soil monitoring profiles. However, their use is limited due to safety concerns related to the radioactive source as well as the high cost and complexity of operation. In addition, neutron probes must be carefully calibrated and corrected for the presence of other hydrogen sources such as organic matter (Evett, 2008).

4. Frequency Domain Reflectometry (FDR).

Frequency domain reflectometry (FDR) is another commonly used method for measuring soil moisture. It works in the frequency range. FDR uses probes that generate an oscillating electrical signal. The frequency of the signal changes as it passes through the soil, influenced by the soil's dielectric constant, which depends on the moisture content. In practice, FDR sensors consist of two electrodes inserted into the ground. When soil moisture changes, the dielectric constant and therefore the frequency of the signal between the electrodes also changes. This change in frequency is measured and used to calculate soil moisture content. FDR is preferred in many applications because it is less expensive than TDR, easier to deploy, and allows for continuous monitoring. However, like TDR, FDR requires careful calibration for different soil types to ensure accurate measurements (Jacobsen & Schjonning, 1993).

5. Time Domain Reflectometry

Time Domain Reflectometry (TDR) is a widely used technique that involves inserting probes into the soil to measure its moisture content. TDR works by sending an electromagnetic pulse along a pair of metal rods or probes that are embedded in the soil. The speed at which this pulse travels through the soil is influenced by the dielectric constant of the soil, which varies with moisture content, water has a much higher dielectric constant compared to air or soil particles.

The TDR device measures the time it takes for the pulse to reflect back to the instrument after reaching the end of the probe. This time delay is then used to calculate the soil’s moisture content. TDR is a non-destructive method that provides continuous, real-time data, making it particularly useful for monitoring soil moisture over time (Topp et al., 1980). However, TDR systems require careful calibration to ensure accuracy and can be expensive compared to other methods. The accuracy of TDR can also be affected by soil properties such as salinity and texture (Robinson et al., 2003).

2.1.2 Remote Sensing estimates of soil moisture.

Remote sensing of soil moisture is primarily conducted using microwave sensors which operates within 0.5 and 100 cm region of the electromagnetic spectrum, exploiting the large difference between the dielectric properties of water and dry soil. Microwave remote sensing methods are particularly effective for soil moisture retrieval due to the distinct dielectric constant of water (~80) compared to soil particles (~4) (Engman, 2015). As detailed by Su (2006), microwave remote sensing, in particular, is highly effective due to its sensitivity to soil moisture. This method can be broadly divided into two approaches, the passive and active.

1. Passive Remote Sensing.

In passive microwave remote sensing, naturally emitted microwave radiation from the Earth's surface is detected. The radiation, referred to as brightness temperature (T_B), is directly influenced by the soil's moisture content. The principle behind this technique is based on the relationship between the dielectric constant of the soil, its emissivity (ϵ_s), and its physical temperature (T_s).

The dielectric constant of water (~80) is significantly higher than that of dry soil (~4), which allows passive microwave sensors to detect variations in soil moisture by measuring the emitted radiation. The observed brightness temperature is a product of the soil's emissivity and its physical temperature:

$$T_B = \epsilon_s \times Ts \qquad \textit{Equation (2)}$$

This relationship is further modelled using the Fresnel equations, which predict the surface reflectivity based on the dielectric constant and the sensor's viewing angle. These equations are fundamental in deriving the dielectric properties of the soil, which are then used to estimate soil moisture content.

However, several environmental factors complicate this retrieval process. Surface roughness and vegetation cover are two critical variables that can distort the observed brightness temperature. Surface roughness can scatter the microwave signal, altering the emissivity, while vegetation can attenuate or add to the thermal emission. To mitigate these effects, various correction algorithms are applied, ensuring that the soil moisture estimates are as accurate as possible under varying conditions.

2. Active Microwave Remote Sensing

Active microwave remote sensing, according to Su (2006), involves the use of radar systems, such as Synthetic Aperture Radar (SAR), which emit microwave pulses toward the Earth's surface and measure the backscattered signal. The strength and characteristics of the backscatter are directly related to the dielectric properties of the soil, which are influenced by its moisture content.

The backscatter coefficient (σ^0) is a key parameter in this approach, representing the fraction of the transmitted microwave signal that is reflected back to the radar sensor. Typically, wet soils produce a stronger backscatter signal compared to dry soils due to their higher dielectric constant. This relationship is modelled using surface scattering models, such as the Integral Equation Model (IEM), which combines aspects of different scattering approaches to account for a broad range of surface roughness conditions. These models enable the estimation of soil moisture by solving the inverse problem, deriving the dielectric properties of the soil from the observed backscatter.

In addition to theoretical models, semi-empirical models are frequently employed. These models establish empirical relationships between the backscatter coefficient and soil moisture, often requiring local calibration to ensure accuracy. Notable examples include the models developed by Oh et al. (1992) and Dubois et al. (1995), which have been widely used in soil moisture studies but necessitate careful application within their calibrated regions.

According to Bauer-Marschallinger et al., (2019), the backscatter model from the Vienna University of Technology (TU Wien) was adopted on the Sentinel-1 sensor with some modifications to take advantage of the high-resolution IW mode measurements and extract SSM1km.

The TU Vienna Change Detection Model calculates soil surface moisture (SSM1km) directly from radar backscatter data, represented by the backscatter coefficient σ0. In this model, fluctuations in backscatter are interpreted as changes in soil moisture, while other surface properties such as geometry, roughness and vegetation structure are treated as constant parameters. The model parameters take into account the maximum dry and wet conditions as well as average signal contributions from vegetation and surface geometry. This model is self-calibrating at the pixel level, with parameters estimated through statistical analysis of long-term backscatter time series data. For SSM1km estimation, the backscatter value $\sigma^0(\theta, t)$ at a given time t and an observation angle θ is normalized to a reference angle Θ and scaled linearly between dry and wet reference values, resulting in the relative surface moisture saturation SSM1km(t), expressed in Percent (Bauer-Marschallinger, et al., 2019).

$$SSM1km(t) = \frac{\Delta\sigma 0(\Theta,t)}{S(\Theta)}\,[\%] \qquad \textit{Equation (3)}$$

The sensitivity to changes in SSM1km at the reference angle Θ is denoted by S(Θ), while the change in normalized backscatter relative to dry conditions is represented by Δσ0(Θ, t). S(Θ) is defined as the difference between the normalized backscatter coefficients under wet and dry conditions. This difference estimates the local backscatter dynamic range, effectively quantifying the sensitivity.

$$S(\Theta) = \sigma_{wet}0\,(\Theta) - \sigma_{dry}0\,(\Theta)\ [dB] \qquad \textit{Equation (4)}$$

Current and near future satellite missions offer opportunities to generate high-resolution soil moisture products. Ongoing missions include the ESA Sentinel-1 European Radar Observatory, the L-band Global Navigation Satellite System (GNSS) signals recorded by the Cyclone Global Navigation Satellite System (CYGNSS), and the SAtélite Argentino de Observación COn Microondas (SAOCOM) mission. Future missions such as the NASA-ISRO Synthetic Aperture Radar (NISAR) mission, the Radar Observing System for Europe L (ROSE-L), the German Aerospace Center (DLR) Tandem-L interferometric radar mission and the ESA Hydrological Global Navigation Satellite System (HydroGNSS) will also improve high-resolution mapping of soil moisture (Brocca, Zhao, & Lu, 2023).

Table 1. Overview of currently available satellite-based surface soil moisture products.

Product	Spatial resolution	Temporal resolution	Spatial coverage	Temporal coverage	Sensing depth	Unit	Product
ASCAT	*25/50 km*	*1-2 days*	*Global*	*2007 - present*	*5 cm*	*%*	*EUMETSAT, n.d.*
ERS2	*25/50 km*	*1-2 days*	*Global*	*1995 - 2011*	*5 cm*	*%*	*European Space Agency [ESA], n.d.-a*
ERS1	*25/50 km*	*1-2 days*	*Global*	*1991 - 2000*	*5 cm*	*%*	*ESA, n.d.-a*
AMSR2	*10/25 km*	*Daily*	*Global*	*2012 - present*	*-*	*%*	*Japan Aerospace Exploration Agency [JAXA], n.d.*
AMSR-E	*25 km*	*Daily*	*Global*	*2002 - 2011*	*-*	*%*	*National Aeronautics and Space Administration [NASA], 2021*
TMI	*25 km*	*Daily*	*Global*	*1997 - 2015*	*-*	*%*	*NASA, n.d.-b*
SMOS	*36 km*	*Daily*	*Global*	*2010 - present*	*2.5 cm*	*m3/m3*	*ESA, n.d.-c*
SMAP	*9 km*	*Daily*	*Global*	*2015 - present*	*5 cm*	*m3/m3*	*NASA, n.d.-a*
Sentinel-1	*1 km*	*Daily*	*Europe*	*2015 - present*	*5 cm*	*%*	*Copernicus Global Land Service [CGLS], n.d.; ESA, n.d.-b*
ESA CCI active	*0.25°*	*Daily*	*Global*	*1991 – 2020*	*5 cm*	*%*	*ESA, 2021*

ESA CCI passive	*0.25°*	*Daily*	*Global*	*1978 – 2020*	*5 cm*	*m3/m3*	*ESA, 2021*
ESA CCI active passive	*0.25°*	*Daily*	*Global*	*1978 - 2020*	*5 cm*	*m3/m3*	*ESA, 2021*
VanderSat L-band	*100 m*	*230 obs/year*	*Global*	*2015 - present*	*5 cm*	*m3/m3*	*VanderSat, 2021b*
VanderSat C-band	*100 m*	*320 obs/year*	*Global*	*2002 - present*	*2 cm*	*m3/m3*	*VanderSat, 2021b*
VanderSat X-band	*100 m*	*320 obs/year*	*Global*	*2002 - present*	*1 cm*	*m3/m3*	*VanderSat, 2021b*

2.1.3 Comparison Techniques.

Several authors have proposed various methods of comparing in-situ soil moisture data with soil moisture data obtained through satellite-based remote sensing (Bi et al., 2016; Chen, 2016; Wang et al., 2016; Crow et al., 2012). Using surface soil moisture data from in situ observations, the spatiotemporal variation pattern of soil moisture in Twente was first mapped and examined in this study. Subsequently, an evaluation was conducted to compare the quality of remotely sensed SSM1km soil moisture data with in-situ observations obtained

from Twente ground stations, focusing on the Twente's spatial and temporal variation pattern. Since point-based ground observations and grid-based satellite retrievals have different spatial scales, point-based data was spatially interpolated to ensure a valid and accurate comparison. Five distinct statistical metrics are employed in the evaluation of the model's performance:

1. Bias

The bias associated with comparing remote sensing estimates of soil moisture with observed soil moisture refers to the systematic difference between the remote sensing soil moisture estimates and the ground-observed soil moisture. It indicates whether the remote sensing model consistently overestimates or underestimates the soil moisture values actually observed on the ground. A positive bias indicates that remote sensing estimates tend to be higher than ground observations, while a negative bias indicates that they are lower. Understanding the bias is crucial for identifying and correcting any systematic errors in the remote sensing model (Willmott and Matsuura, 2005).

$$Bias = \frac{1}{n}\sum_{i=1}^{n}(y_i - \hat{y}) \qquad \textit{Equation (5)}$$

where:

- $\boldsymbol{n}$ is the total number of observations.
- $\boldsymbol{y_i}$ represents the ground-observed soil moisture for the *i*-th data point.
- $\boldsymbol{\hat{y}}$: represents the remote sensing estimated soil moisture for the *i*-th data point.

2. Root Mean Square Error (RMSE).

Root Mean Square Error (RMSE) measures the average magnitude of errors between remote sensing estimates and soil moisture values observed on the ground. It is calculated as the square root of the average squared differences between the remote sensing predictions and the ground observations. RMSE provides a measure of the overall accuracy of the remote sensing model, regardless of whether the model consistently over- or underestimates soil moisture (Chai & Draxler, 2014).

$$RMSE = \sqrt{\frac{1}{n}\sum_{i=1}^{n}(y_i - \hat{y})^2} \qquad \textit{Equation (6)}$$

where:

- $\boldsymbol{n}$: is the total number of observations.
- $\mathbf{y_i}$: represents the ground-observed soil moisture for the *i*-th data point.
- $\boldsymbol{\hat{y}}$: represents the remote sensing estimated soil moisture for the *i*-th data point.

3. The coefficient of determination (R^2).

The **Coefficient of Determination (R^2)** quantifies the proportion of variance in observed soil moisture that can be predicted from the remote sensing estimates. A value close to 1 indicates that the remote sensing model fits well and accurately predicts the variability of soil moisture observed on the ground, while a value close to 0 indicates that the model has poor predictive power (Nagelkerke, 1991).

$$R^2 = 1 - \frac{\frac{1}{n}\sum_{i=1}^{n}(y_i - \hat{y}_i)^2}{\frac{1}{n}\sum_{i=1}^{n}(y_i - \bar{y})^2} \qquad \textit{Equation (7)}$$

where:

- $\mathbf{y_i}$ represents ground-observed soil moisture.
- $\hat{\boldsymbol{y}}_{\boldsymbol{i}}$ represents the predicted soil moisture from the remote sensing model.
- $\bar{\mathbf{y}}$ is the mean of the ground-observed soil moisture values.
- $\boldsymbol{n}$ is the number of observations (or data points).

4. Pearson correlation

The Pearson correlation measures the linear relationship between remote sensing estimates and observed soil moisture on the ground. A Pearson correlation value of 1 implies a perfect positive linear relationship, indicating that increases in remote sensing estimates correspond directly to increases in ground observations. Conversely, a value of -1 indicates a perfect negative relationship, and 0 implies no linear relationship between the two sets of measurements (Benesty et al., 2009).

$$r = \frac{\sum_{i=1}^{n}(x_i - \bar{x})(y_i - \bar{y})}{\sqrt{\sum_{i=1}^{n}(x_i - \bar{x})^2}\sqrt{\sum_{i=1}^{n}(y_i - \bar{y})^2}} \qquad \textit{Equation (8)}$$

Where:

- $\boldsymbol{x_i}$ and $\boldsymbol{y_i}$ are the remote sensing soil moisture estimates and ground-observed soil moisture values, respectively, for each data point.
- $\bar{\boldsymbol{x}}$ is the mean of the x values.
- $\bar{\boldsymbol{y}}$ is the mean of the y values.
- $\boldsymbol{n}$ is the number of sample points.

5. Spearman correlation (ρ)

Spearman correlation is used to evaluate the strength and direction of the monotonic relationship between the ranks of remote sensing estimates and observed soil moisture values on the ground. Unlike Pearson correlation, which evaluates linear relationships, Spearman correlation is particularly useful when the relationship between remote sensing estimates and ground-observation data is not linear but still follows a consistent pattern (monotonic). This nonparametric measure is robust to outliers and does not require the data to meet the assumptions of normality or linearity.

$$\rho = 1 - \frac{6\sum d_i^2}{n(n^2-1)} \qquad \textit{Equation (9)}$$

Where:

- **ρ** is the Spearman rank correlation coefficient.
- ***n*** is the number of data points.
- $\boldsymbol{d_i}$ is the difference between the ranks of corresponding values of remote sensing soil moisture estimates and ground-observed soil moisture.

6. Percent error

Percent error is a statistical measure that evaluates the accuracy of remote sensing estimates by comparing the deviation between these estimates and actual soil moisture observed on the ground. This is particularly useful in assessing how well remote sensing data reflects actual soil moisture levels observed on the ground and helps assess the reliability and precision of the remote sensing model.

$$\textit{Percent Error} = \left|\frac{y_i - \hat{y}_i}{y_i}\right| * 100 \qquad \textit{Equation (10)}$$

where:

- $\mathbf{y_i}$ represents ground-observed soil moisture.
- $\boldsymbol{\hat{y}_i}$ represents the remote sensing soil moisture estimates.
- * represents multiplication.

2.2 Data

2.2.1 Ground-based observations.

Daily in-situ soil moisture observations in m3/m3 were downloaded from the 11 measuring stations within Twente Monitoring Network. Table 2 gives detailed information of the measuring stations. These stations are part of the International Soil Moisture Network (ISMN). ISMN was initiated in 2009 to serve as a reference database for research and scientific applications. It provides open-access to long-term, harmonized and quality controlled near-surface to deep root zone in-situ soil moisture observations. The Vienna University of Technology has managed the implementation and functioning of ISMN since 2009. Nevertheless, the German Federal Ministry for Digital and Transport has pledged ongoing financial support for the service. As a result, ICWRGC and the German Federal Institute of Hydrology (BfG) will collaboratively oversee the hosting of ISMN (ISMN, n.d.). The table below gives detailed information of the in-situ data used in this study.

Table 2 Selected soil moisture monitoring station within the Twente monitoring network. (Dante et al., 2011)

Station ID	Lat, Lon	Elevation (masl)	Depth (cm)	Land Cover	Soil Type	Soil Type from 1:50000 map
ITCSM_01b	*52.41472, 6.96583*	*3*	*5, 10, 20*	*Grass bush*	*NA*	Sandy clay loam on subsoil of fine sand
ITCSM_02b	*52.39083 6.86011*	*28*	*5, 10, 20*	*Grassland*	*Sand*	Man-made sandy thick earth soil
ITCSM_03b	*52.35024 6.78951*	*7*	*5, 10*	*Grassland*	*Loamysand*	Loamy fine sand
ITCSM_04b	*52.27158 6.92133*	*44*	*5, 10,20*	*Grassland*	*Loamysand*	Loam
ITCSM_07b	*52.37328 6.96228*	*17*	*5, 10,20*	*Corn*	*Loamysand*	Sandy clay loam on subsoil of fine sand
ITCSM_08b	*52.13578 6.74507*	*21*	*5, 10,20,*	*Corn*	*Sand*	Fine sand

ITCSM_10c	*52.19104 6.66827*	*11*	*5, 10,20*	*Grassland*	*Sand*	Fine sand
ITCSM_11d	*52.22005 6.54288*	*7*	*5, 10 20*	*Grassland*	*Loamysand*	Man-made sandy thick earth soil
ITCSM_12b	*52.14035 6.55965*	*8*	*5, 10,20*	*Grassland*	*Sand*	Sandy clay loam on subsoil of fine sand
ITCSM_13	*52.19389 6.41750*	*8*	*5, 10,20*	*Grassland*	*Sand*	Fine sand
ITCSM_14c	*52.19594 6.30484*	*7*	*5, 10, 20*	*Grassland*	*Loamysand*	Loamy fine sand

2.2.2 Remote Sensing Data

1) Sentinel 1.

Since 2014, the Sentinel-1 satellites with high-resolution radar sensors have enabled unprecedented spatial-temporal coverage of the Earth's surface. They operate in the C-band (CSAR, at 5.405 GHz) and have a Synthetic Aperture Radar (SAR) system that provides information about surface properties regardless of daylight and cloud cover. The mission consists of two identical spacecraft, Sentinel-1A (S-1A), launched in April 2014, and Sentinel-1B (S-1B), launched in April 2016, and is part of the European Earth observation program Copernicus. The Sentinel-1 SAR works with the Copernicus constellation's multispectral sensors on board Sentinel-2 and Sentinel-3 (Bauer-Marschallinger et al., 2019).

With support for co-polarization and cross-polarization receive channels, the CSAR instrument on board the Sentinel-1 satellites offer four different acquisition modes. Designed to meet most user requirements, IW Swath mode is the primary acquisition mode over (non-polar) land, with three modes focused on maritime and emergency operations (ESA, 2013). In IW mode, CSAR collects data over a 250-kilometers swath over flat terrain, covering the incidence angle range of 29.1° to 46.0°. More specifically, it uses the Terrain Observation with Progressive Scans SAR imaging technique to sequentially capture and merge three

parallel sub-strips (De Zan & Guarnieri, 2006). After multiple viewing, the high-resolution product (IWGRDH) results in a ground resolution of 20 m × 22 m. The spatial resolution of the single view is 5 m × 20 m. A default of 1 dB (3σ) is used for radiometric accuracy.

The basic idea behind microwave remote sensing of soil moisture is the huge difference in dielectric properties between soil particles (<4) and water (~80). Microwave sensors can detect the change in the dielectric equilibrium state of the soil-water mixture as it becomes wetter (Njoku & Kong, 1977). The most promising ability to thoroughly verify soil moisture types has been demonstrated by both latent and dynamic microwave remote sensing techniques.

2) Sentinel-1 Surface Soil Moisture (SSM1km).

The Sentinel-1 SSM1km product measures relative soil moisture saturation in the top 5 cm of soil, expressed as a percentage, and is available every 2-4 days across Europe. The coverage area is determined by the orbit configuration of the Sentinel-1 mission. Currently, soil moisture products from SSM1km are only available for the European region as sufficient observations are required to create reliable model parameters (Bauer-Marschallinger et al., 2017).

The SSM1km data is provided by Copernicus Global Land Services (CGLS) and is derived from Sentinel-1 radar backscatter images acquired in interferometric Wide Swath (IW) mode and VV polarization. This raw satellite data (Level 1) is provided jointly by the European Space Agency (ESA) and the European Commission (EC). The output products are daily images showing the relative soil moisture of the top 5 cm depth of the soil as a percentage of saturation at a resolution of 1 km. The Copernicus SSM1km version 1 product is available for the European continent every 3-8 days (from January 2015 to October 2016) and from October 2016 every 1.5-4 days (CGLOPS-1, n.d.). The total number of 410 scenes from June 1, 2017, to December 31 was downloaded from the Copernicus Land Service data portal, which provides free biogeophysical products of the global land surface.

The Copernicus Global Land Service offers a wide range of harmonized and co-formatted biogeophysical products available in near real-time through the Copernicus Global Land Service. Globally, these products address energy, water, cryosphere, and vegetation variables, among other aspects of the land surface. These parameters are produced and delivered by the CGLS on time, which also creates long-term time series. Leaf area index (LAI), fraction of photosynthetically active radiation absorbed (FAPAR), surface albedo, land surface temperature, soil moisture, burned area, water bodies and additional vegetation indices are among the essential climate variables (ECVs) that the CGLS has been offering since 2013. With frequencies ranging from hourly to daily to every ten days, these variables are automatically and consistently generated from Earth observation satellite (Bauer-Marschallinger, et al., 2017).

3) SMAP Derived 1km Downscaled Surface Soil Moisture Data.

In this study, we also used a global daily surface soil moisture data product derived from the L-band radiometer of the Soil Moisture Active Passive (SMAP) mission with a resolution of 1 km as a reference dataset for rescaling. Using a complex downscaling algorithm, the SMAP Enhanced Level 2 (L2) Radiometer Half-Orbit 9 km Equal-Area Scalable Earth Grid (EASE-Grid) Soil Moisture product is integrated with the MODIS land surface temperature data to produce this high-resolution data. To ensure accurate estimates of soil moisture in a variety of environments and terrains, the accuracy of this dataset was verified using in situ measurements from dense networks representing several types of land cover found worldwide. The data covers a significant period from April 1, 2015, to September 29, 2022, and allows for in-depth analysis (Lakshmi & Fang, 2023).

The main parameter of this product is the surface moisture of the soil in m^3/m^3, which usually corresponds to the top 5 cm of the soil column. Every day the data is updated and divided into bands corresponding to the ascending and descending half-tracks of the SMAP L-band radiometer. This separation makes it easier to understand daily variations in soil moisture and provides insightful information for a range of agricultural and environmental applications (Lakshmi & Fang, 2023).

2.2.1 Interpolation of ground-based observations.

To estimate the spatial distribution of soil moisture across the study area, I utilized the Inverse Distance Weighting (IDW) interpolation method within the QGIS environment. IDW is a deterministic interpolation technique that assumes that the influence of a measured value decreases with distance from the measurement location. This method was chosen due to its simplicity and effectiveness in generating continuous surface data from discrete measurement points, making it particularly suitable for environmental data such as soil moisture.

The process began by collecting soil moisture readings from various measuring stations distributed across the study area. These point measurements, while accurate at their specific locations, needed to be interpolated to produce a comprehensive surface that could represent the area as a whole.

In QGIS, I first inputted the point data, ensuring that each station's coordinates and corresponding soil moisture values were accurately georeferenced. The IDW interpolation was then applied, with the power parameter adjusted to reflect the influence of nearby points more strongly than those further away. Specifically, I set the distance coefficient to 2, which is a commonly used value in environmental studies to balance local influence and smoothness of the interpolated surface.

The result of this interpolation was a continuous raster surface that provided an area-average estimation of soil moisture across the entire study region. This interpolated surface was then used for further analysis, allowing for a more comprehensive understanding of the spatial variability of soil moisture, which is critical for assessing hydrological patterns and informing agricultural practices within the region.

2.2.2 Twente Soil Moisture Network.

The Twente soil moisture network, which covers the Twente region as well as part of the Salland region and the province of Gelderland, is located in the eastern part of the Dutch province of Overijssel. Its boundaries are 50°05'–53°27'N and 6°05'–7°00'E (Dante et al., 2012). Figure 1 shows a map of the Netherlands with the Twente region and the Overijssel province. It also shows the area the network covers, with all monitored locations highlighted by red circles.

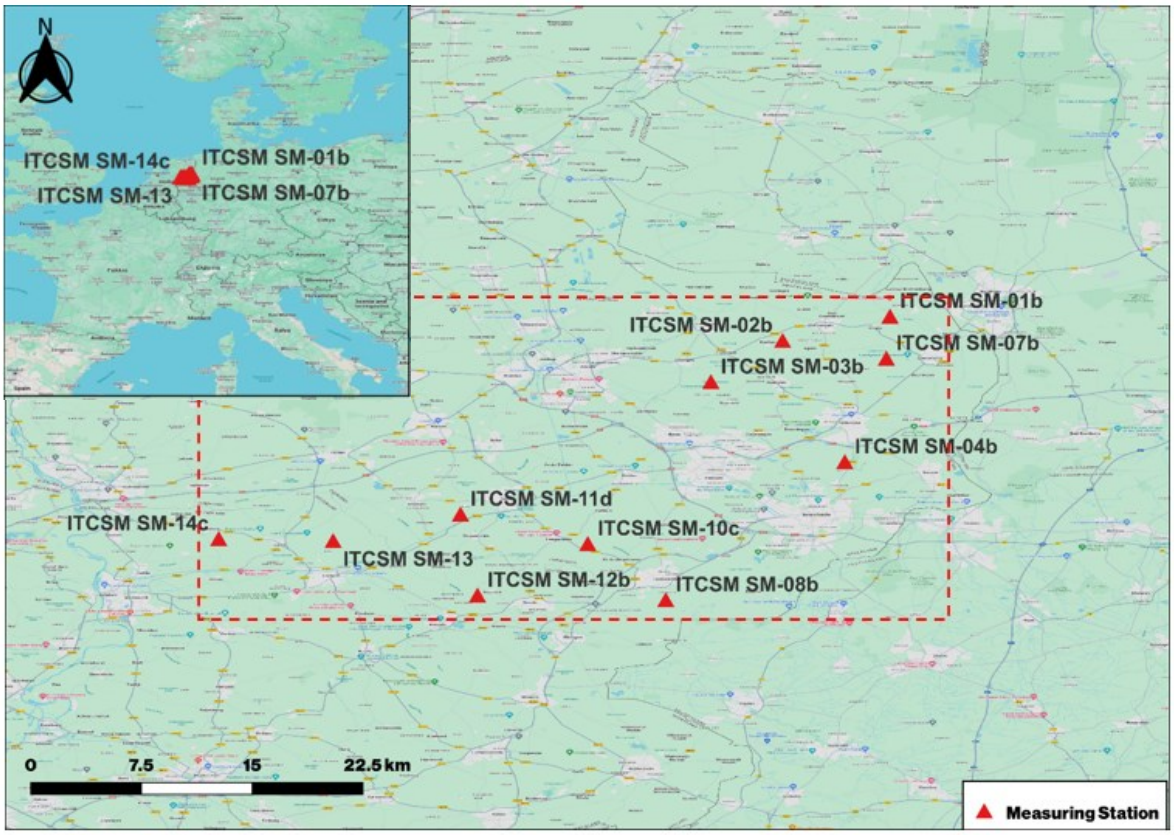

Figure 2. Shows the measuring stations located within the Twente soil monitoring network, shown by the red dotted line. (Source: QGIS open street map)

Twenty stations measuring soil temperature and moisture were placed over an area of approximately 50 km x 40 km (52°05' to 52°27'N, 6°05' to 7°00'E). Installation of the soil moisture monitoring stations began in November 2008 and ended in June 2009. The entire network has been operational since July 2009, with all 20 monitoring stations spread over an area of approximately 50 km x 40 km (Dente et al., 2012). These locations were selected to ensure comprehensive monitoring of the area, covering all soil types and land covers.

In this study, a total of eleven monitoring stations, shown with black dots in Figure 1, were selected for analysis from June 1, 2017, to December 31, 2020. Further details about these

monitoring stations are shown in Table 1. The Twente soil moisture monitoring network was selected for this analysis because it met the following requirements.

1. Availability of measurements of near-surface or near-surface soil moisture at 3 different depths, 5 cm, 10 cm and 20 cm from 06/01/2017 to 12/31/2020.
2. Located in the coverage area of the Sentinel-1 surface soil moisture product Sentinel-1 surface moisture (SSM1km).
3. Equipped with a spatially dense network configuration that enables spatial analysis.

The region is flat, with elevation differences ranging from -3 to 50 meters above sea level. Grassland used for pasture, which is harvested and fertilized several times a year, is the most common land cover type. Nevertheless, the land use of this region is a patchwork of urban areas, forests and agricultural fields. The main crop is corn, which is sown in April and harvested in September. Other crops grown there include potatoes and other grains. The Netherlands has a temperate climate, based on the Koeppen classification system. Annual precipitation is distributed throughout the year and averages around 760 mm. The average monthly air temperature varies between about 3 °C in January and 17 °C in July (Dante et al., 2012).

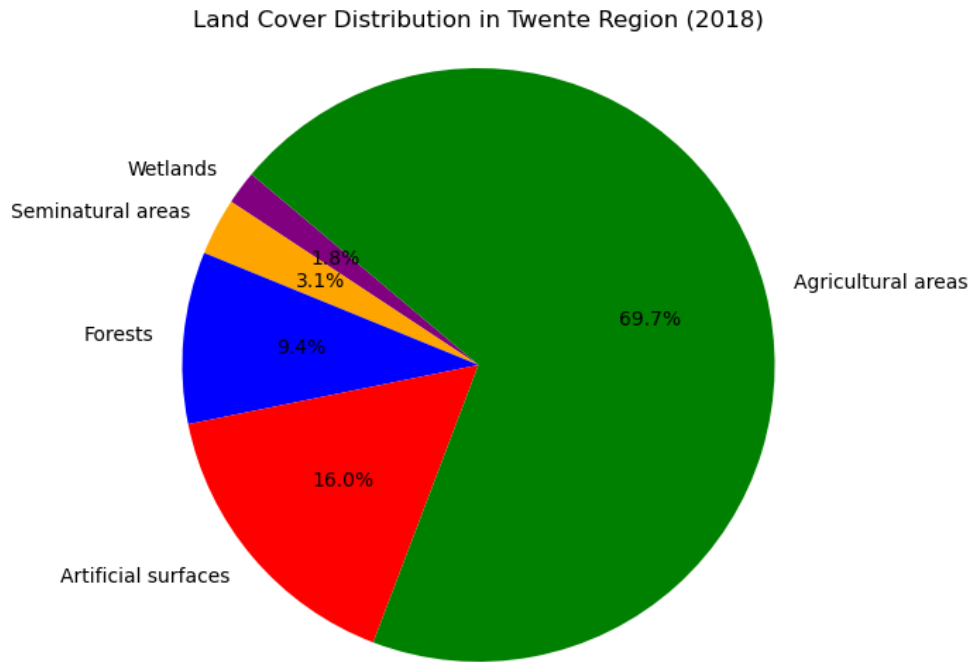

Figure 3 Land use map of Twente region in the Netherlands according to ESRI land cover (ESRI, Land Cover, n.d.)

2.2.3 The areas flooded during the May 2023 Romagna event

Hydrometeorological events of exceptional intensity affected the Emilia-Romagna Region's territory from the evening of May 1, 2023, to May 3, 2023, resulting in a serious and critical situation, especially in the provinces of Forlì-Cesena, Ravenna, Bologna, Modena, and Reggio Emilia. Another exceptionally strong weather event struck on May 16 and 17, severely impacting not only the aforementioned regions of the provinces of Bologna and Romagna but also the region of the province of Rimini (Brath et al., 2023).

As of May 23, there have been fourteen confirmed deaths from the floods and 36,000 people have been forced to find alternative shelter. There were 27,000 displaced people in the Ravenna region, 4,830 in the province of Forlì-Cesena and 4,012 in the Bologna region. In addition, the floods caused 305 landslides and the total or partial closure of five hundred roads. In addition to the coastal cities of Ravenna, Rimini and Riccione on the Adriatic, the cities of Bologna, Imola, Castel Bolognese, Faenza, Lugo, Forlì and Cesena were also badly flooded (MashMcLennan, 2023). The Idice River (Reno) basin in Castenaso and Sillaro River basin in Sesto Imolese will be the subject of the analysis as shown in Figure 4. The average areal rainfall heights recorded during these two events are given in Table 3.

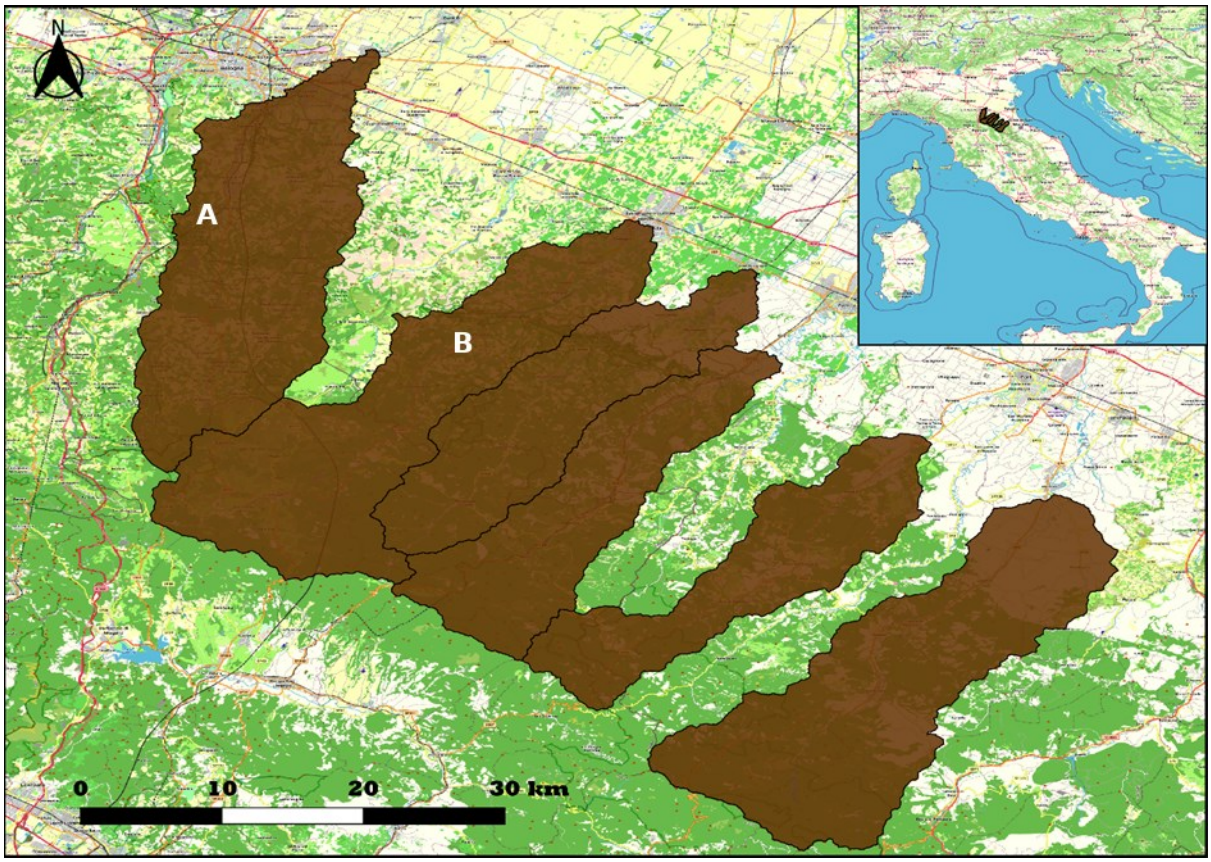

Figure 4. The map shows the basins affected by the May 2023 event in the Emilia-Romagna Region of Italy. Basin (A) represents the Idice River (Reno) in Castenaso, while basin (B)

corresponds to the Sillaro River in Sesto Imolese. The analysis of soil moisture variation is focused exclusively on these two basins.

Table 3 Shows the average areal rainfall heights for Idice (Reno) and Sillaro basins (Brath et al., 2023).

Basin	**Area (*km*^{2})**	**Precipitation (*mm*) (1-3 May)**	**Precipitation(*mm*) (15-17 May)**
Idice (Reno) in Castenaso	*393.1*	*170.3*	*144.4*
Sillaro in Sesto Imolese	*247.3*	*173.2*	*156.4*

.

Chapter 3 Results.

This chapter presents the results of the comparative analysis between soil moisture estimates derived from microwave remote sensing products (Sentinel-1 SSM1km and SMAP) and ground-based observations. The analysis is structured around key themes, including temporal variation analysis, statistical comparison of point-based and area-averaged data, and the impact of land cover on soil moisture retrieval accuracy. Additionally, the spatial variation of soil moisture before, during, and after the May 2023 flood events in Emilia Romagna, Italy, is examined.

3.1 Temporal Variation Analysis of SSM1km and Ground Observations.

The temporal variation of soil moisture captured by the Sentinel-1 SSM1km product was compared with in-situ ground observations from various stations within the Twente region. Figures 5 through 15 illustrate the time series of soil moisture measurements for selected stations, where the brown line represents in-situ measurements, and the blue dotted line represents SSM1km estimates. Since SSM1km is in relative units (%) and the in-situ soil moisture values are in absolute units (m^3/m^3), data scaling was required to enable a valid comparison. The piece-wise linear Cumulative Distribution Function (CDF) matching (Liu, et al., 2011) of the SSM1km data with the local in situ soil moisture, which gave an absolute soil water content in m^3/m^3 between 0.0 and 0.5 was carried out. SMAP-derived soil moisture with a spatial and temporal resolution similar to SSM1km was used as a reference dataset in scaling as it was found to meet the requirements. CDF matching compares the distributions of two time series and thus enables a direct comparison.

3.1.1 Station-Specific Analysis.

- **Station 1B (Figure 5):** The SSM1km data generally followed the trends observed in ground measurements but showed deviations during peak moisture events. The SSM1km data tended to slightly overestimate soil moisture levels during wetter periods, as indicated by a positive bias of 0.0814.
- **Station 2B (Figure 6):** The temporal patterns of soil moisture were well captured by the SSM1km data, although the bias was negative (-0.0322), indicating slight underestimation. The Pearson correlation was moderate (0.563), suggesting a reasonable linear relationship.
- **Stations 3B to 14C (Figures 7-15):** Similar trends were observed across other stations, with varying degrees of accuracy. Notably, Station 11D showed the highest RMSE (0.306) and a negative R^2, indicating poor predictive power of the SSM1km data at this location.

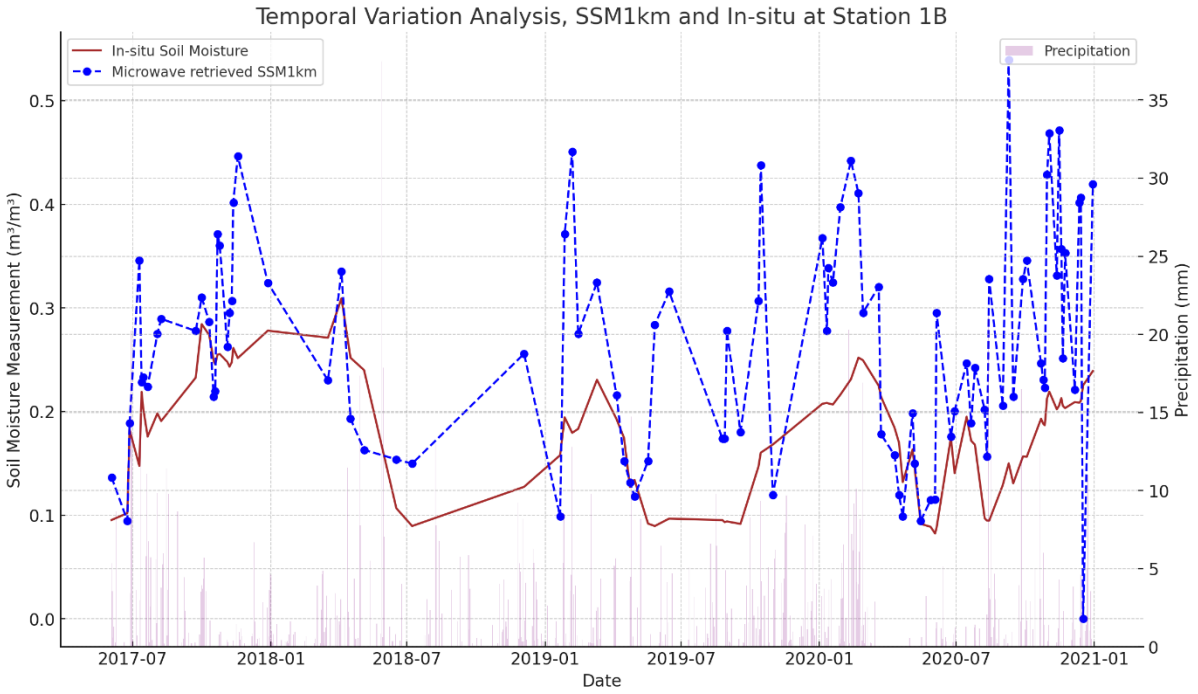

Figure 5 Temporal variation of soil moisture at point station 1B from June 3, 2017, to December 31, 2020, the in-situ measurements are represented by the brown line and absolute SSM1km by the blue dotted line.

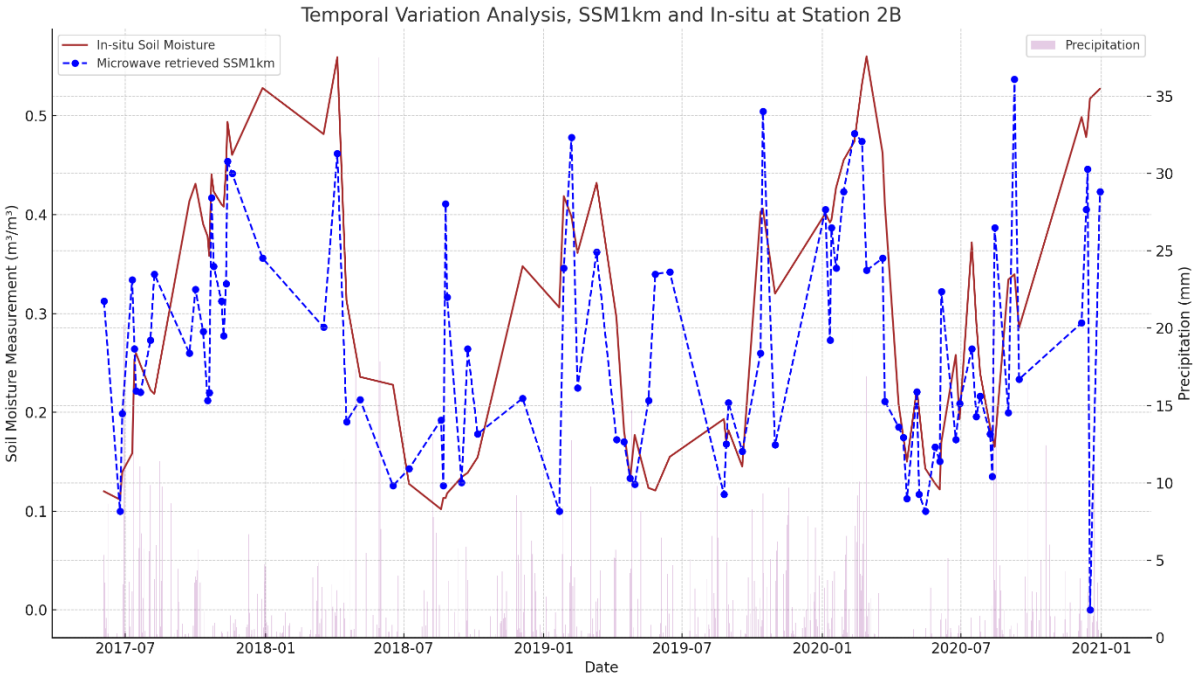

Figure 6 Temporal variation of soil moisture at point station 2B from June 3, 2017, to December 31, 2020, the in-situ measurements are represented by the brown line and absolute SSM1km by the blue dotted line.

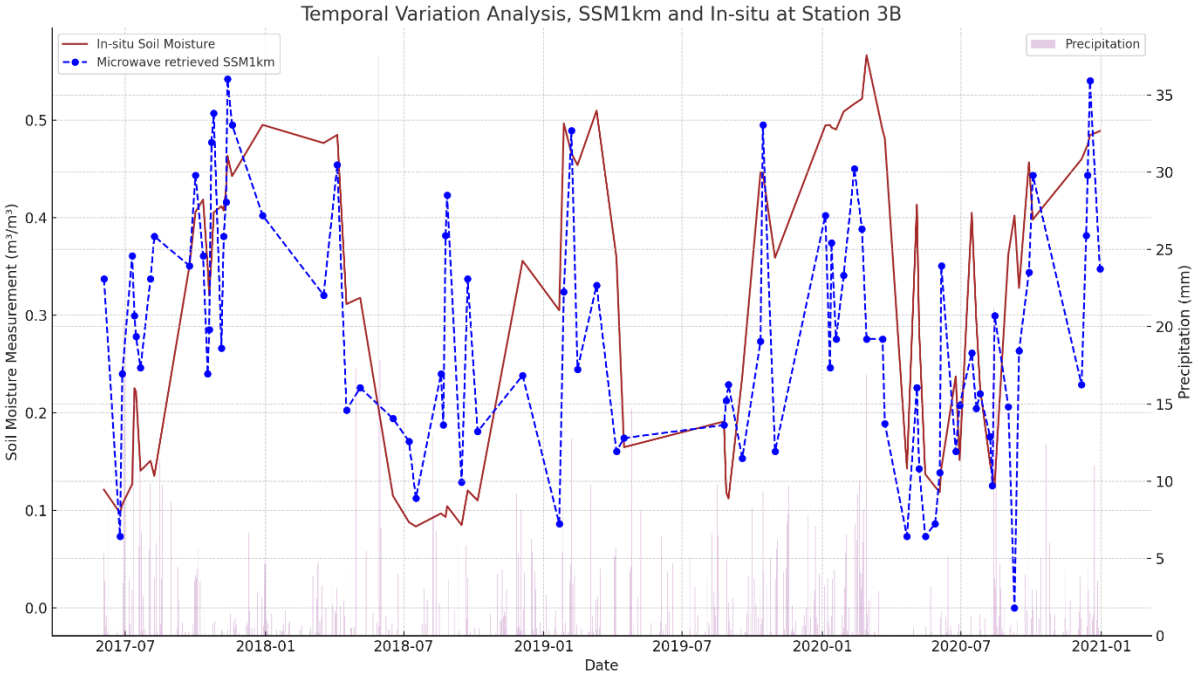

Figure 7 Temporal variation of soil moisture at point station 3B from June 3, 2017, to December 31, 2020, the in-situ measurements are represented by the brown line and absolute SSM1km by the blue dotted line.

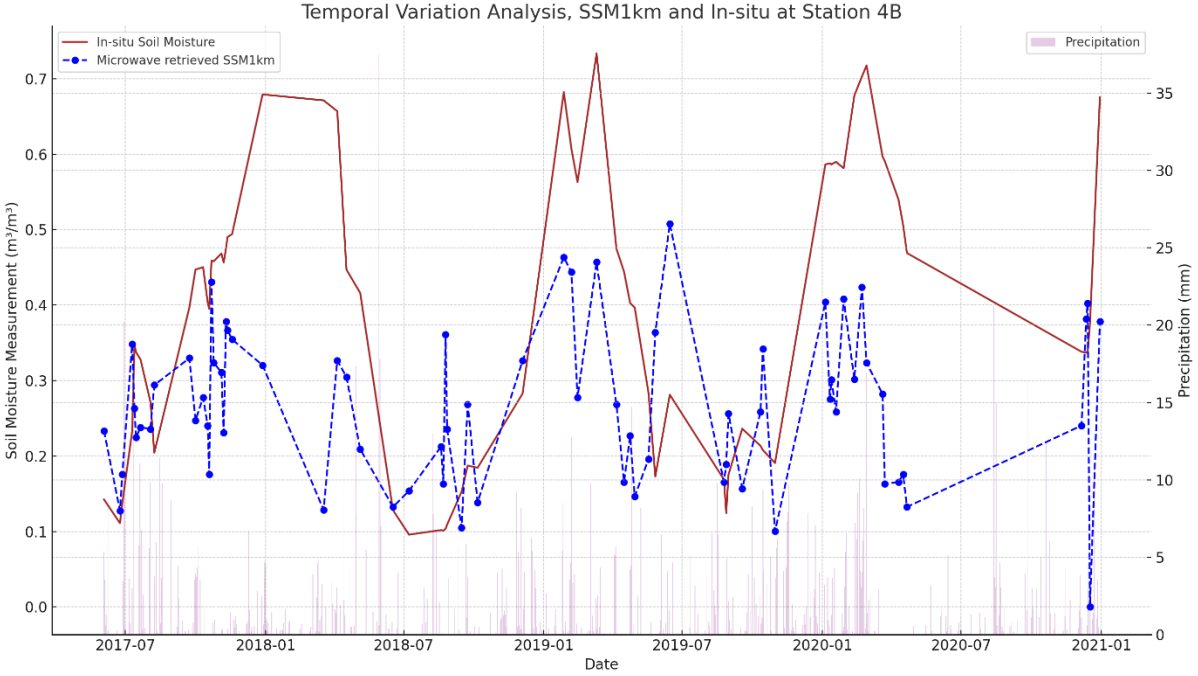

Figure 8 Temporal variation of soil moisture at point station 4B from June 3, 2017, to December 31, 2020, the in-situ measurements are represented by the brown line and absolute SSM1km by the blue dotted line.

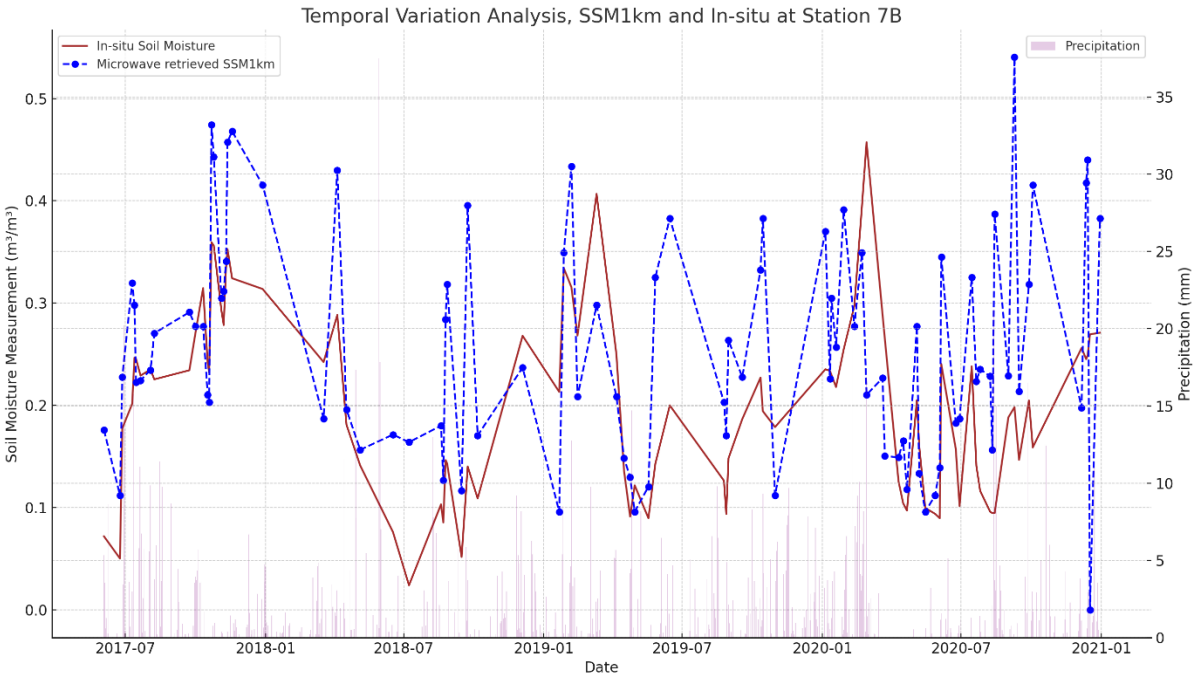

Figure 9 Temporal variation of soil moisture at point station 7B from June 3, 2017, to December 31, 2020, the in-situ measurements are represented by the brown line and absolute SSM1km by the blue dotted line.

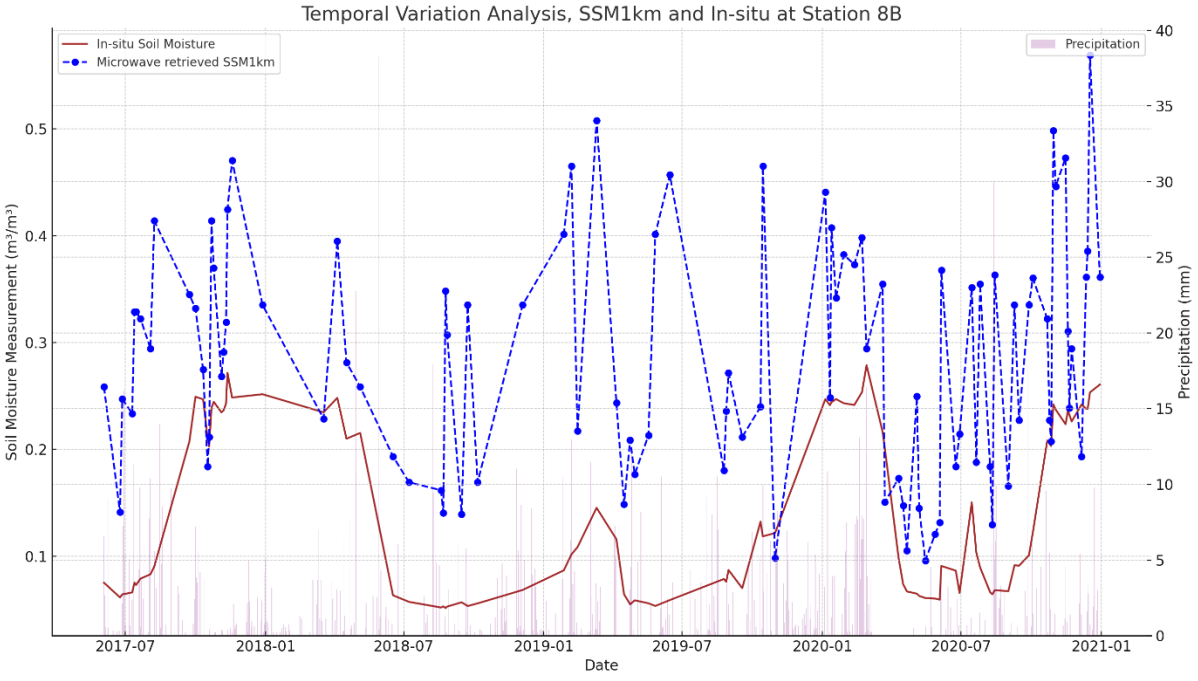

Figure 10 Temporal variation of soil moisture at point station 8B from June 3, 2017, to December 31, 2020, the in-situ measurements are represented by the brown line and absolute SSM1km by the blue dotted line.

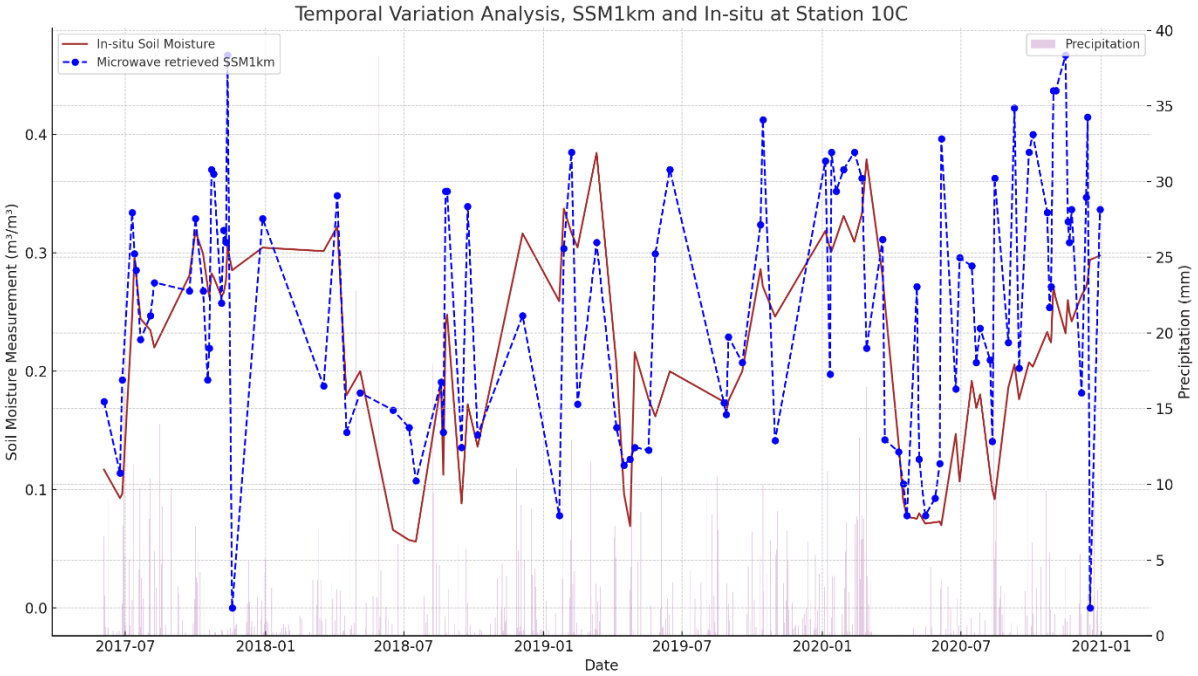

Figure 11 Temporal variation of soil moisture at point station 10C from June 3, 2017, to December 31, 2020, the in-situ measurements are represented by the brown line and absolute SSM1km by the blue dotted line.

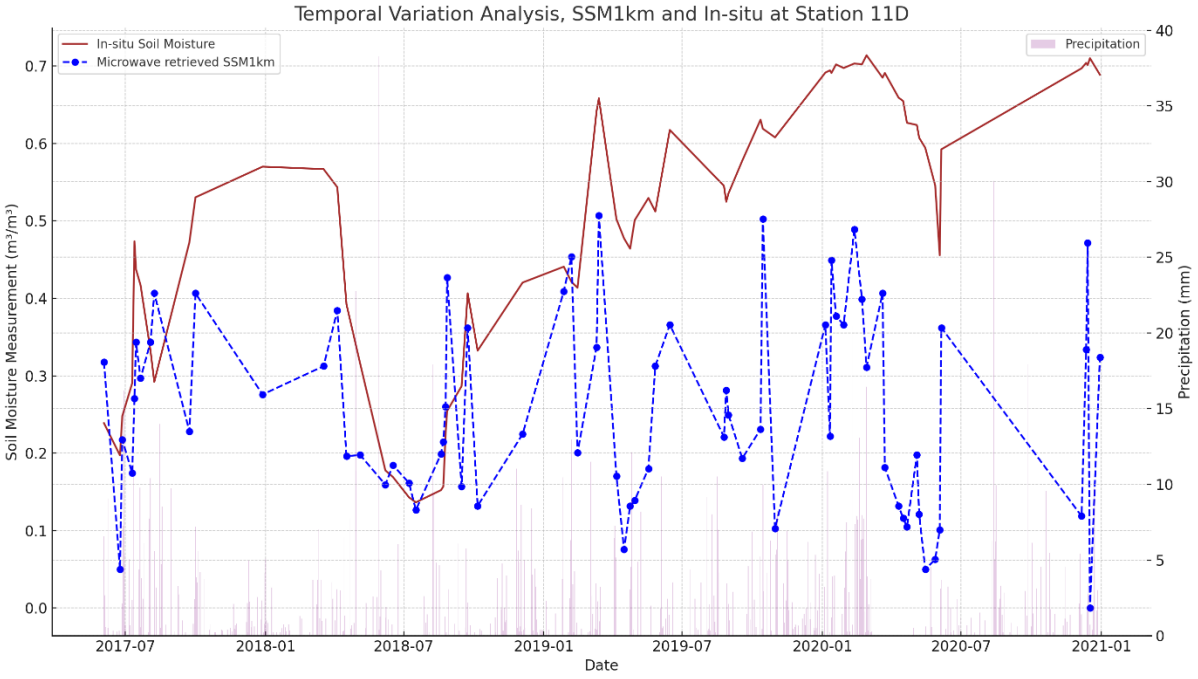

Figure 12 Temporal variation of soil moisture at point station 11D from June 3, 2017, to December 31, 2020, the in-situ measurements are represented by the blue dotted line.

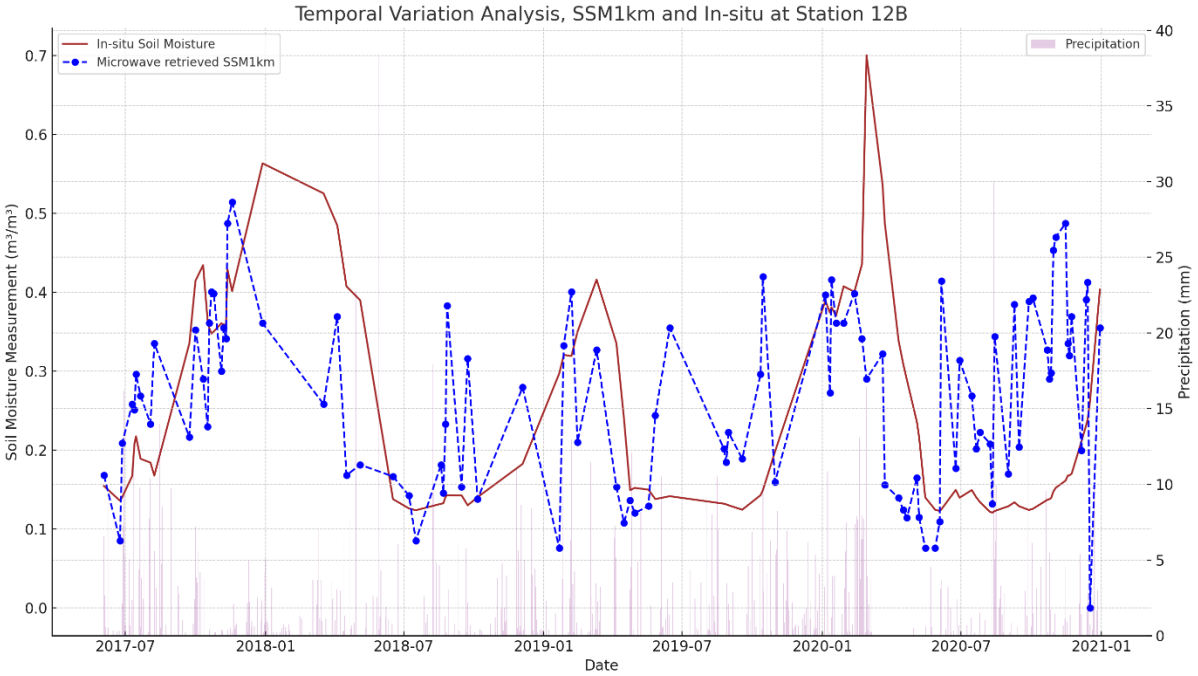

Figure 13 Temporal variation of soil moisture at point station 12B from June 3, 2017, to December 31, 2020, the in-situ measurements are represented by the brown line and absolute SSM1km by the blue dotted line.

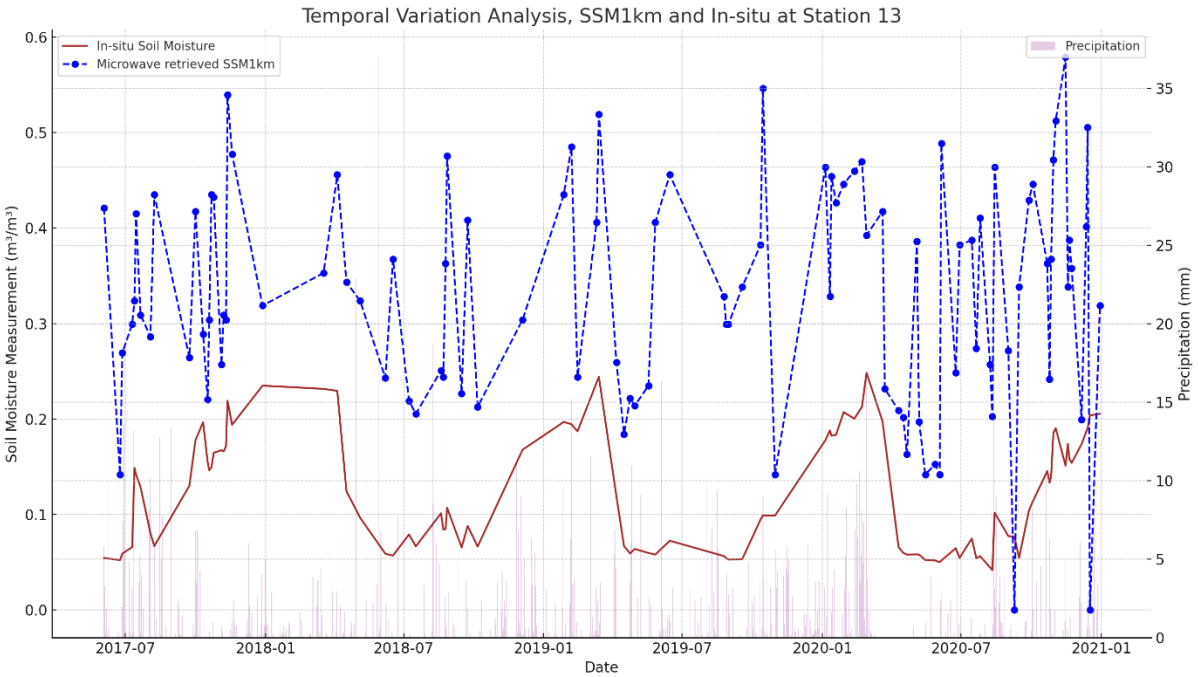

Figure 14 Temporal variation of soil moisture at point station 13 from June 3, 2017, to December 31, 2020, the in-situ measurements are represented by the brown line and absolute SSM1km by the blue dotted line.

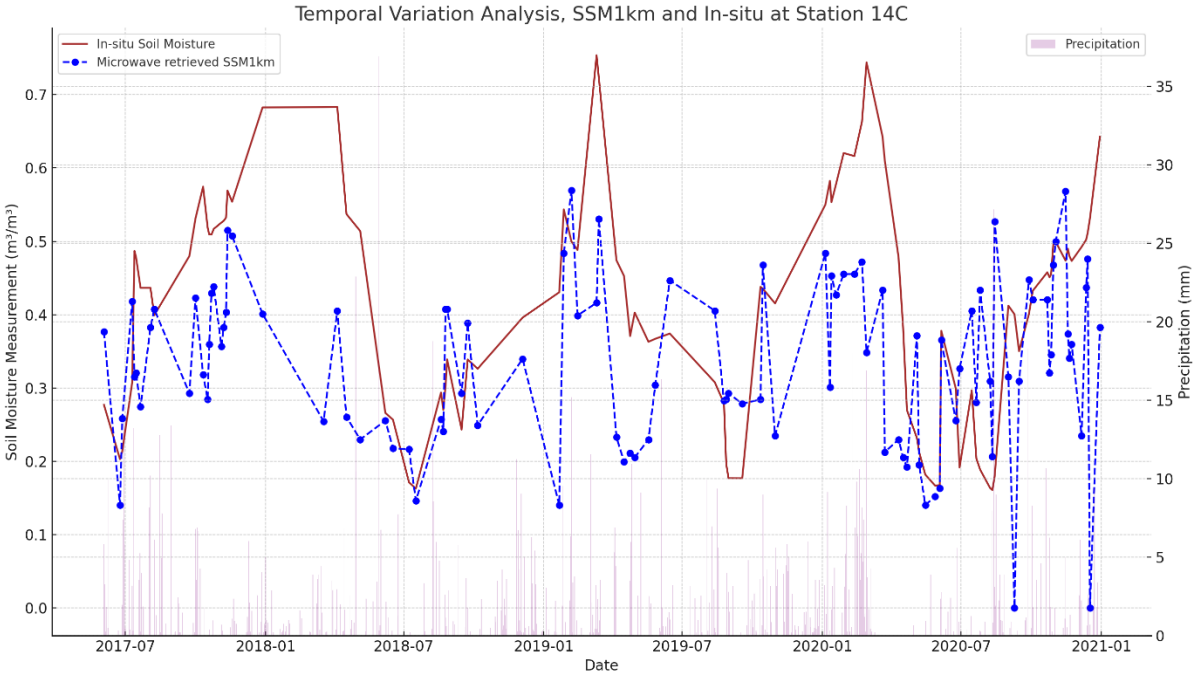

Figure 15 Temporal variation of soil moisture at point station 14C from June 3, 2017, to December 31, 2020, the in-situ measurements are represented by the brown line and absolute SSM1km by the blue dotted line.

3.1.2 Statistical Metrics

Table 4 summarizes the statistical metrics, including Bias, RMSE, R^2, Pearson correlation, Spearman correlation, and Percentage Error for each station. The results indicate that while the SSM1km product captured general trends, it often struggled with extreme variations and exhibited varying accuracy across different stations.

Table 4 The statistical metrics showing resulting of the comparative analysis of SSM1km and ground-based observations.

Station	Depth (cm)	Bias	RMSE	Coefficient of Determination (R^2)	Pearson Correlation (r)	Spearman Correlation (ρ)	Percentage Error (%)
1B	*5*	*0.0814*	*0.1261*	*-3.867*	*0.4364*	*0.4849*	*60.71*
2B	*5*	*-0.0322*	*0.1239*	*0.1917*	*0.563*	*0.5765*	*37.68*

3B	*5*	*-0.0286*	*0.1454*	*0.1168*	*0.4887*	*0.5051*	*53.43*
4B	*5*	*-0.122*	*0.2128*	*-0.2734*	*0.4046*	*0.4308*	*47.5*
7B	*5*	*0.0536*	*0.1109*	*-0.5273*	*0.5351*	*0.5897*	*56.73*
8B	*5*	*0.1435*	*0.1749*	*-3.7377*	*0.4626*	*0.5257*	*157.73*
10C	*5*	*0.0371*	*0.1065*	*-0.571*	*0.4835*	*0.5036*	*47.42*
11D	*5*	*-0.2405*	*0.306*	*-2.0515*	*0.2354*	*0.227*	*47.96*
12B	*5*	*0.0208*	*0.1495*	*-0.3274*	*0.2612*	*0.2875*	*59.79*
13	*5*	*0.2092*	*0.2344*	*-13.6561*	*0.4156*	*0.4509*	*233.59*
14C	*5*	*-0.0856*	*0.1715*	*-0.2671*	*0.4066*	*0.4543*	*32.84*

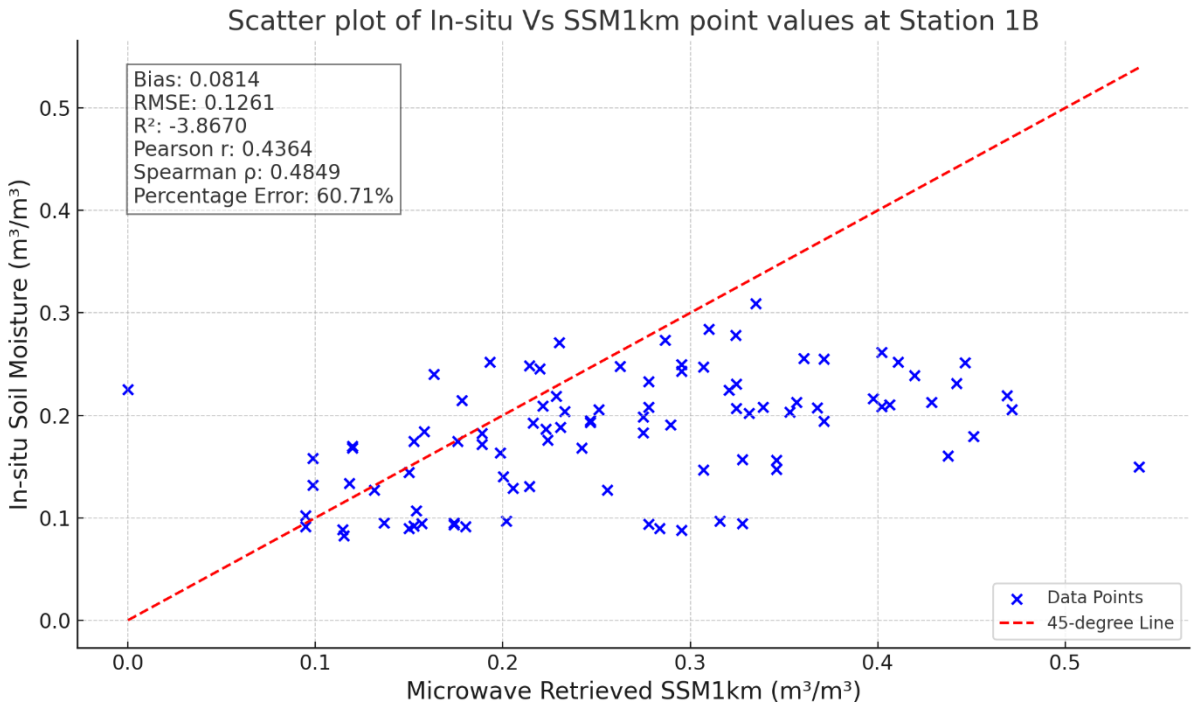

Figure 16 The graph above shows the scatter plot of absolute soil moisture (SSM1km) and In-situ soil moisture measurements at Station 1B.

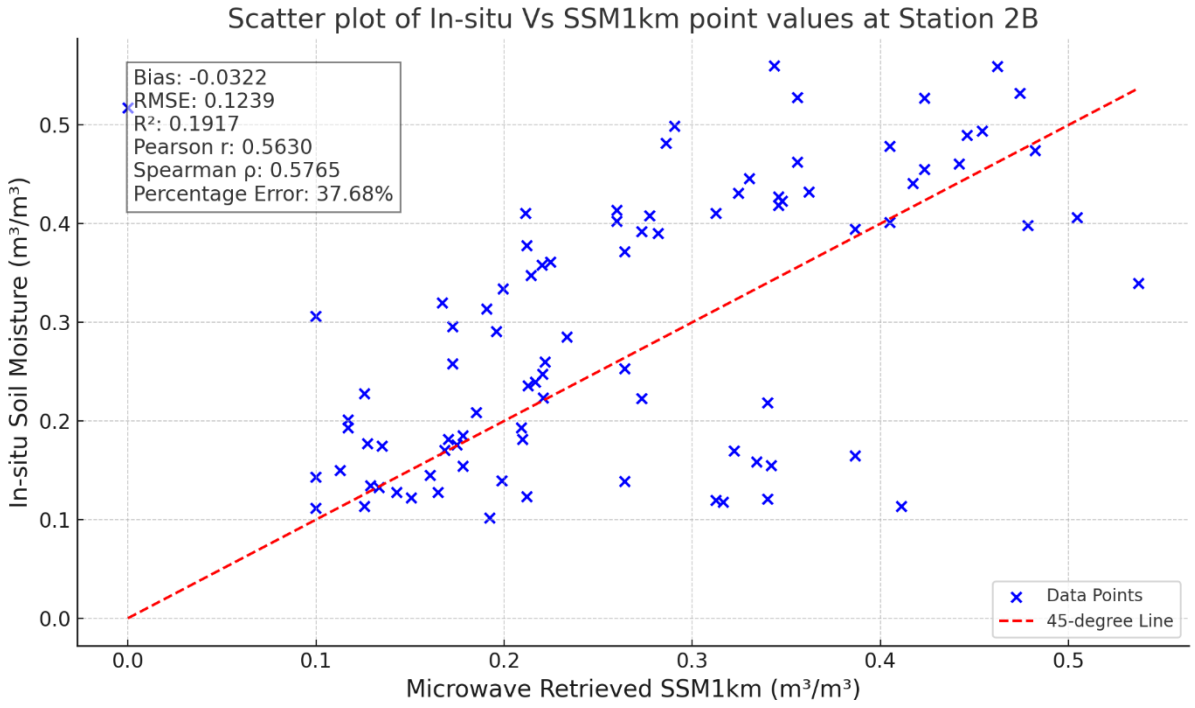

Figure 17 The graph above shows the scatter plot of absolute soil moisture (SSM1km) and In-situ soil moisture measurements at Station 2B.

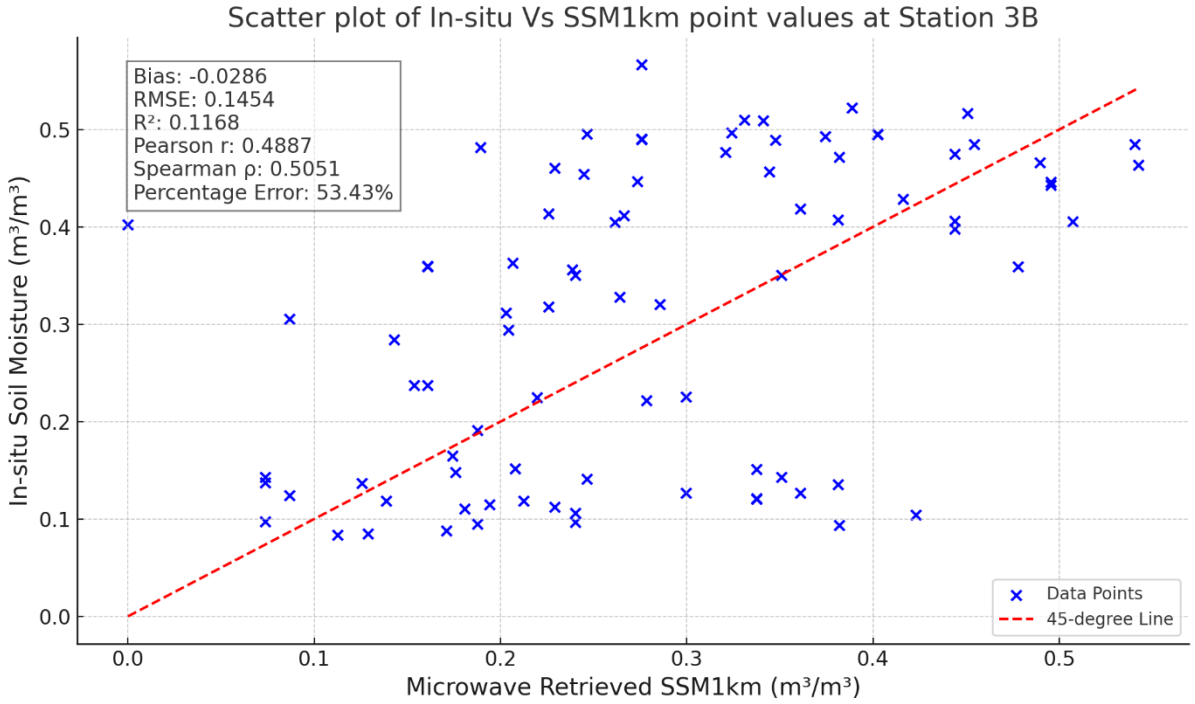

Figure 18 The graph above shows the scatter plot of absolute soil moisture (SSM1km) and In-situ soil moisture measurements at Station 3B.

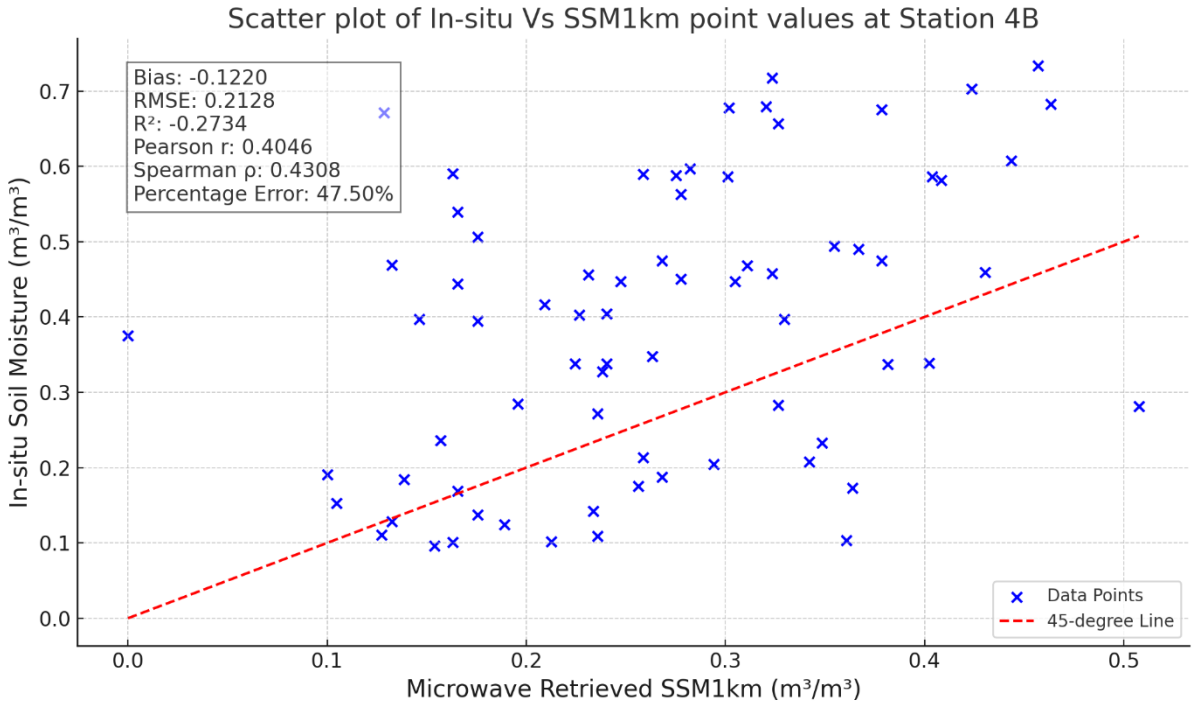

Figure 19 The graph above shows the scatter plot of absolute soil moisture (SSM1km) and In-situ soil moisture measurements at Station 4B.

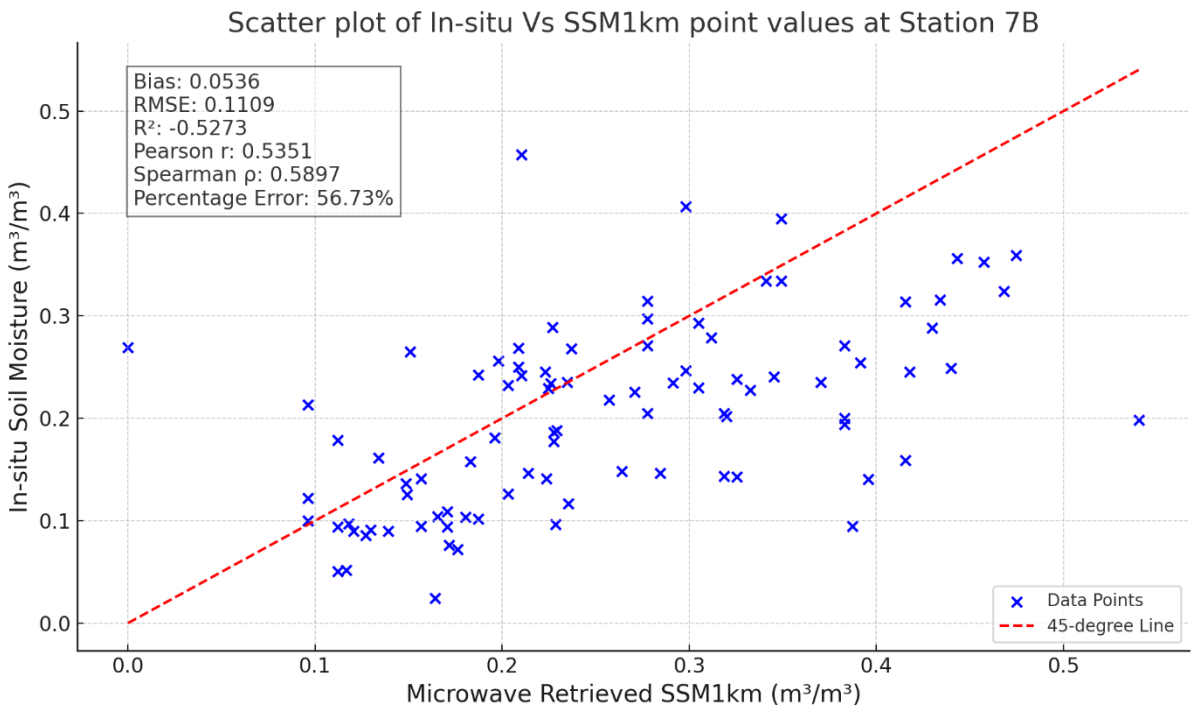

Figure 20 The graph above shows the scatter plot of absolute soil moisture (SSM1km) and In-situ soil moisture measurements at Station 7B.

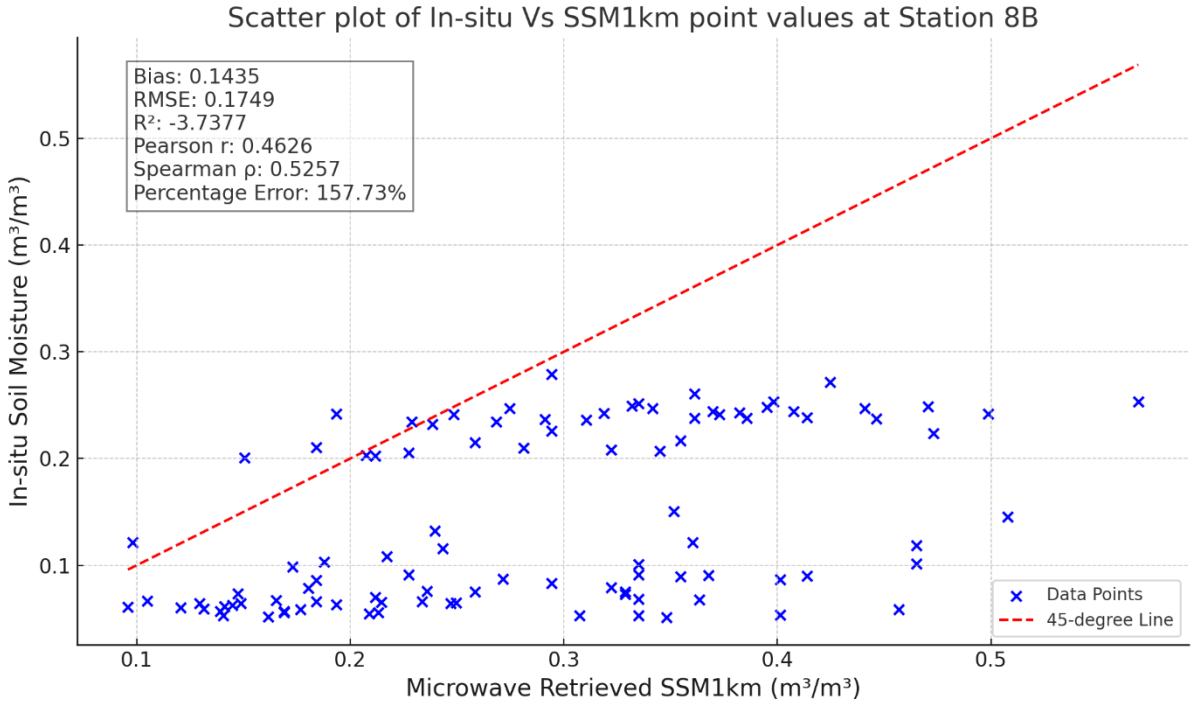

Figure 21 The graph above shows the scatter plot of absolute soil moisture (SSM1km) and In-situ soil moisture measurements at Station 8B.

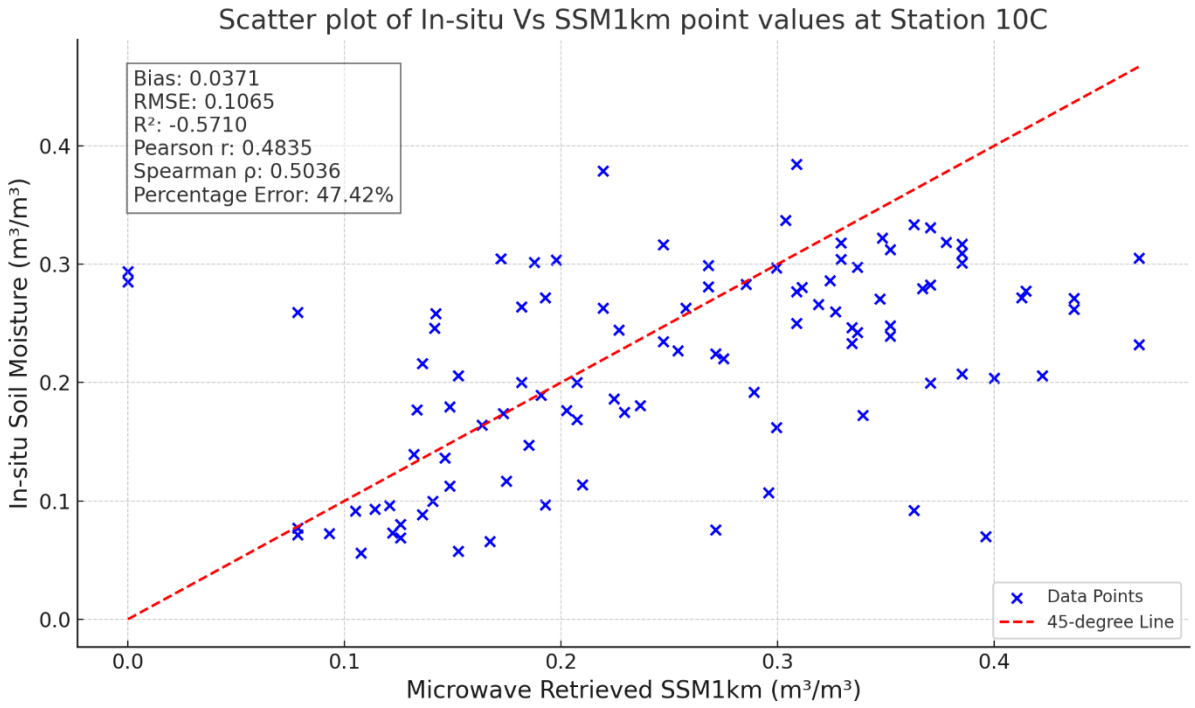

Figure 22 The graph above shows the scatter plot of absolute soil moisture (SSM1km) and In-situ soil moisture measurements at Station 10C.

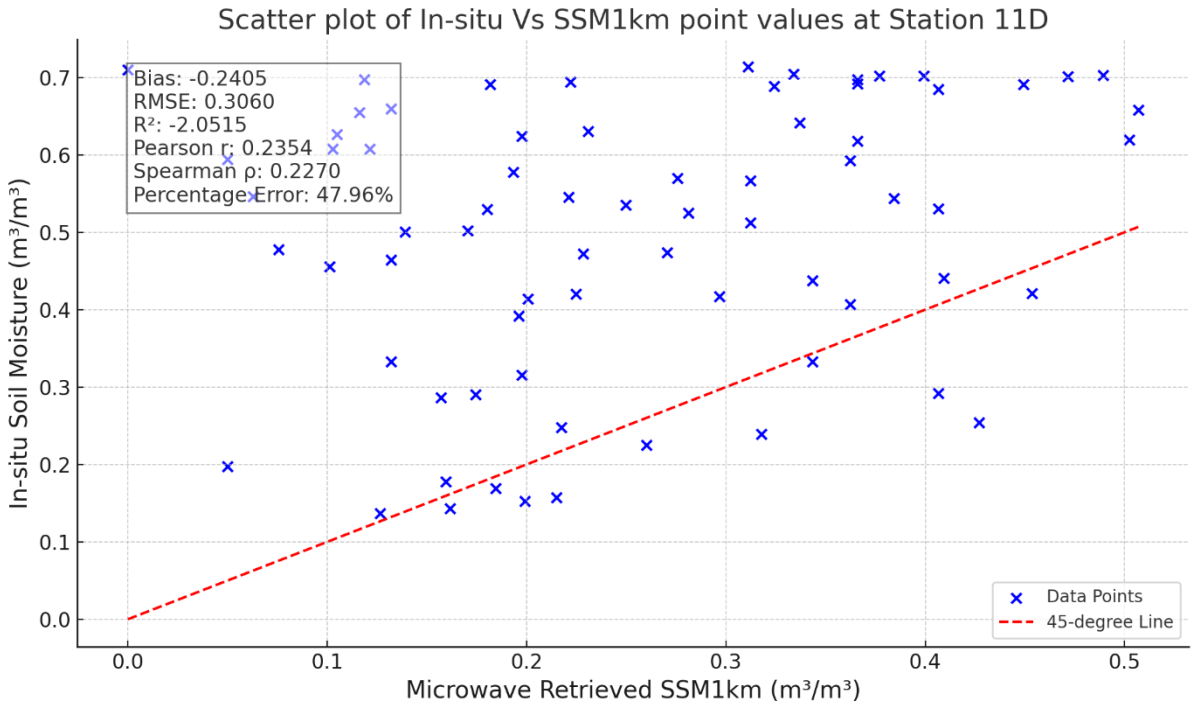

Figure 23 The graph above shows the scatter plot of absolute soil moisture (SSM1km) and In-situ soil moisture measurements at Station 11D.

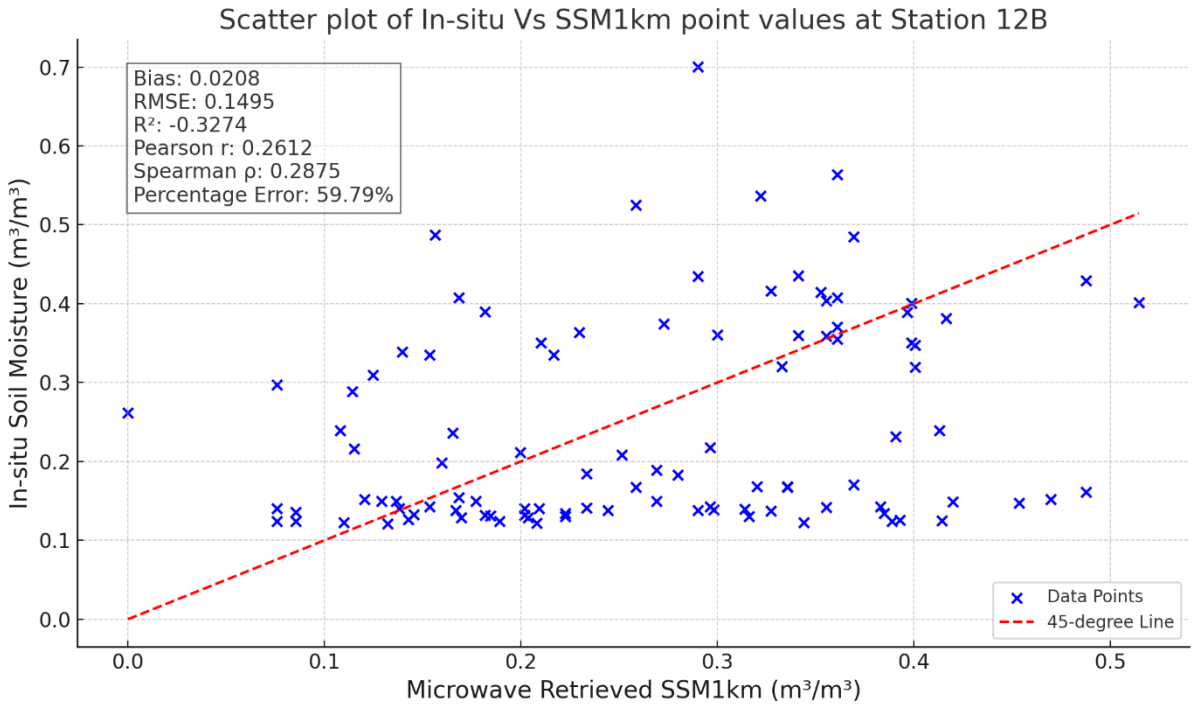

Figure 24 The graph above shows the scatter plot of absolute soil moisture (SSM1km) and In-situ soil moisture measurements at Station 12B.

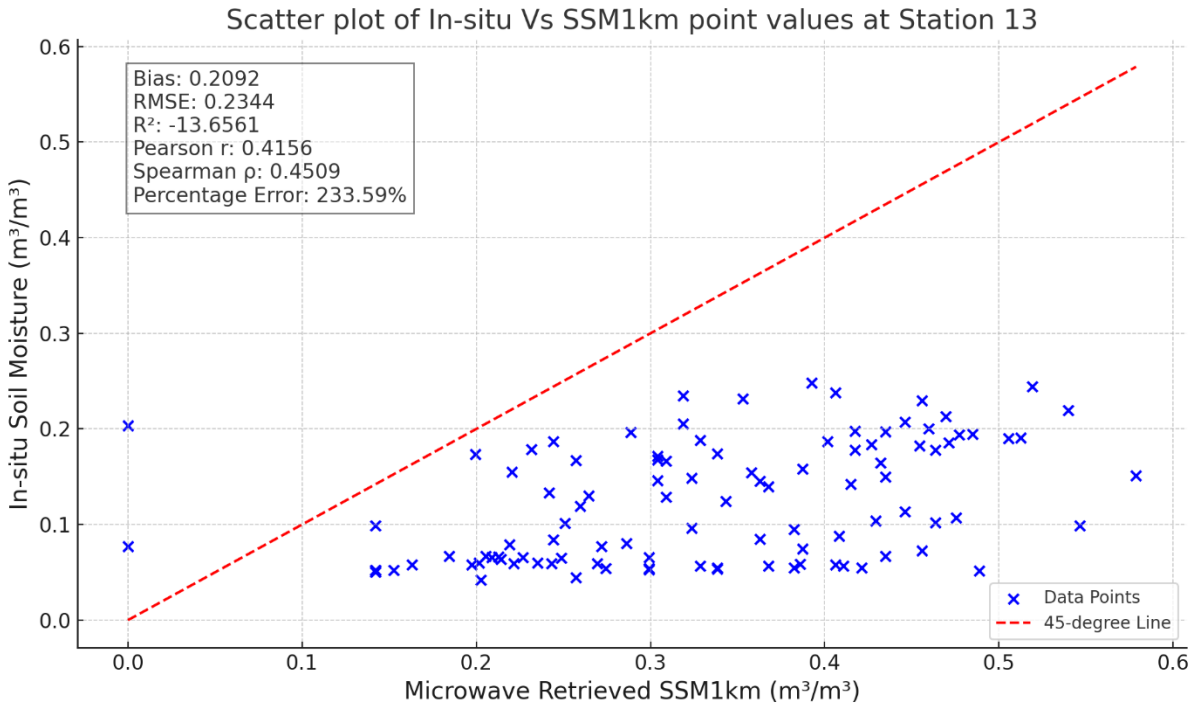

Figure 25 The graph above shows the scatter plot of absolute soil moisture (SSM1km) and In-situ soil moisture measurements at Station 13.

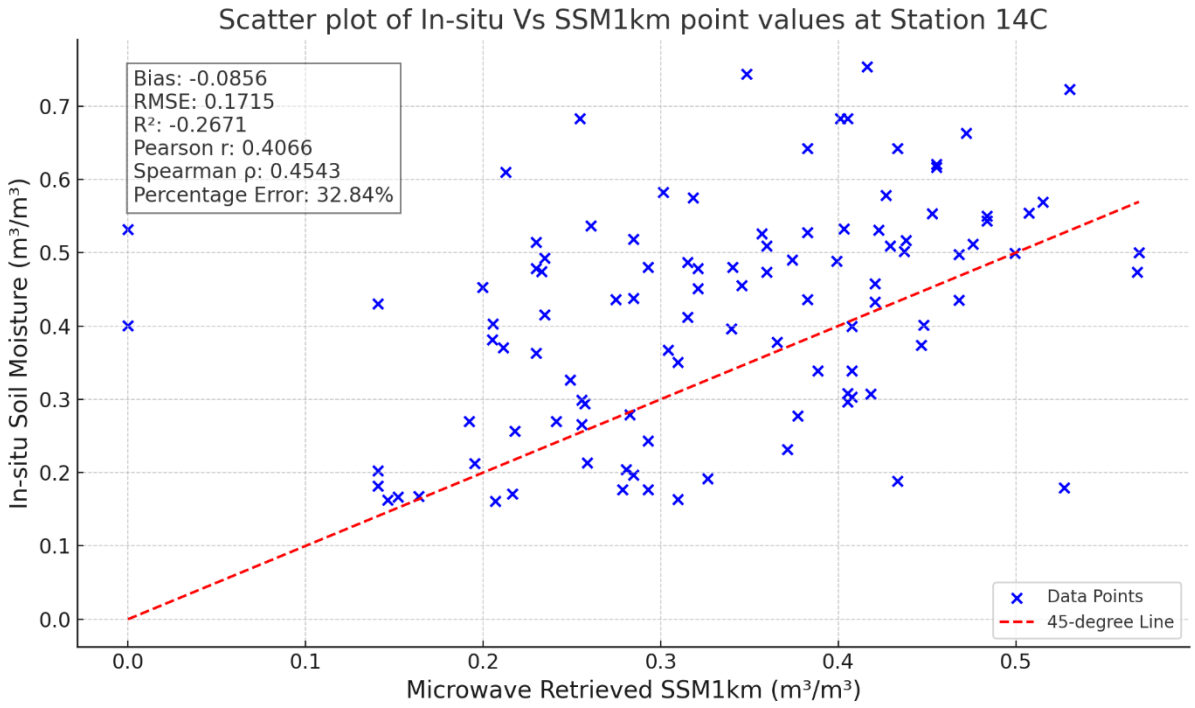

Figure 26 The graph above shows the scatter plot of absolute soil moisture (SSM1km) and In-situ soil moisture measurements at Station 14C.

3.2 Temporal Variation Analysis of SMAP and Ground Observations.

The SMAP-derived soil moisture estimates were also compared with ground observations. Figures 43 through 53 present the time series data for various stations, with in-situ measurements shown in brown and SMAP estimates in blue.

3.2.1 Station-Specific Analysis.

- **Station 1B (Figure 43):** SMAP data followed the observed trends closely, with a low bias and reasonable RMSE, indicating better performance compared to SSM1km at this station.
- **Station 2B (Figure 44):** The SMAP data showed a negative bias (-0.0286) and a moderate Pearson correlation (0.4887), suggesting a slight underestimation but overall good agreement with ground observations.
- **Stations 3B to 14C (Figures 45-53):** The SMAP data generally performed well across the stations, with lower RMSE values and higher correlation coefficients compared to SSM1km, although some discrepancies were still noted in stations with complex land cover.

The SMAP-derived pixel values are converted into time series and then compared to the observations from the ground stations that overlap each pixel using statistical metrics listed in Chapter 2.2.2.

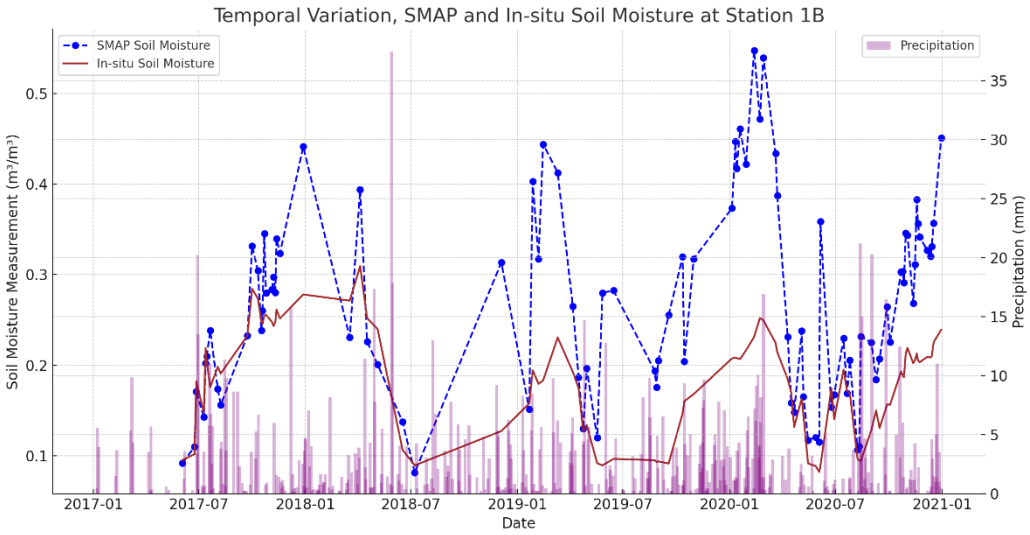

Figure 27 Temporal variation of soil moisture at point station 1B from June 3, 2017, to December 31, 2020, the in-situ measurements are represented by the brown line and absolute SMAP derived soil moisture by the blue dotted line.

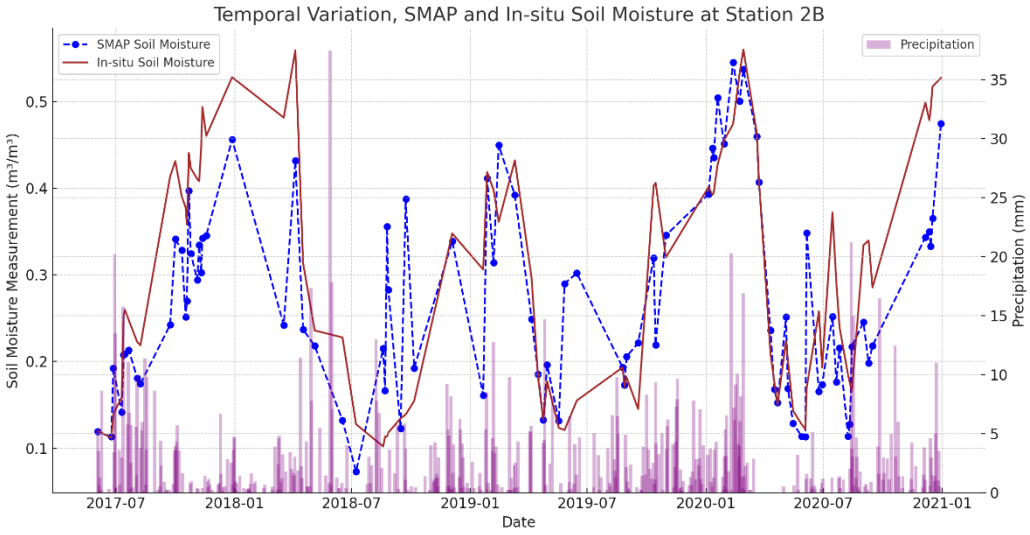

Figure 28 Temporal variation of soil moisture at point station 2B from June 3, 2017, to December 31, 2020, the in-situ measurements are represented by the brown line and absolute SMAP derived soil moisture by the blue dotted line.

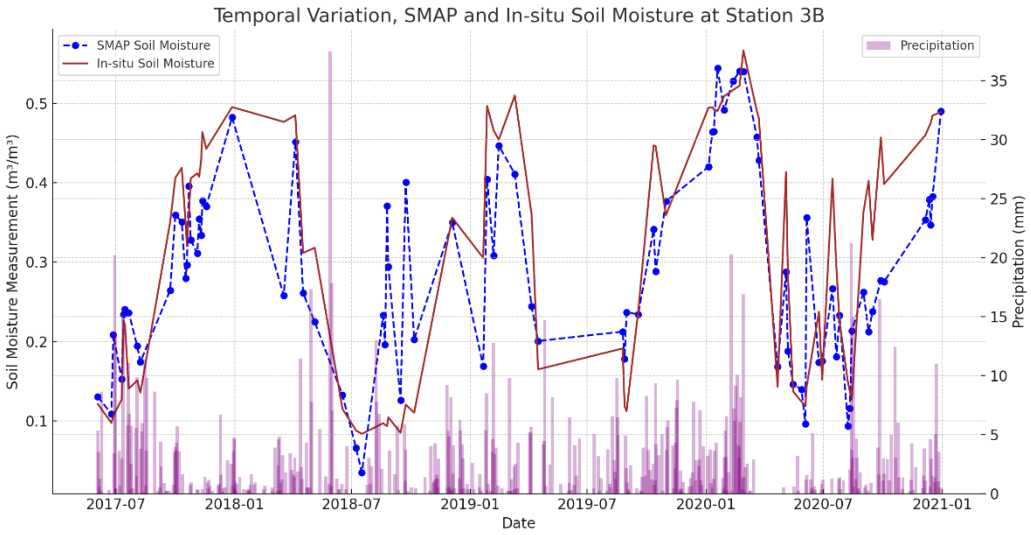

Figure 29 Temporal variation of soil moisture at point station 3B from June 3, 2017, to December 31, 2020, the in-situ measurements are represented by the brown line and absolute SMAP derived soil moisture by the blue dotted line.

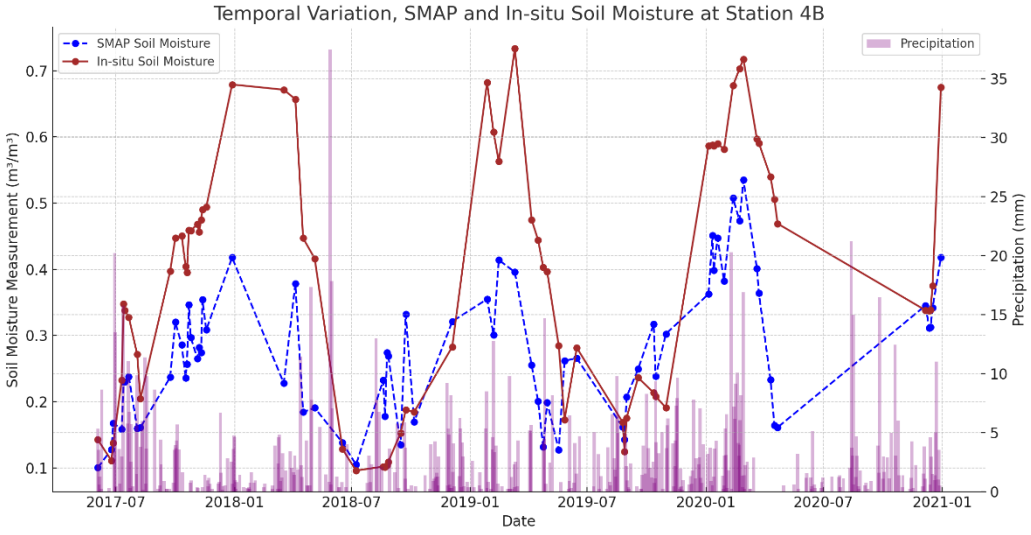

Figure 30 Temporal variation of soil moisture at point station 4B from June 3, 2017, to December 31, 2020, the in-situ measurements are represented by the brown line and absolute SMAP derived soil moisture by the blue dotted line.

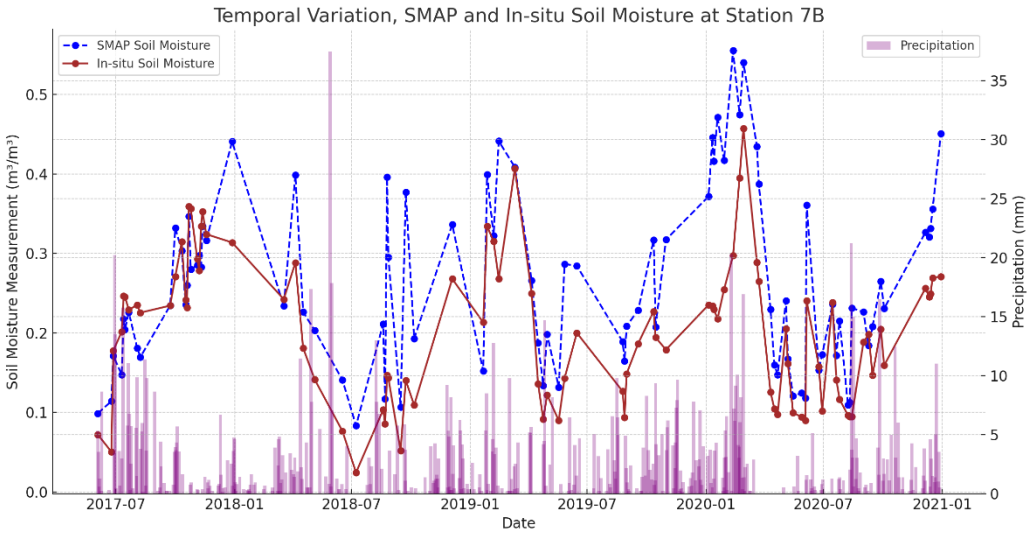

Figure 31 Temporal variation of soil moisture at point station 7B from June 3, 2017, to December 31, 2020, the in-situ measurements are represented by the brown line and absolute SMAP derived soil moisture by the blue dotted line.

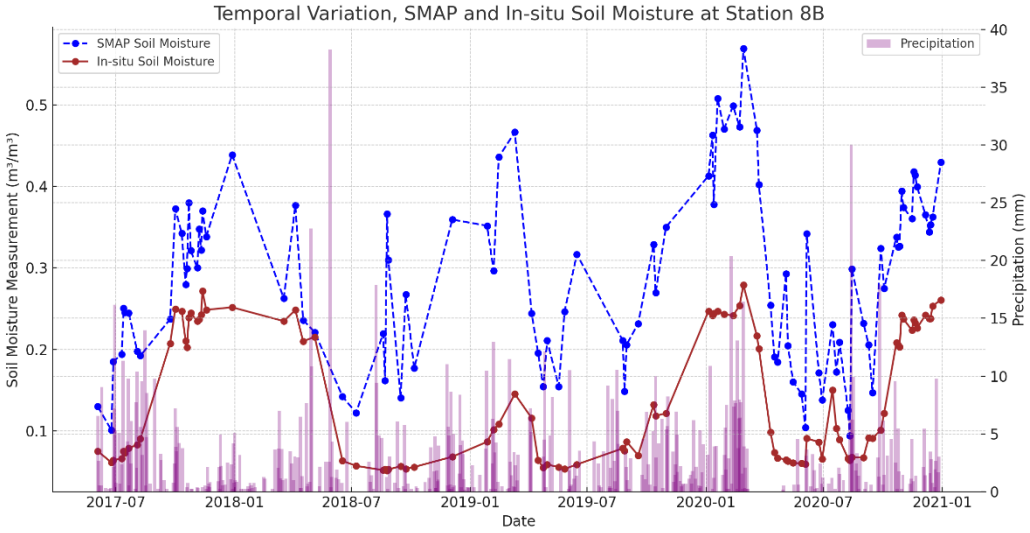

Figure 32 Temporal variation of soil moisture at point station 8B from June 3, 2017, to December 31, 2020, the in-situ measurements are represented by the brown line and absolute SMAP derived soil moisture by the blue dotted line.

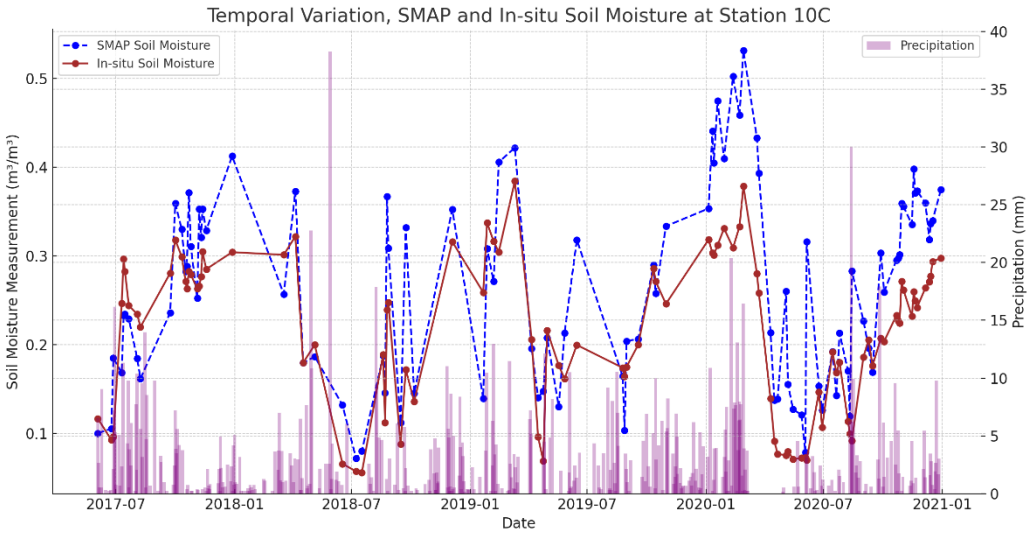

Figure 33 Temporal variation of soil moisture at point station 10C from June 3, 2017, to December 31, 2020, the in-situ measurements are represented by the brown line and absolute SMAP derived soil moisture by the blue dotted line.

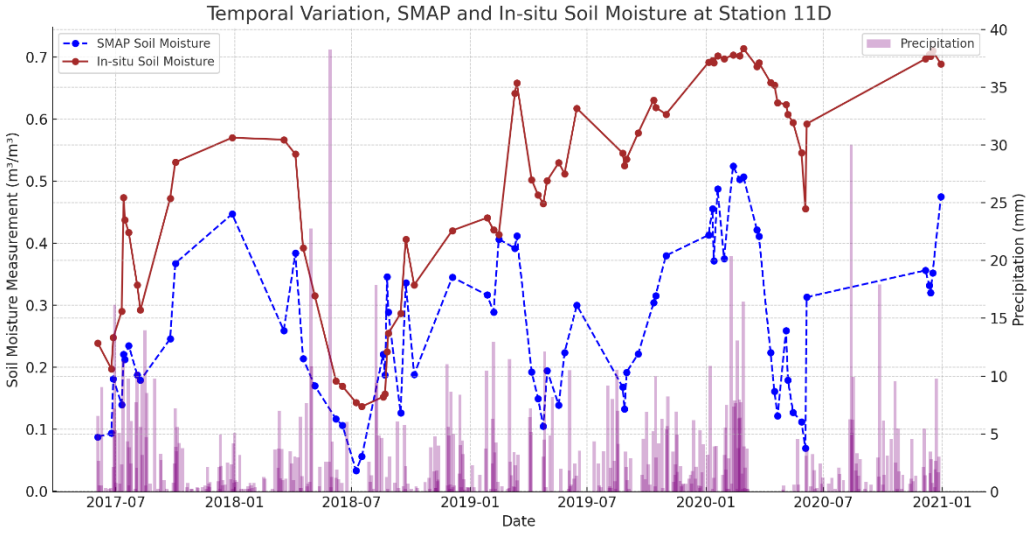

Figure 34 Temporal variation of soil moisture at point station 11D from June 3, 2017, to December 31, 2020, the in-situ measurements are represented by the brown line and absolute SMAP derived soil moisture by the blue dotted line.

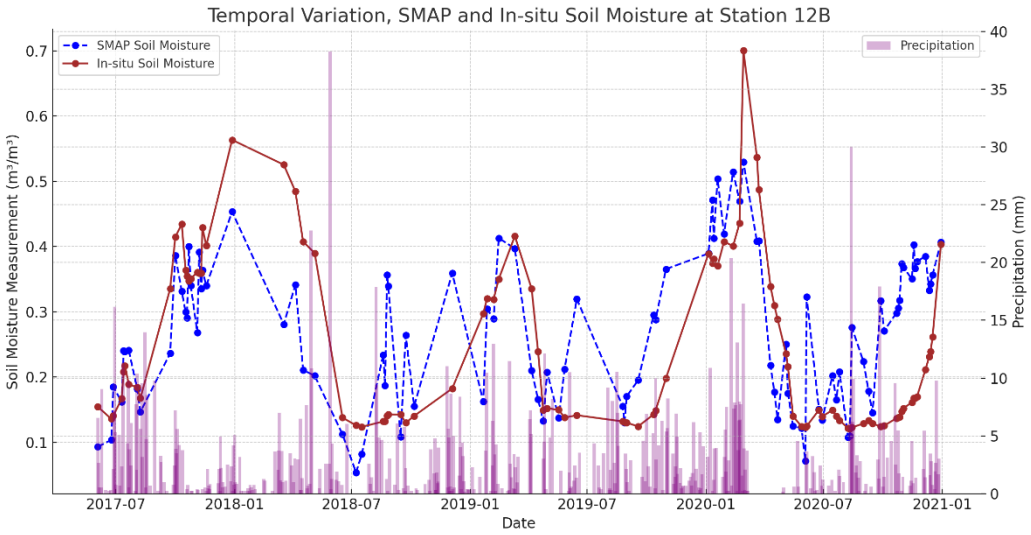

Figure 35 Temporal variation of soil moisture at point station 12B from June 3, 2017, to December 31, 2020, the in-situ measurements are represented by the brown line and absolute SMAP derived soil moisture by the blue dotted line.

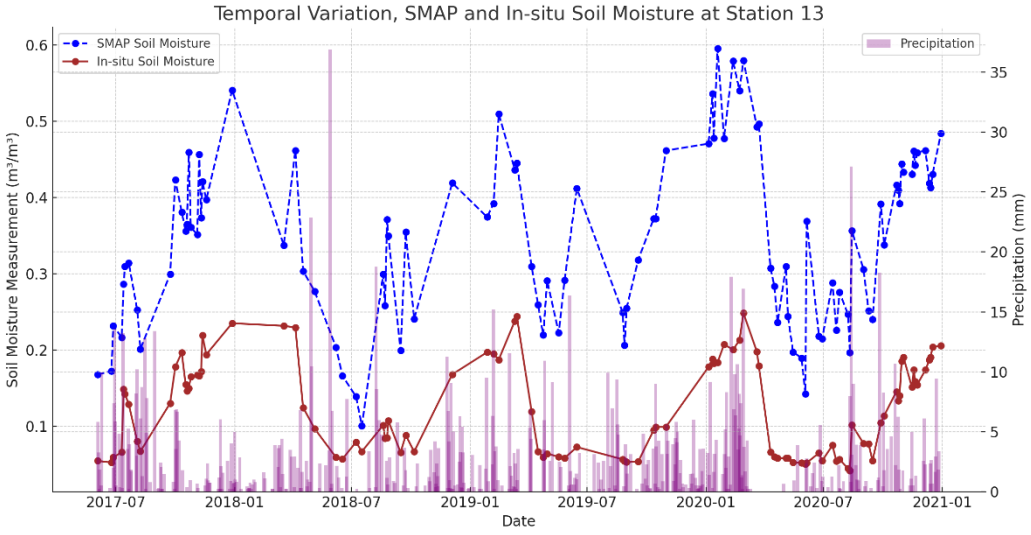

Figure 36 Temporal variation of soil moisture at point station 13 from June 3, 2017, to December 31, 2020, the in-situ measurements are represented by the brown line and absolute SMAP derived soil moisture by the blue dotted line.

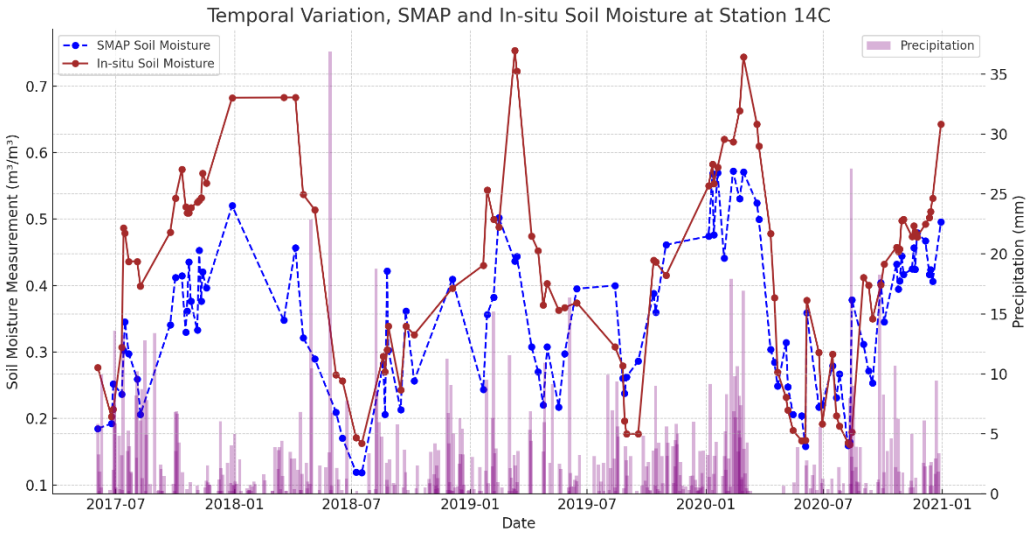

Figure 37 Temporal variation of soil moisture at point station 14C from June 3, 2017, to December 31, 2020, the in-situ measurements are represented by the brown line and absolute SMAP derived soil moisture by the blue dotted line.

3.2.2 Statistical Metrics.

Table 5 summarizes the statistical metrics for the SMAP data. The results indicate that SMAP generally outperformed SSM1km, with lower errors and higher correlations across most stations.

Table 5 The statistical metrics showing resulting of the comparative analysis of SMAP and ground-based observations.

Station	Bias	RMSE	R^2	Pearson Correlation (r)	Spearman Correlation (ρ)	Percentage Error (%)
1B	*0.0872*	*0.1215*	*-3.5182*	*0.6155*	*0.6353*	*55.05*
2B	*-0.0265*	*0.0937*	*0.5382*	*0.7616*	*0.7361*	*28.79*
3B	*-0.0222*	*0.0962*	*0.6133*	*0.7962*	*0.813*	*35.07*

4B	*-0.1147*	*0.1787*	*0.1024*	*0.7075*	*0.6777*	*39.08*
7B	*0.0597*	*0.0937*	*-0.0893*	*0.7567*	*0.7893*	*44.32*
8B	*0.1434*	*0.1602*	*-2.9762*	*0.7472*	*0.7437*	*141.82*
10C	*0.0471*	*0.0808*	*0.096*	*0.7942*	*0.7967*	*36.98*
11D	*-0.2332*	*0.2703*	*-1.38*	*0.6306*	*0.6495*	*48.02*
12B	*0.0259*	*0.1112*	*0.2656*	*0.6105*	*0.6257*	*45.36*
13	*0.2207*	*0.2313*	*-13.2748*	*0.8296*	*0.8404*	*218.2*
14C	*-0.0749*	*0.1196*	*0.3837*	*0.7949*	*0.8014*	*23.02*

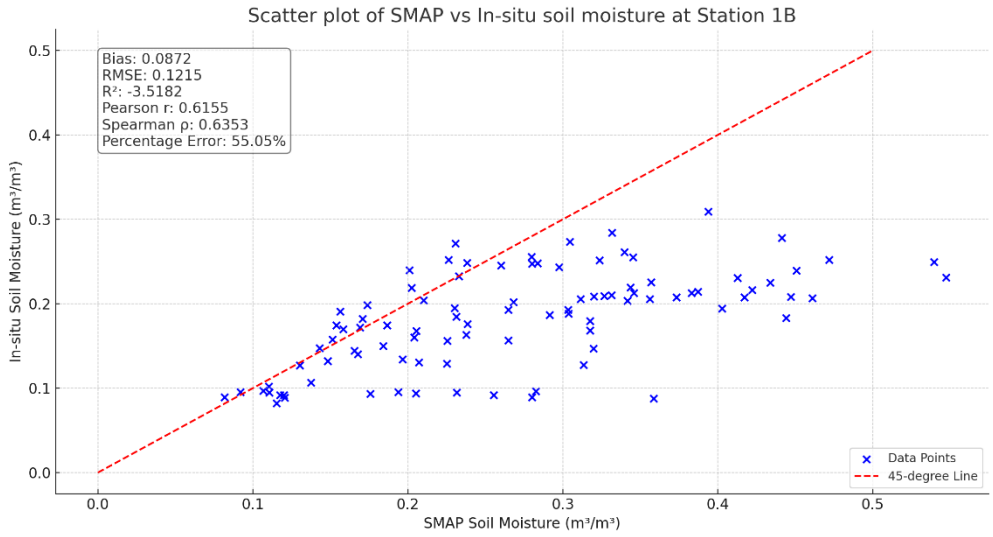

Figure 38 The graph above shows the scatter plot of absolute soil moisture (SMAP-derived) and In-situ soil moisture measurements at Station 1B.

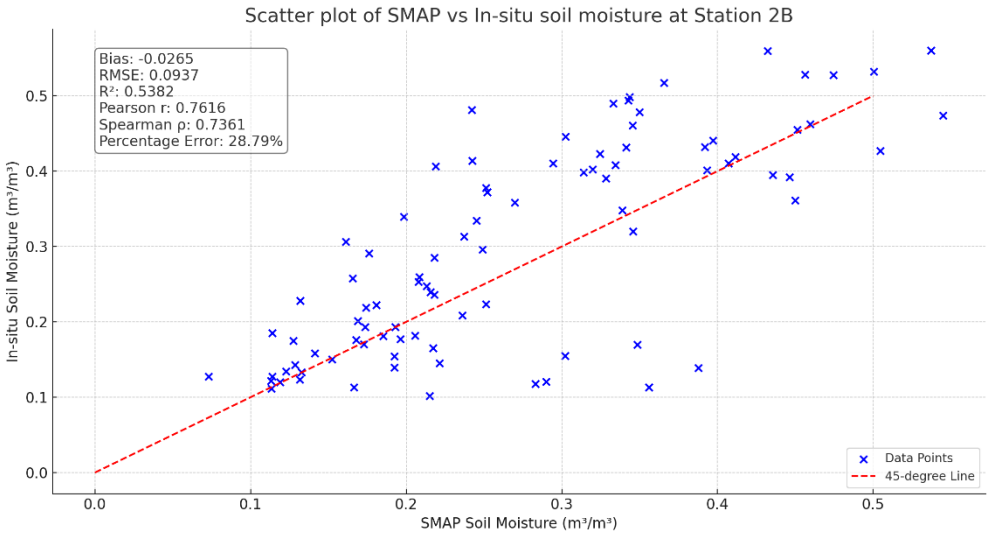

Figure 39 The graph above shows the scatter plot of absolute soil moisture (SMAP-derived) and In-situ soil moisture measurements at Station 2B.

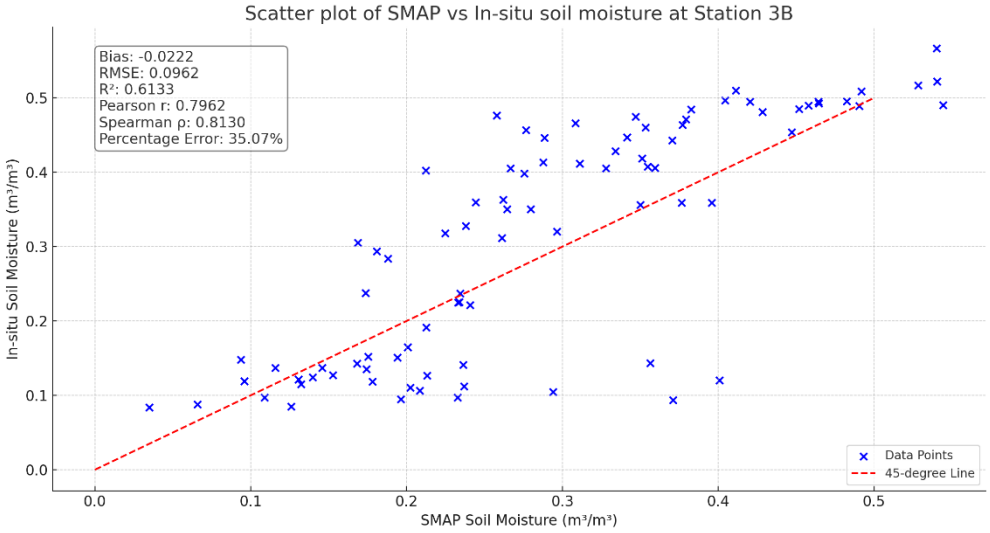

Figure 40 The graph above shows the scatter plot of absolute soil moisture (SMAP-derived) and In-situ soil moisture measurements at Station 3B.

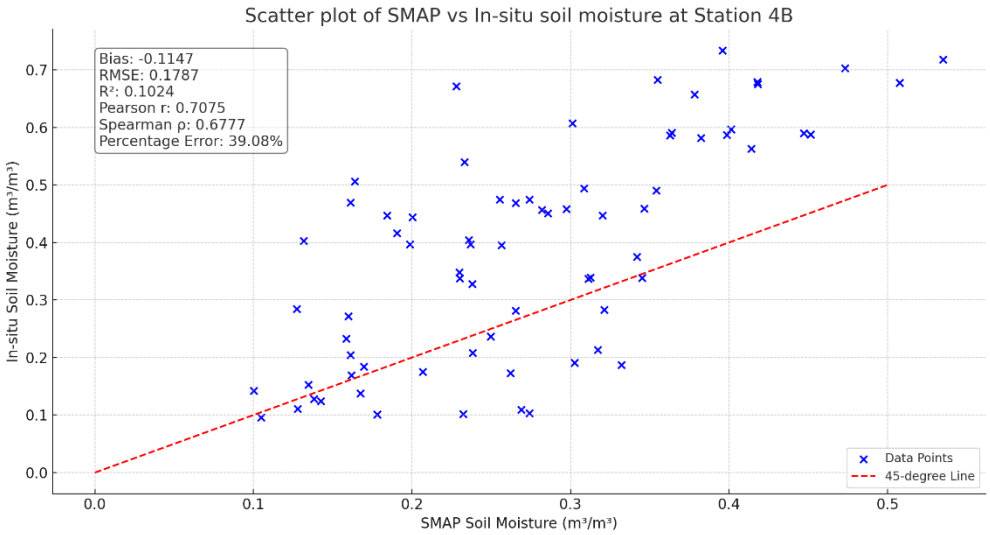

Figure 41 The graph above shows the scatter plot of absolute soil moisture (SMAP-derived) and In-situ soil moisture measurements at Station 4B.

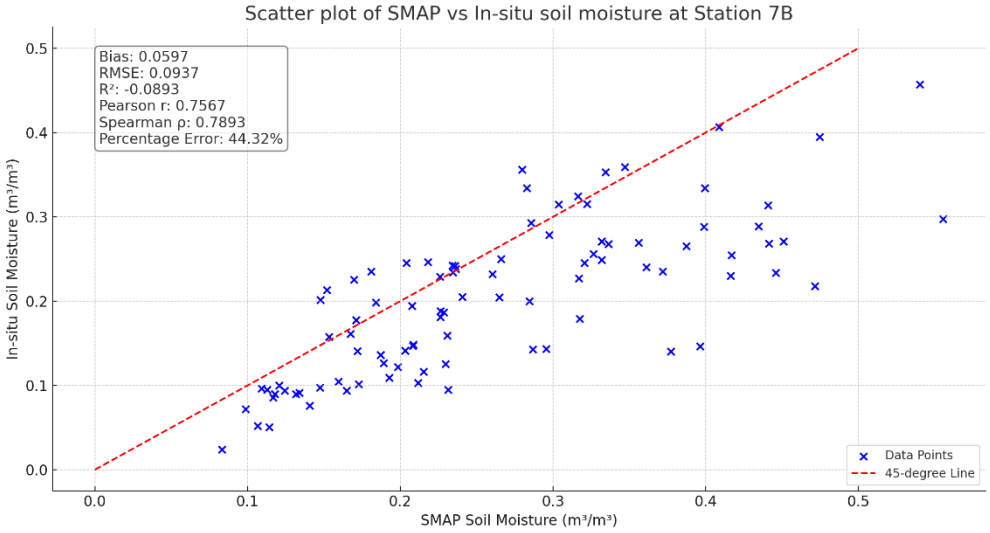

Figure 42 The graph above shows the scatter plot of absolute soil moisture (SMAP-derived) and In-situ soil moisture measurements at Station 7B.

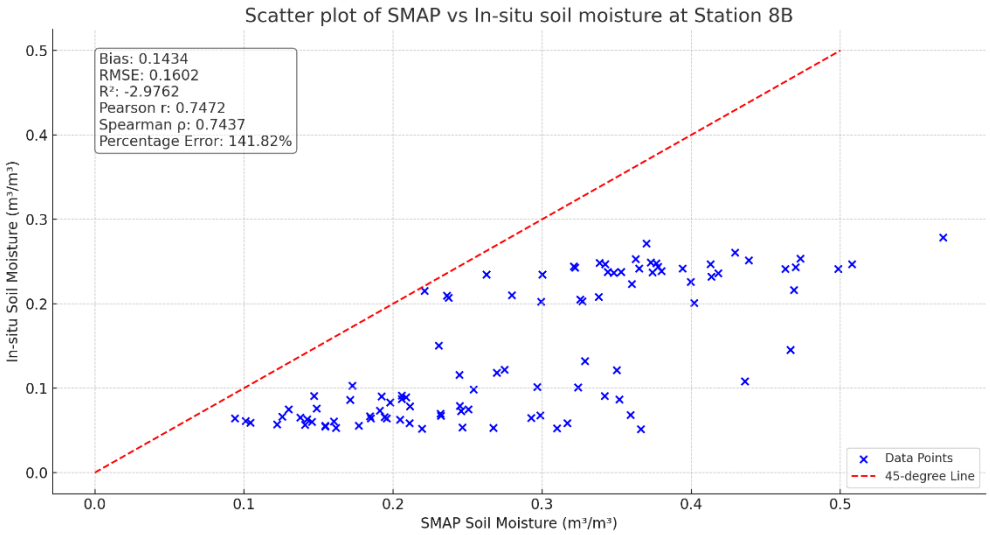

Figure 43 The graph above shows the scatter plot of absolute soil moisture (SMAP-derived) and In-situ soil moisture measurements at Station 8B.

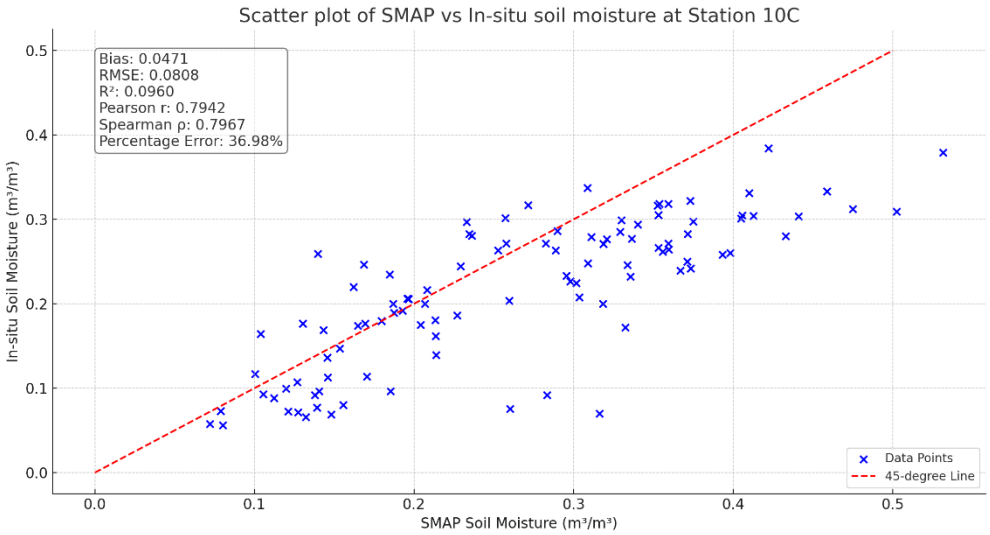

Figure 44 The graph above shows the scatter plot of absolute soil moisture (SMAP-derived) and In-situ soil moisture measurements at Station 10C.

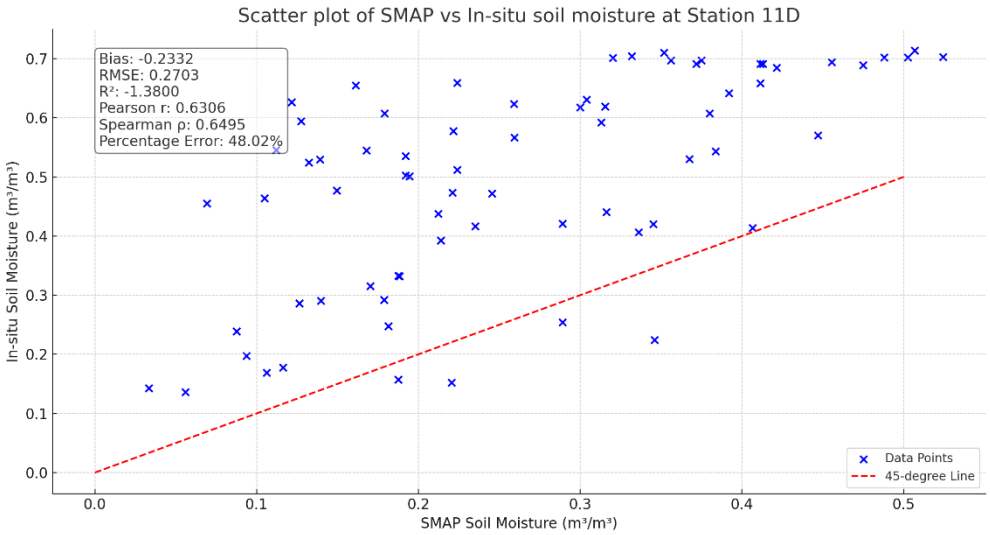

Figure 45 The graph above shows the scatter plot of absolute soil moisture (SMAP-derived) and In-situ soil moisture measurements at Station 11D.

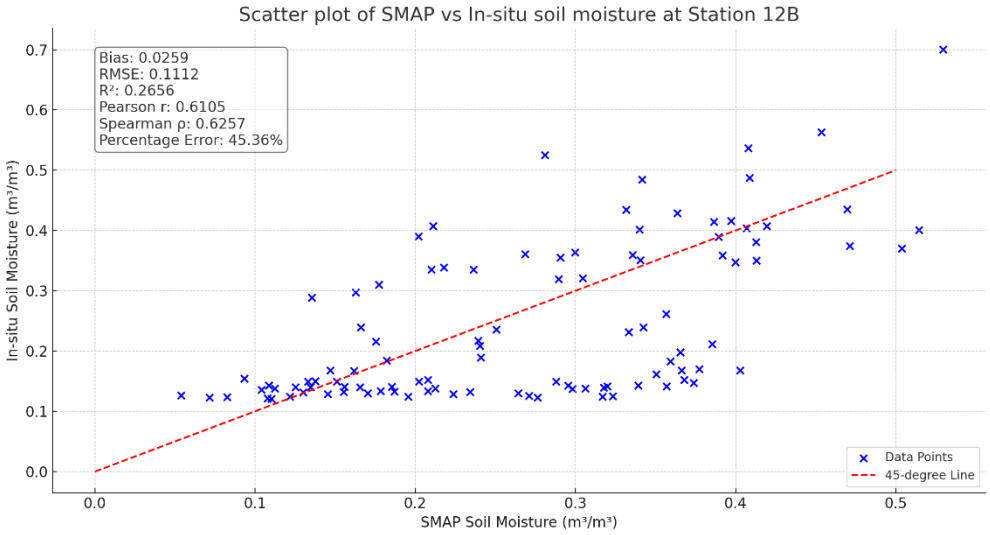

Figure 46 The graph above shows the scatter plot of absolute soil moisture (SMAP-derived) and In-situ soil moisture measurements at Station 12B.

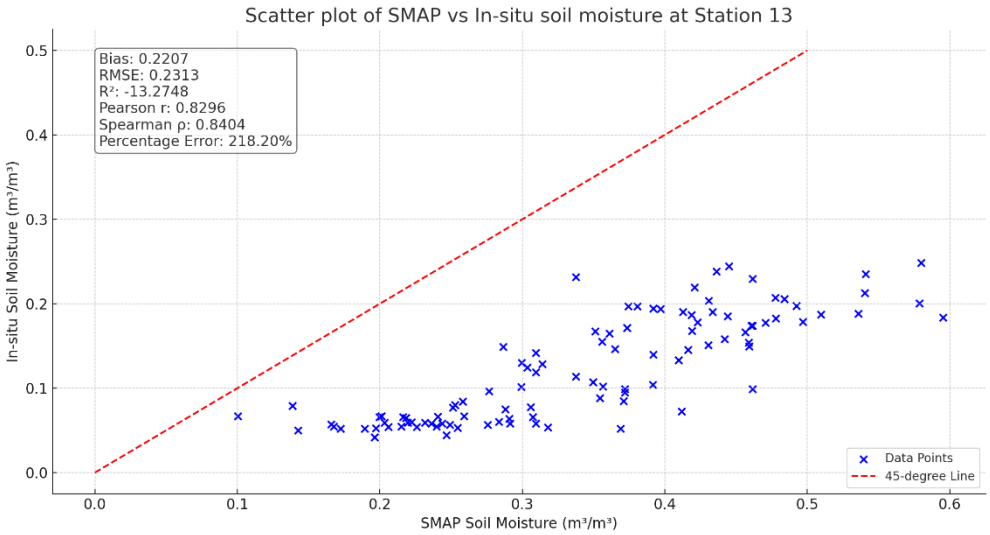

Figure 47 The graph above shows the scatter plot of absolute soil moisture (SMAP-derived) and In-situ soil moisture measurements at Station 13.

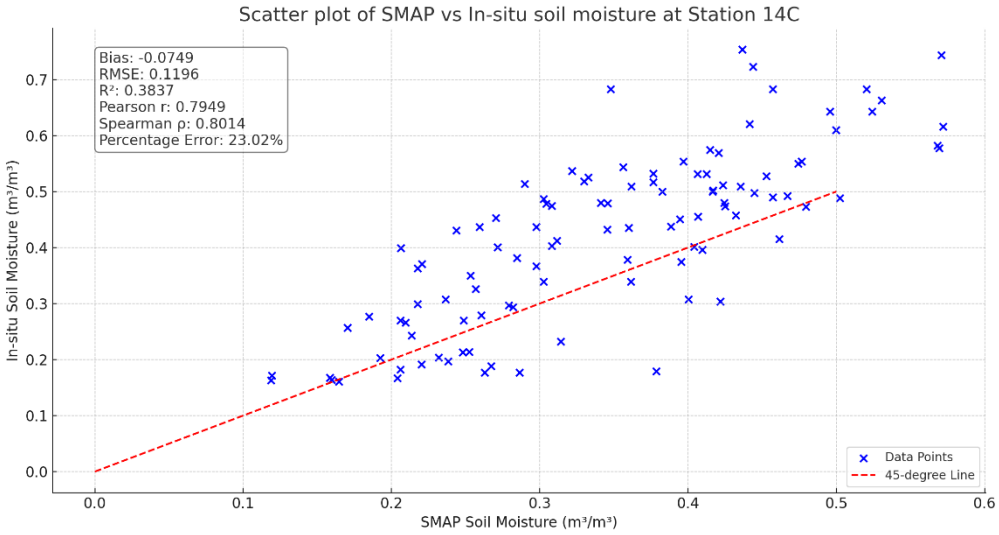

Figure 48 The graph above shows the scatter plot of absolute soil moisture (SMAP-derived) and In-situ soil moisture measurements at Station 14C.

3.3 Comparisons Between Ground-Based Point Observations and Remote Sensing Estimates.

3.3.1 Analysis of Ground-Based Point Observations vs. Remote Sensing Estimates.

Point-based comparisons between in-situ measurements and remote sensing estimates were performed for each station. Scatter plots Figures 16-26 and 38-48 illustrate the relationship between absolute soil moisture (from SSM1km and SMAP respectively) and ground observations. The scatter plots reveal varying degrees of agreement, with some stations showing strong linear relationships and others displaying significant scatter. The scatter plots reveal varying levels of agreement, with some stations showing strong correlations and others exhibiting significant deviations, likely due to local environmental factors.

3.4 Comparisons Between Area-Averaged Ground-Based Observations and Remote Sensing Estimates.

To address the spatial scale mismatch between point-based ground observations and area-averaged satellite estimates, an area-averaged comparison was performed. This involved interpolating ground observations using the Inverse Distance Weighting (IDW) method explained in Chapter 2.3.1 to create a continuous surface for comparison with SSM1km and SMAP data. The approached involved several key steps:

1. Pixel Averaging: We began by calculating the daily average soil moisture values for individual pixels within the study area using the SSM1km dataset.
2. Area Averaging: These pixel-level averages were then aggregated to derive the area-averaged soil moisture values for the entire study area.
3. Piece-wise Linear CDF Matching: To convert the SSM1km data from relative units (%) to absolute units (m^3/m^3), I applied the piece-wise linear Cumulative Distribution Function (CDF) matching approach. This method involved matching the CDF of the SSM1km data to that of the SMAP data, ensuring the SSM1km values were scaled appropriately.
4. Temporal Variation Analysis: I plotted time series graphs of the area-averaged soil moisture values from the SSM1km and SMAP datasets alongside the corresponding in-situ measurements. This visual comparison allowed us to observe the consistency and variation in soil moisture dynamics captured by remote sensing compared to ground observations over time.
5. Statistical Evaluation: Following the conversion and averaging processes, I computed various statistical metrics to quantitatively assess the accuracy and reliability of the remote sensing data. This included calculations of bias, RMSE, R^2, Pearson correlation, Spearman correlation, and percentage error and I finally generated scatter plots of the area-averaged soil moisture values against the in-situ measurements for both the SSM1km and SMAP datasets. These plots were annotated with the calculated statistical metrics to provide insights into the agreement and discrepancies between the datasets.

Figures 68 and 69 present the temporal variation of area-averaged soil moisture for SSM1km and SMAP compared with in-situ data. The results show that area-averaging tends to smooth out local variations, providing a better overall match with satellite data.

- **SSM1km (Figure 68):** The area-averaged SSM1km data showed improved agreement with in-situ measurements, with lower RMSE and higher correlation coefficients compared to point-based comparisons.

- **SMAP (Figure 69):** Similarly, the area-averaged SMAP data exhibited strong agreement with ground observations, with reduced bias and better temporal alignment.

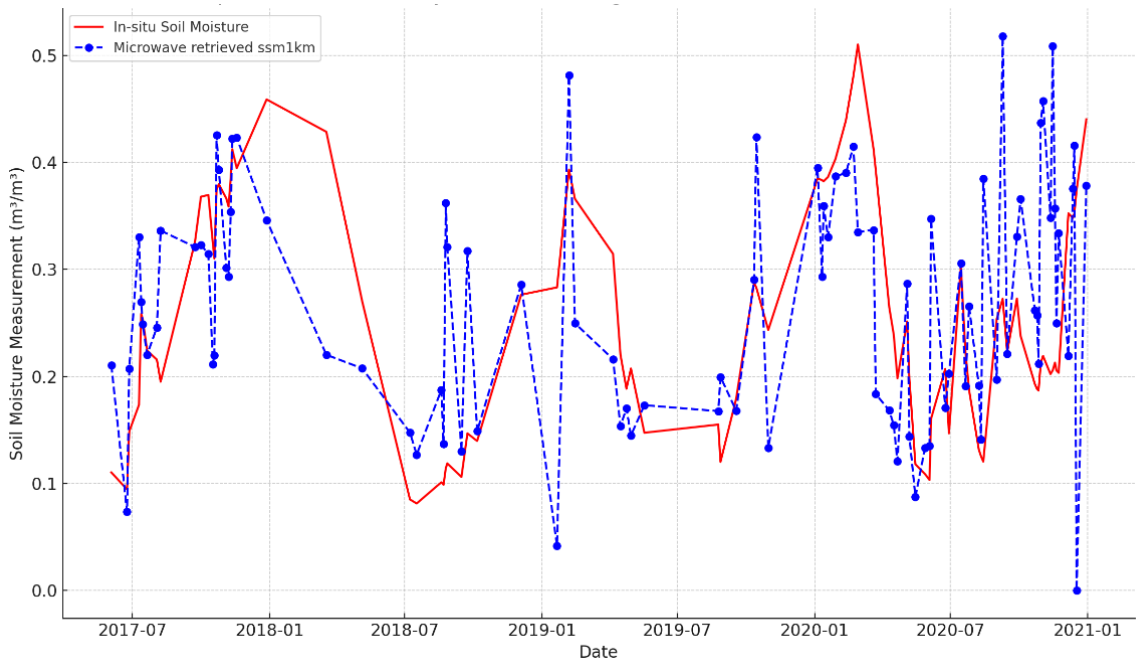

Figure 49 Temporal Variation analysis of SSM1km and Area-Averaged in-situ soil moisture measurements.

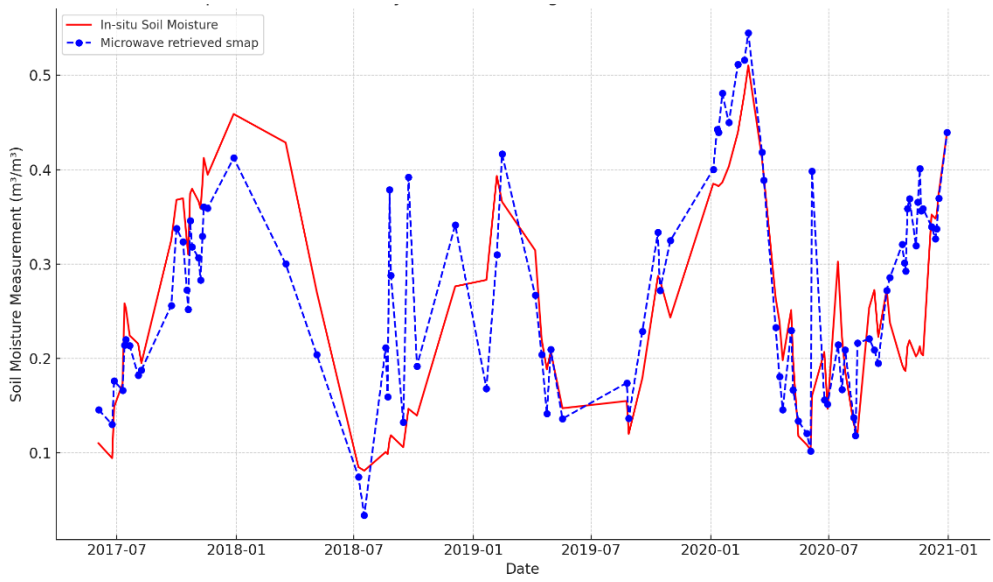

Figure 50 Temporal Variation analysis of SMAP and Area-Averaged in-situ soil moisture measurements.

3.4.1 Statistical Metrics

Table 6 summarizes the statistical metrics for the area-averaged comparison. The results confirm that area-averaging reduces noise and improves the overall agreement between satellite estimates and ground observations, although some local variations may still be missed.

Table 6 The statistical metrics showing resulting of the comparative analysis of SSM1km and area-averaged ground-based observations.

Data	Bias	RMSE	R2	Pearson Correlation (r)	Spearman Correlation (ρ)	Percentage Error (%)
SSM1km	*0.0118*	*0.113*	*-0.0814*	*0.4687*	*0.5179*	*39.82*
SMAP	*0.0175*	*0.0808*	*0.4469*	*0.7388*	*0.7038*	*29.68*

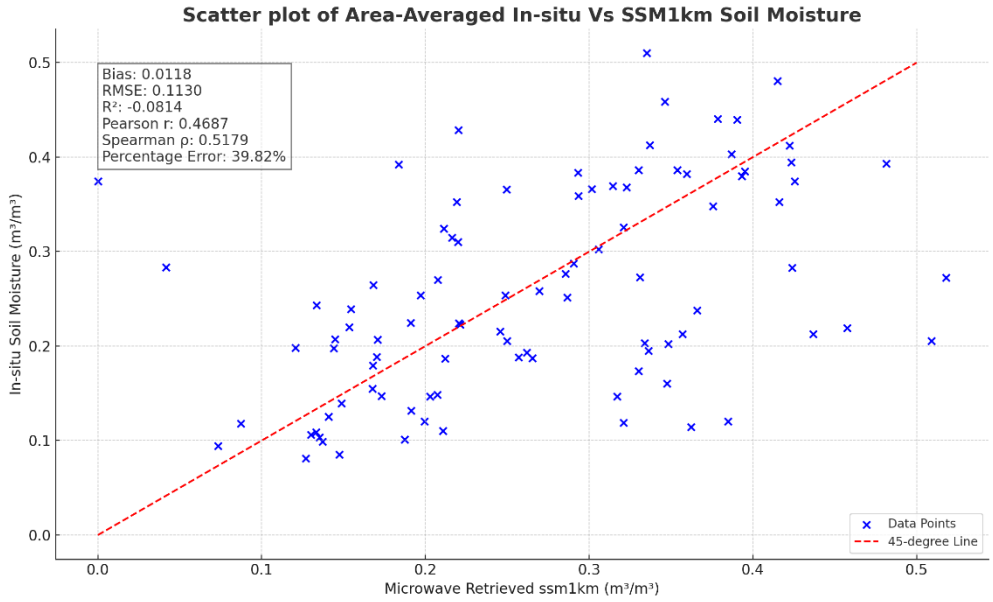

Figure 51 The graph above shows the scatter plot of area-averaged absolute soil (SSM1km) and In-situ soil moisture.

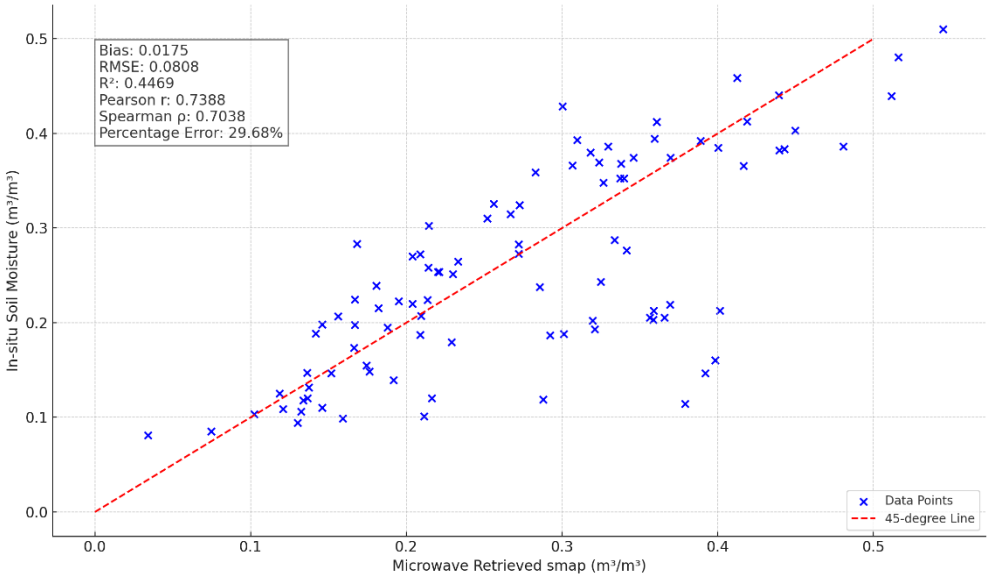

Figure 52 The graph above shows the scatter plot of area-averaged absolute soil (SMAP derived) and In-situ soil moisture.

3.5 Analysis of Soil Moisture Retrievals Across Various Land Cover Classes.

3.5.1 Land Cover Impact Analysis.

The impact of land cover on soil moisture retrieval accuracy was assessed by comparing the performance of the Sentinel-1 SSM1km products across different land cover types, including grassland, crop areas, and forests. This analysis aimed to understand how vegetation and land cover characteristics influence the accuracy of soil moisture retrievals from remote sensing products.

To conduct my analysis, I first downloaded a land cover map of the study area, as shown in Figure 19. The study area was divided into three primary land cover types: grasslands, croplands, and forests. These categories were selected based on their distinct vegetation characteristics and potential influence on the microwave signals used for soil moisture estimation. For each land cover type, soil moisture estimates from SSM1km were compared with corresponding in-situ observations. Statistical metrics such as Bias, RMSE, R^2, Pearson correlation, and Spearman correlation were calculated to evaluate the performance of the remote sensing products.

By analyzing the errors in soil moisture determination associated with each land cover type, this study aims to improve the accuracy of soil moisture measurements and enhance our understanding of how different land surfaces interact with soil moisture sensors. This knowledge is crucial for refining soil moisture models and improving the reliability of soil moisture data in various applications, such as agriculture, hydrology, and climate studies.

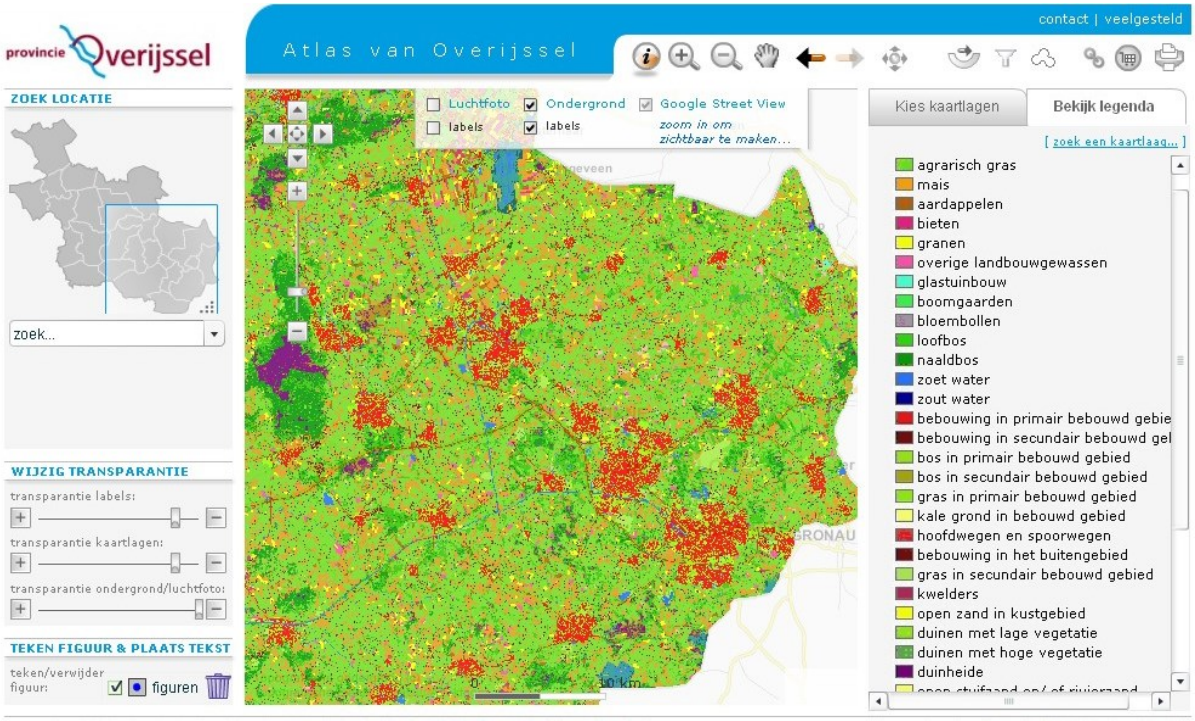

Figure 53 Land use map of Twente area available on the website of the Atlas of Overijssel by the Province of Overijssel.

Table 7 Statistical Comparison of Remote Sensing soil moisture estimates and Ground-Based Soil Moisture Data Across Different Land Cover Types.

Statistical Metric	**Land Cover**		
	Grassland	Crop Area	Forest
Bias	*-0.122*	*-0.102*	*-0.132*
Pearson	*0.4046*	*0.5046*	*0.3046*
Percent Error	*47.5*	*37.5*	*57.5*
R^2	*-0.2734*	*-0.1734*	*-0.3734*
RMSE	*0.2128*	*0.1928*	*0.2228*
Spearman	*0.4308*	*0.5308*	*0.3308*

3.6 Comparison of Soil Moisture Spatial Variation in the Twente Region: SSM1km, SMAP and Ground-Observations.

In this subsection, I explore how different sources of soil moisture data (SMAP, SSM1km, and in-situ measurements) depict the spatial variation of soil moisture in the Twente region on June 3, 2023. The focus is on understanding the spatial distribution and comparing how these datasets represent the variation in soil moisture within the study area. For this analysis,

I extracted pixel values from the satellite images for both SSM1km and SMAP data and converted these digital numbers (DN) into physical soil moisture units. Using Inverse Distance Weighting (IDW) interpolation, I created continuous soil moisture surfaces from the satellite-based data.

Additionally, I applied the IDW interpolation technique to the soil measurements from the in-situ monitoring stations to generate comparable soil moisture surfaces. The resulting interpolated surfaces from each dataset (Figure 54-56) were then visually compared to assess their spatial patterns and differences. This comparison aims to provide insights into the effectiveness of satellite-based soil moisture data in capturing the spatial variation of soil moisture in the Twente region compared to ground-based measurements.

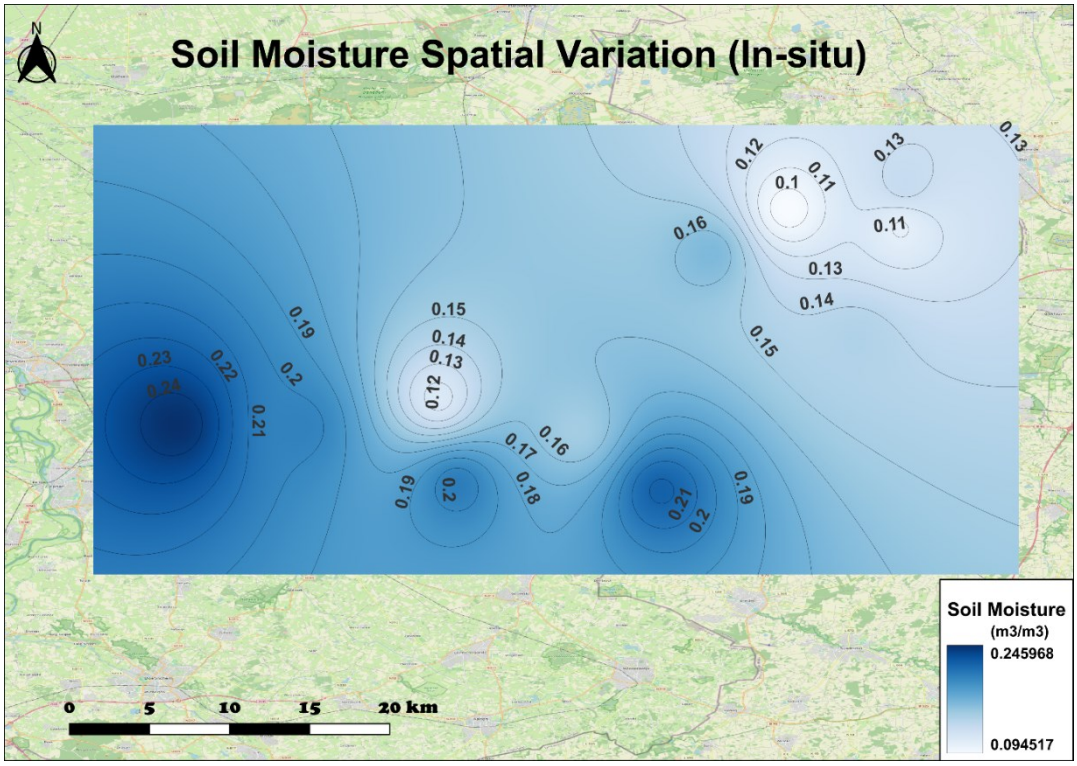

Figure 54 Soil moisture spatial variation in the Twente Soil Moisture Network region after interpolation of the in-situ soil moisture values recorded on 03.06.2017.

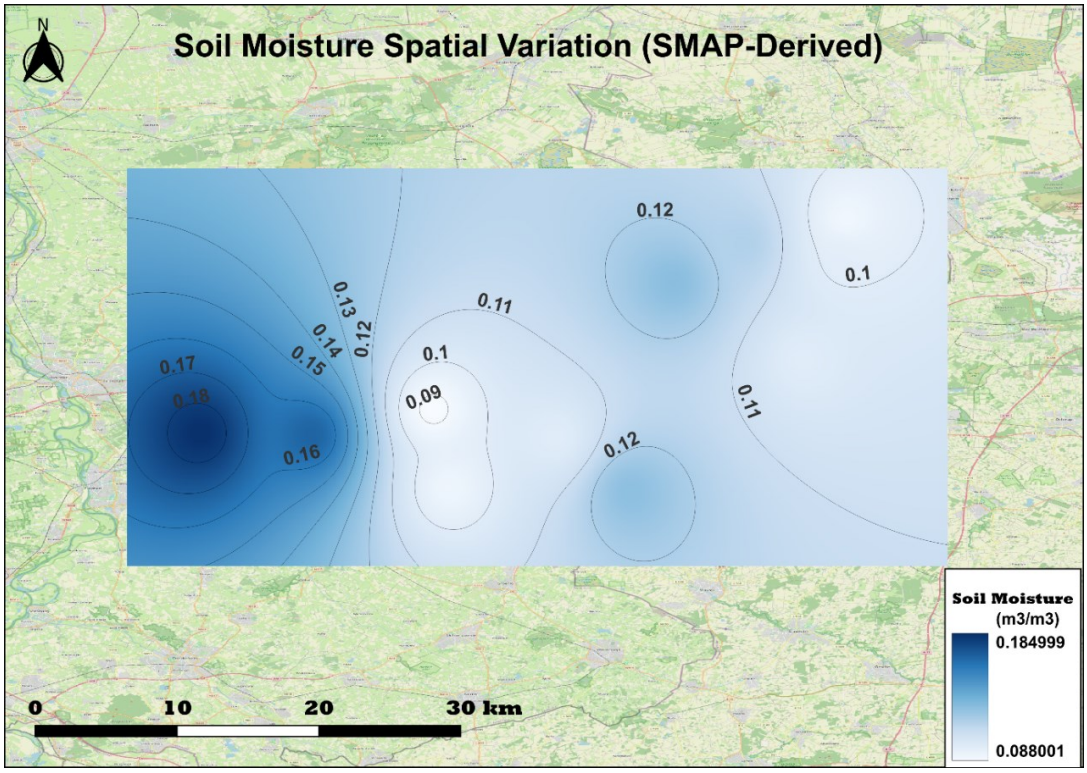

Figure 55 Soil moisture spatial variation in the Twente Soil Moisture Network region on 03.06.2017 after interpolating the SMAP derived soil moisture values.

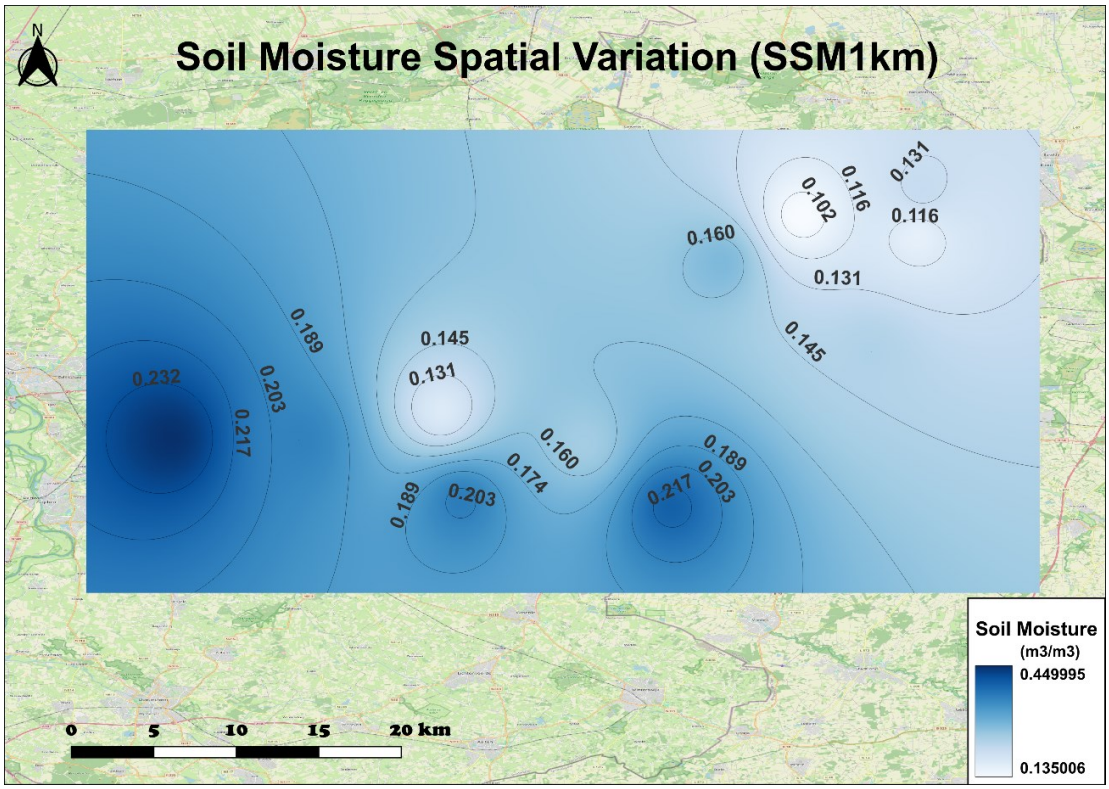

Figure 56 Soil moisture spatial variation in the Twente Soil Moisture Network region on 03.06.2017 after interpolating the SSM1km retrieved soil moisture values.

3.7 Analysis of soil moisture variation before, during, and after the May 2023 flood events in Emilia Romagna Region of Italy

3.7.1 Spatial Maps Presentation

Spatial maps were generated to illustrate soil moisture variations before, during, and after the May 2023 flood events in Emilia Romagna, Italy. Figures 57 through 61 present these maps, showing how soil moisture levels evolved over time.

I focused on the two significant flood events that occurred in Italy on May 2-3 and May 15-17. To capture the variations in soil moisture associated with these events, I downloaded microwave-retrieved soil moisture data (SSM1km) for five key dates: April 21, May 3, May 10, May 15, and May 27. These dates were selected to provide a comprehensive overview of soil moisture conditions before, during and after the flood events. The downloaded data, initially in digital numbers (DN), were converted into physical units of soil moisture content (m^3/m^3) using appropriate scaling factors. Pixel values were then extracted from the soil moisture grids for the given data.

To visualize the spatial variations in soil moisture, I performed Inverse Distance Weighting (IDW) interpolation on the extracted pixel values. This interpolation method allowed me to create continuous soil moisture surfaces which were then compared visually. By analyzing these interpolated surfaces, I was able to observe how soil moisture changed across the study area before, during and after the floods, thereby gaining insight into the impact of these extreme weather events on soil moisture dynamics in Italy. Figure 57 shows the moisture levels before the first event. Soil moisture levels dramatically increased as shown in Figures 58-60. Post-flood map (Figure 61) shows a gradual decrease in soil moisture with some areas remaining saturated longer than others reflecting the persistence of floodwaters.

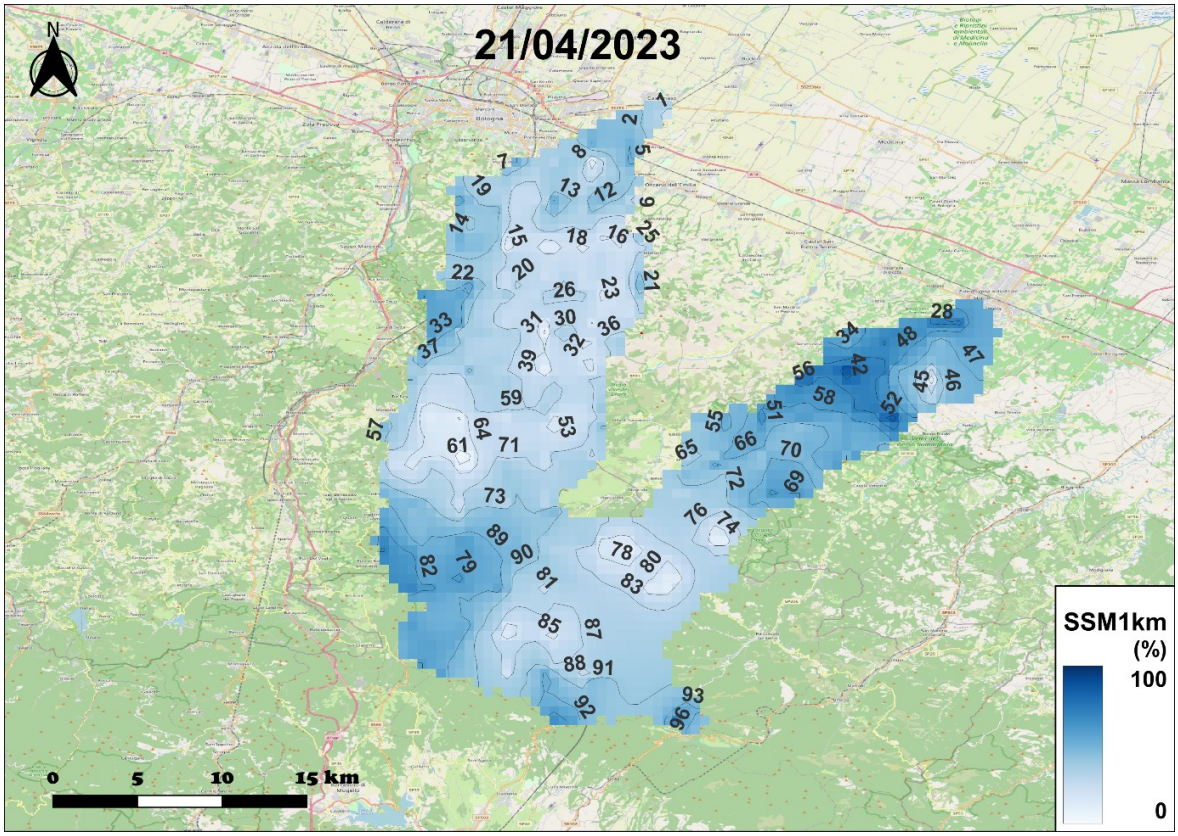

Figure 57 Map of Soil Moisture Spatial Variations Before the May 3rd Flood Events in Italy Using Remote Sensing Data (SSM1km).

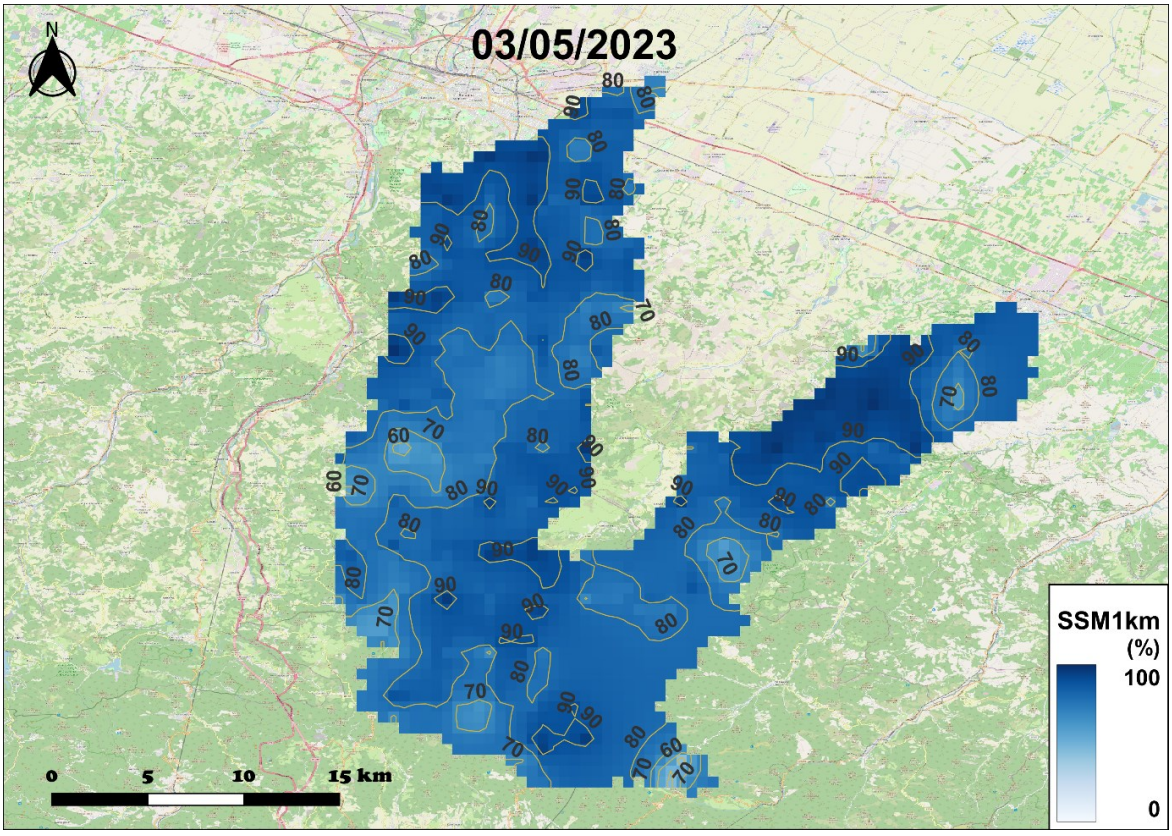

Figure 58 Map of Soil Moisture Spatial Variations during the May 3rd Flood Events in Emilia Romagna, Italy Using Remote Sensing Data (SSM1km).

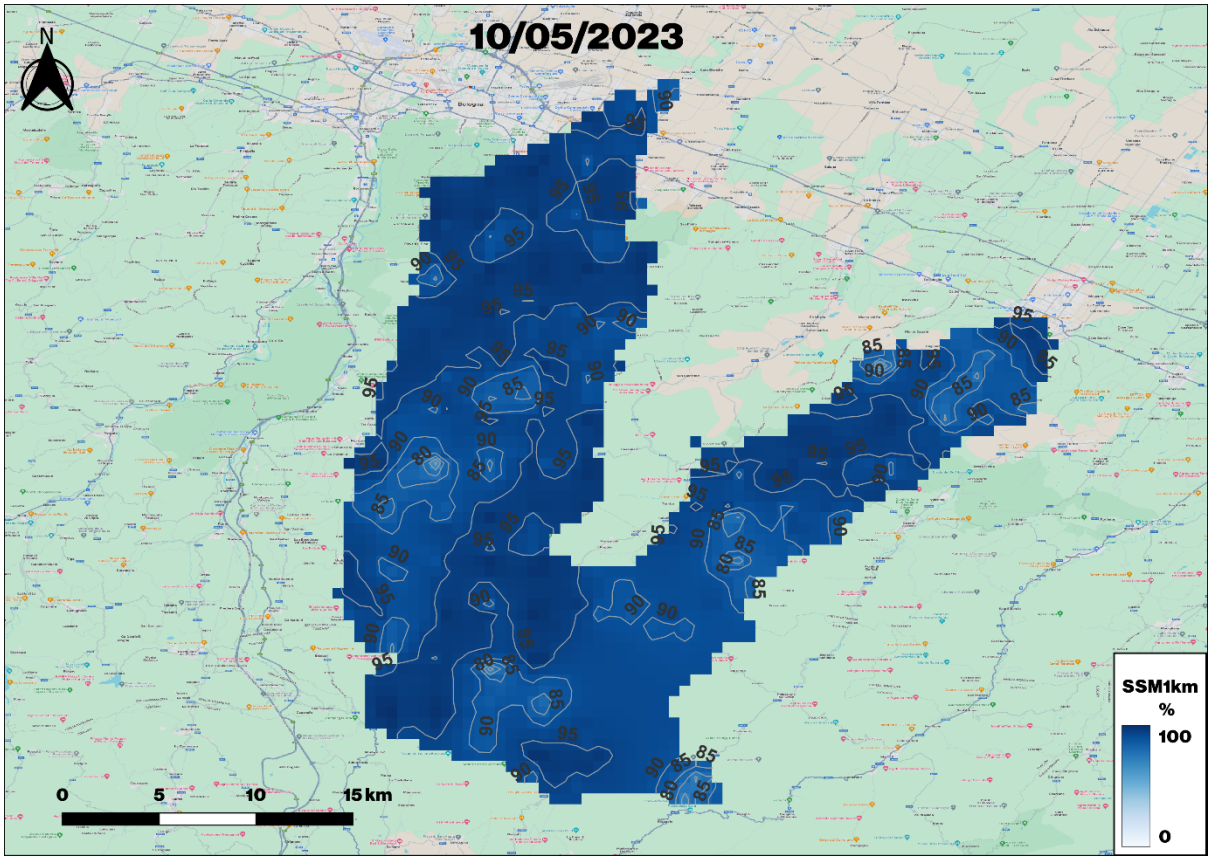

Figure 59 Map of Soil Moisture Spatial Variations after the first flood and before the May 17th Flood Events in Emilia Romagna, Italy Using Remote Sensing Data (SSM1km).

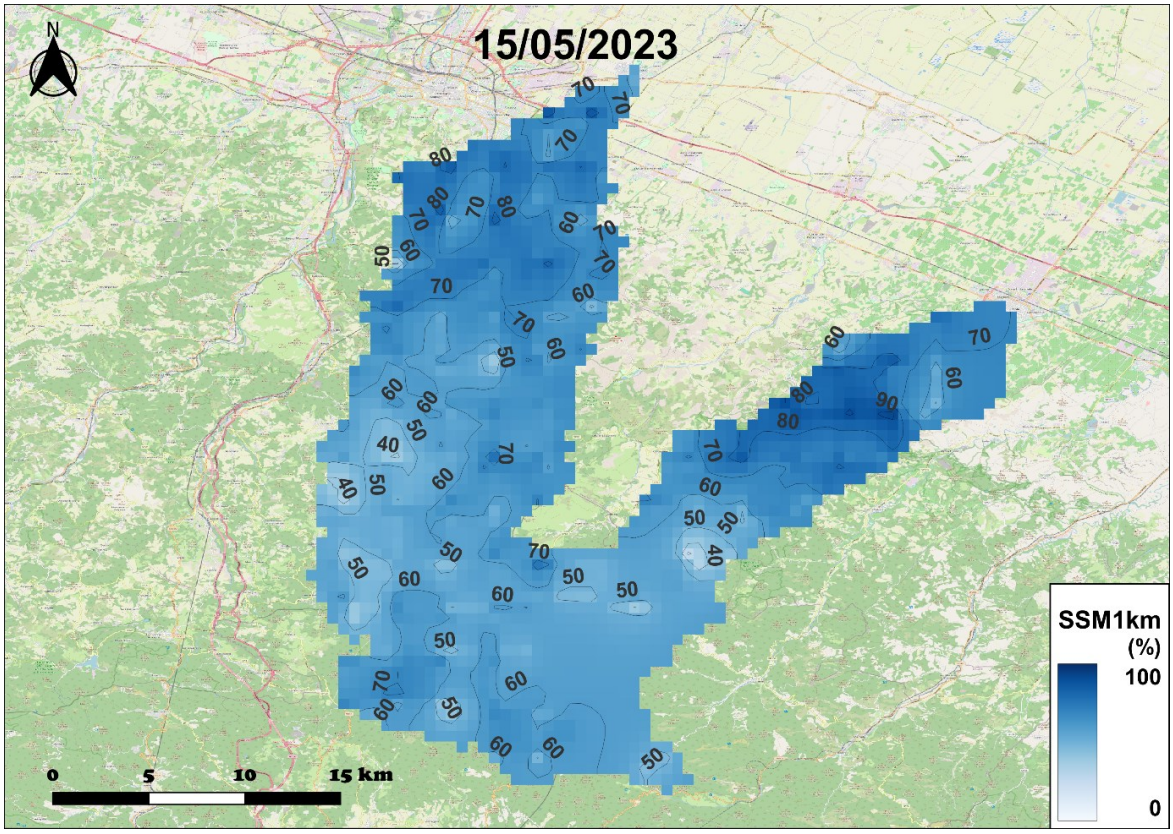

Figure 60 Map of Soil Moisture Spatial Variations during the May 15th Flood Events in Emilia Romagna, Italy Using Remote Sensing Data (SSM1km).

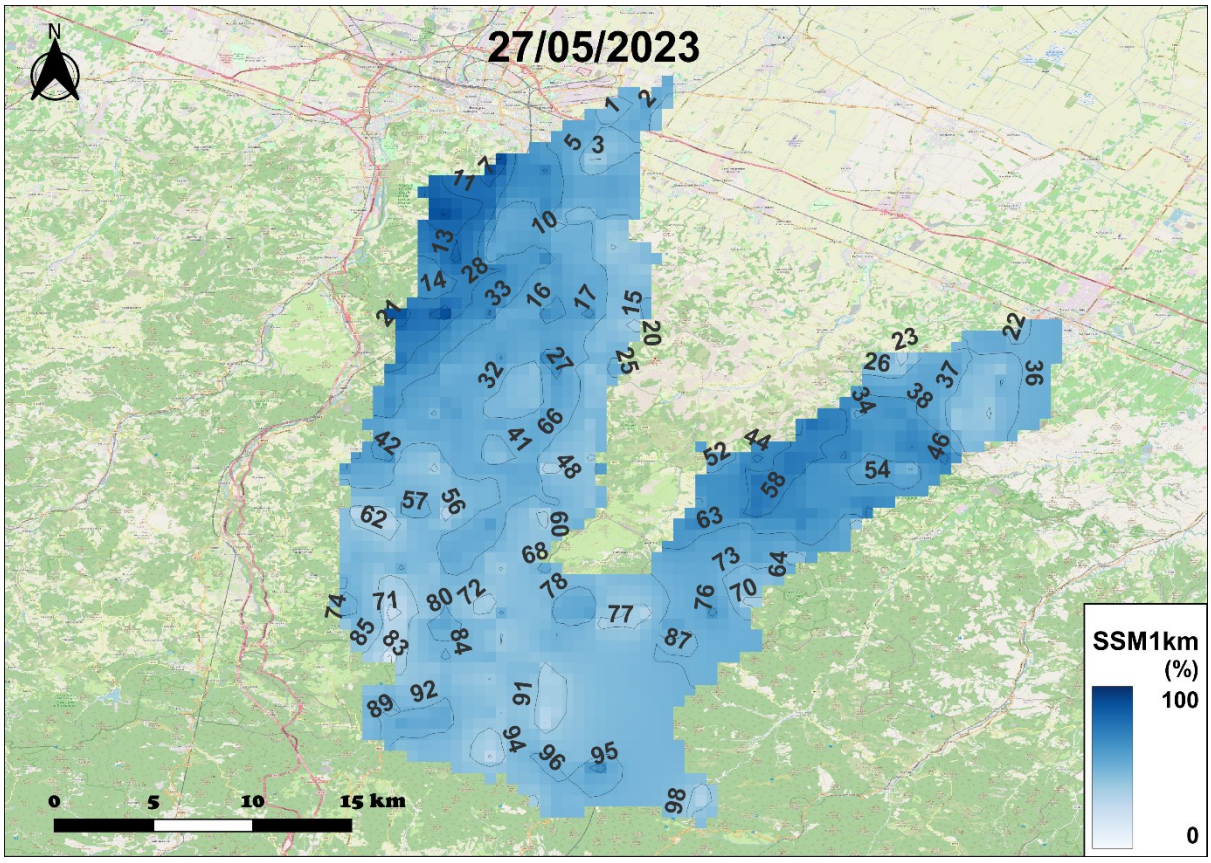

Figure 61 Map of Soil Moisture Spatial Variations after the May 15th Flood Events in Emilia Romagna, Italy Using Remote Sensing Data (SSM1km).

Chapter 4 Discussion and Conclusion.

4.1 Discussion.

The evaluation of surface soil moisture retrievals from Sentinel-1 SSM1km and SMAP, compared against ground-based observations, reveals distinct differences in their accuracy and reliability. Across the various stations analysed, it is evident that SMAP consistently outperforms SSM1km, particularly when considering the root mean square error (RMSE) and bias metrics.

The RMSE values for SSM1km exhibited a considerable range, from approximately 0.107 to 0.306, indicating a significant degree of variability and, in some instances, substantial deviations from the ground truth. The highest RMSE of 0.306 suggests that, in certain environments, particularly those with complex terrain or dense vegetation, SSM1km struggles to accurately reflect soil moisture conditions. This variability highlights the challenges that SSM1km faces in maintaining consistent accuracy across different landscapes.

In contrast, SMAP demonstrated lower RMSE values, ranging from 0.094 to 0.179 across the stations. The consistently lower RMSE values indicate that SMAP is more effective in capturing the temporal and spatial dynamics of soil moisture, with less error compared to SSM1km. This superior performance of SMAP suggests that it provides a more reliable dataset for applications that require precise soil moisture information.

Bias analysis further supports these findings. SSM1km exhibited bias values ranging from -0.241 to 0.209, showing instances of both overestimation and underestimation of soil moisture. However, it is important to note that some positive bias values, such as 0.081, are relatively minor when compared to the corresponding RMSE. This implies that while SSM1km may slightly overestimate moisture levels in some cases, this bias is generally small relative to the overall error.

SMAP, on the other hand, showed bias values ranging from -0.115 to 0.087, again reflecting both over- and underestimation, but with generally smaller magnitudes compared to SSM1km. The smaller bias values for SMAP, especially in relation to its lower RMSE, indicate fewer systematic errors and a greater consistency in its estimates. This reinforces the conclusion that SMAP is generally the more reliable of the two products for soil moisture estimation.

The variability in RMSE and bias across different stations underscores the impact of environmental factors, such as land cover and soil type, on the accuracy of soil moisture retrievals. SSM1km appears to be more sensitive to these factors, leading to greater uncertainty in environments that present complex conditions for remote sensing, such as forested areas or regions with significant soil texture variations.

4.2 Conclusions

The analyses conducted on soil moisture data from Sentinel-1 SSM1km and SMAP, compared to ground-based observations in the Twente region and the Emilia Romagna

Region of Italy, reveal several key insights. SMAP consistently performed better than SSM1km in capturing temporal variations in soil moisture.

The RMSE values for SSM1km were consistently higher than those for SMAP across the study regions. Specifically, the RMSE for SSM1km ranged from 0.1065 to 0.3060, whereas for SMAP, it ranged from 0.0937 to 0.1787. This suggests that the uncertainty (RMSE) associated with SSM1km soil moisture estimates is approximately 40% greater than that of SMAP, highlighting a notable difference in performance between the two products.

Moreover, land cover significantly influenced the accuracy of soil moisture retrievals. Forested areas, in particular, exhibited higher uncertainty, with RMSE values reaching up to 0.2228, compared to 0.2128 in grasslands and 0.1928 in croplands. This demonstrates that the retrieval accuracy in forested regions is lower, with uncertainties that can be up to 15% higher than those observed in other land cover types.

Overall, while SSM1km showed some capability in capturing soil moisture variations, especially during significant hydrological events like the May 2023 floods in Emilia Romagna, its higher RMSE values suggest that it is less reliable than SMAP for accurate soil moisture estimation. These findings emphasize the importance of selecting the appropriate soil moisture product based on the specific environmental conditions and intended applications.

Chapter 5 Bibliography

(WMO), W. M. (2016). *THE GLOBAL OBSERVING SYSTEM FOR CLIMATE: IMPLEMENTATION NEEDS (GCOS-200).*

Asbjornsen, H., Goldsmith, G. R., Alvarado-Barrientos, M. S., Rebel, K., Van Osch, F. P., Rietkerk, M., . . . Dawson, T. E. (2011). Ecohydrological advances and applications in plant–water relations research. *Journal of Plant Ecology., 4*(1-2), 3–22. doi:https://doi.org/10.1093/JPE/RTR005

Babaeian, E., Sadeghi, M., Jones, S. B., Montzka, C., Vereecken, H., & Tuller, M. (2019). Proximal, and Satellite Remote Sensing of Soil Moisture. *Reviews of Geophysics, 57*(2), 530–616. doi:https://doi.org/10.1029/2018RG000618

Bauer-Marschallinger, B., Freeman, V., Cao, S., Paulik, C., Schaufler, S., Stachl, T., . . . Wagner, W. (2019). Toward Global Soil Moisture Monitoring with Sentinel-1: Harnessing Assets and Overcoming Obstacles. *GEOSCIENCE AND REMOTE SENSING, 57*(1), 520-539. doi:doi: 10.1109/TGRS.2018.2858004

Bauer-Marschallinger, B., Schaufler., Giannakos., A., T., J., C., P., . . . W, W. (2017). 1KM SOIL MOISTURE FROM SENTINEL-1 AND ASCAT:EVOLUTIONS ACTIVITIES WITHIN THE COPERNICUS GLOBAL LAND SERVICE. Rome.

Benesty, J., Chen, J., Huang, Y., & Cohen, I. (2009). Pearson correlation coefficient. In Noise reduction in speech processing. *Springer*, 1-4.

Bi, H., Haiyun., Jiangyuan., Zeng., Zheng, W., & Fan, X. (2016). Validation of SMAP Soil Moisture analysis product using in-situ measurements over the Little Washita watershed. *IEEE International Geoscience and Remote Sensing Symposium*, 3086-3089. doi:doi: 10.1109/IGARSS.2016.7729798.

Brath, A., Casagli, N., Marani, M., Mercogliano, P., & Motta, R. (2023). *Relationship of the technical-scientific commission established with resolution of the Regional Council no. 984/2023 and determination management 14641/2023, in order to analyze the extreme meteorological events of the month of May 2023.* Retrieved from https://www.regione.emilia-romagna.it/alluvione/rapporto-della-commissione-tecnico-scientifica/20231212_rapporto_commissione_rer.pdf

Brocca, L., Zhao, W., & Lu, H. (2023). High-resolution observations from space to address new applications in hydrology. *The innovation, 4*(3), 100437. doi: https://doi.org/10.1016/j.xinn.2023.100437

Byun, K., Liaqat, U., & Choi, M. (2014). Dual-model approaches for evapotranspiration analyses over homogeneous and heterogeneous land surface conditions. *Agricultural and Forest Meteorology 197(3/4):169–187, 197*(3-4), 169–187. doi:DOI:10.1016/j.agrformet.2014.07.001

CGLOPS-1. (n.d.). *Copernicus Global Land Operations*. Retrieved from https://land.copernicus.eu/en/technical-library/product-user-manual-surface-soil-moisture-version-1/@@download/file

Chai, T., & Draxler, R. R. (2014). Root mean square error (RMSE) or mean absolute error (MAE)?– Arguments against avoiding RMSE in the literature. *Geoscientific Model development, 7*, 1247–1250. doi:https://doi.org/10.5194/gmd-7-1247-2014

Chen, J. (2016). Validation of Passive Microwave Remotely Sensed Soil Moisture (Amsr-E) Products in the Yihe Catchment, Shandong Province of China. *International Journal of Engineering Research and Applications, 6*(11), 80-84. Retrieved from https://www.ijera.com/papers/Vol6_issue11/Part-2/L0611028084.pdf

Copernicus. (n.d.). *Data portal*. Retrieved from Data portal: https://land.copernicus.eu/en/products/soil-moisture/daily-surface-soil-moisture-v1.0#download

Crow, Berg, A. A., Cosh, M. H., Loew, A., Mohanty, B. P., Panciera, R., . . . Walker, J. P. (2012). Upscaling sparse ground-based soil moisture observations for the validation of coarse-resolution satellite soil moisture products. *Reviews of Geophysics, 50*(2). doi:https://doi.org/10.1029/2011RG000372

Crow, W., Berg, A., Cosh, H., Loew, A., Mohanty, P., Panciera, R., . . . Walker, P. (2012). Upscaling Sparse Ground- based Soil Moisture Observations for the Validation of Coarse- resolution Satellite Soil Moisture Products. *Reviews of Geophysics, 50*(2). doi: https://doi.org/10.1029/2011RG000372

De Zan, F., & Guarnieri, A. (2006). TOPSAR: Terrain observation by progressive scans. *IEEE Trans. Geosci. Remote Sens, 44*(9), 2352–2360. doi:DOI: 10.1109/TGRS.2006.873853

Decagon. (2005). EC-5 soil moisture sensor operator's manual.

Dente, L., Su, Z., & Wen, J. (2012). Validation of SMOS Soil Moisture Products over the Maqu and Twente region. *Sensors, 12*, 9965-9986. doi:doi:10.3390/s120809965

Dorigo, W. A., Wagner, W., Hohensinn, R., Hahn, S., Paulik, C., Xaver, A., . . . Jackson, T. (2011). The International Soil moisture Network: A data hosting facility for global in situ soil moisture measurements. *Hydrology and Earth System Sciences, 15*(5), 1675–1698. doi:https://doi.org/10.5194/HESS-15-1675-2011

Dorigo, W. A., Wagner, W., Hohensinn, R., Hahn, S., Paulik, C., Xaver, A., . . . Jackson, T. (2011). The International Soil Moisture Network: A data hosting facility for global in situ soil moisture measurements. *Hydrology and Earth System Sciences., 15*(5), 1675–1698. doi:https://doi.org/10.5194/HESS-15-1675-2011

Engman, E. (1991). Application of microwave remote sensing of soil moisture for water resources and agriculture. *Remote sensing of environment., 35*(2-3), 213-226. doi:doi:10.1016/0034-4257(91)90013-V

Engman, E. T. (2015). Progress in Microwave Remote Sensing of Soil Moisture. *Canadian Journal of Remote Sensing., 16*(3), 6-14. doi: https://doi.org/10.1080/07038992.1990.11487620

ESA. (2013). *Sentinel-1 User Handbook.* doi:https://sentinel.esa.int/documents/247904/349449/S1_SP-1322_1.pdf

ESRI. (n.d.). *Esri Land Cover*. Retrieved from https://livingatlas.arcgis.com/landcover/

ESRI. (n.d.). *Land Cover*. Retrieved from https://livingatlas.arcgis.com/landcoverexplorer/#mapCenter=-82.38194%2C36.37212%2C4.263157556358316&mode=step&timeExtent=2017%2C2023&year=2023

Evett, S. R. (2008). Neutron moisture meters. In *Field estimation of soil water content: A practical guide to methods, instrumentation, and sensor technology* (pp. 39-54). University of Georgia.

Forman, B., Reichle, R., & Derksen, C. (2014). Estimating Passive Microwave Brightness Temperature Over Snow-Covered Land in North America Using a Land Surface Model and an Artificial Neural Network. *Geoscience and Remote Sensing*, 235-248. doi:doi:10.1109/TGRS.2013.2237913

GLDAS_NOAH025_3H_2.1. (n.d.). *GLDAS_NOAH025_3H_2.1.* Retrieved from https://disc.gsfc.nasa.gov/datasets/GLDAS_NOAH025_3H_2.1/summary

Graldi, G., Zardi, D., & Vitti, A. (2023). Retrieving Soil Moisture at the Field Scale from Sentinel-1 Data over a Semi-Arid Mediterranean Agricultural Area. *Remote Sensing, 15*(12), 2997. doi: https://doi.org/10.3390/rs15122997

Hillel, D. (2003). Introduction to Environmental Soil Physics. *Academic Press*. doi:https://doi.org/10.1016/B978-0-12-348655-4.X5000-X

ICWRGC. (2023). *ICWRGC*. Retrieved from Data: https://waterandchange.org/en/data/#gtn-h

ISMN. (n.d.). *Soil Moisture*. Retrieved from https://ismn.earth/en/

Jacobsen, O. H., & Schjonning, P. (1993). Field evaluation of time domain reflectometry for soil water measurements. *Journal of Hydrology, 151*(2-4), 159-172. doi:https://doi.org/10.1016/0022-1694(93)90234-Z

Kerr, Y. H. (2006). Soil moisture from space: Where are we? *Hydrogeology Journal, 15*(1), 117–120. doi:https://doi.org/10.1007/S10040-006-0095-3

Koster, R. D., Guo, Z., Yang, R., Dirmeyer, P. A., Mitchell, K., & Puma, M. J. (2009). On the Nature of Soil Moisture in Land Surface Models. *Journal of Climate., 22*(16), 4322–4335. doi:https://doi.org/10.1175/2009JCLI2832.1

Lakshmi, V., & Fang, B. (2023). *SMAP-Derived 1-km Downscaled Surface Soil Moisture Product Version 1.* Retrieved from https://doi.org/10.5067/U8QZ2AXE5V7B

Liu, Y., Parinussa, R., Dorigo, W., De Jeu, R., Wagner, W., Van Dijk, A., . . . Evans, J. (2011). Developing an improved soil moisture dataset by blending passive and active microwave satellite-based retrievals. *Hydrology and Earth Systems Science, 15*, 425–436. doi:doi:10.5194/hess-15-425-2011

MashMcLennan. (2023). *Post Event Report: 2023 Mid-May Emilia-Romagna Floods.* Retrieved from https://www.guycarp.com/insights/2023/06/Italy_Emilia-Romagna_Flood_2023-05.html

Moene, A. F., & Dam, J. C. (2014). Transport in the Atmosphere-Vegetation-Soil Continuum. *Cambridge University Press*. doi:https://doi.org/10.1017/CBO9781139043137

Nagelkerke, N. J. (1991). A note on a general definition of the coefficient of determination. *Biometrika, 78*(3), 691-692.

Njoku, G., & Kong, J. (1977). Theory for PassiveMicrowave Remote SensingofNear-Surface Soil Moisture. *Journal of Geophysical of Research, 82*(20), 3108 - 3118. doi:https://doi.org/10.1029/JB082i020p03108

Oommen, B. A., & Philip, J. (2023). Soil moisture evaluation with spiral fringing field capacitive sensors. *International Journal of Environmental Science and Technology, 21*, 3735–3746. doi:https://doi.org/10.1007/s13762-023-05218-8

Petropoulos, G. P., Ireland, G., & Barrett, B. (2015). Surface soil moisture retrievals from remote sensing: Current status, products & future trends. *Physics and Chemistry of the Earth, 83–84*, 36–56. doi:https://doi.org/10.1016/J.PCE.2015.02.009

Rahimzadeh-Bajgiran, P., Berg, A., Champagne, C., & Omasa, K. (2013). Estimation of soil moisture using optical/thermal infrared remote sensing in the Canadian Prairies. *ISPRS Journal of Photogrammetry and Remote Sensing, 83*, 94–103. doi:https://doi.org/10.1016/j.isprsjprs.2013.06.004

Reichle, R. H., Koster, R. D., Dong, J., & Berg, A. A. (2004). Global Soil Moisture from Satellite Observations, Land Surface Models, and Ground Data: Implications for Data Assimilation. *Journal of Hydrometeorology., 5*(3), 430–442. doi:https://doi.org/10.1175/1525-7541(2004)005<0430:GSMFSO>2.0.CO;2

Robinson, D. A., Jones, S. B., Wraith, J. M., Or, D., & Friedman, S. P. (2003). A review of advances in dielectric and electrical conductivity measurement in soils using time domain reflectometry. *Vadose Zone Journal, 2*(4), 444-475. doi:https://doi.org/10.2136/vzj2003.4440

Rodell, M., Houser, P. R., Jambor, U., Gottschalck, J., Mitchell, K., Meng, C.-J., . . . Toll, D. (2004). The Global Land Data Assimilation System. Bulletin of the American Meteorological Society, 85(3),. *85*(3), 381-394. doi:https://doi.org/10.1175/BAMS-85-3-381

Rodríguez-Iturbe, I., & Porporato, A. (2005). *Ecohydrology of Water-Controlled Ecosystems:Soil Moisture and Plant Dynamics.* Cambridge University Press. doi:https://doi.org/10.1017/CBO9780511535727

Sabaghy, S., Walker, J. P., Renzullo, L. J., & Jackson, T. J. (2018). Spatially enhanced passive microwave derived soil moisture: Capabilities and opportunities. *Remote Sensing of Environment, 209*, 551–580. doi:https://doi.org/10.1016/J.RSE.2018.02.065

Seneviratne, S. I., Corti, T., Davin, E. L., Hirschi, M., Jaeger, E. B., Lehner, I., . . . Teuling, A. J. (2010). Investigating soil moisture–climate interactions in a changing climate. *Earth-Science Reviews., 99*(3–4), 125–161. doi:https://doi.org/10.1016/J.EARSCIREV.2010.02.004

Srivastava, P., Han, D., Rico Ramirez, M., & Islam, T. (2013). Appraisal of SMOS soil moisture at a catchment scale in a temperate maritime climate. *Journal of Hydrology, 498*, 292–304. doi:DOI: 10.1016/j.jhydrol.2013.06.021

Topp, G. C., Davis, J. L., & Annan, A. P. (1980). Electromagnetic determination of soil water content: Measurements in coaxial transmission lines. *Water Resources Research, 16*(3), 574-582. doi:https://doi.org/10.1029/WR016i003p00574

Tuttle, E., & Salvucci, G. (2014). A new approach for validating satellite estimates of soil moisture using large-scale precipitation: Comparing AMSR-E products. *Remote Sensing of Environment., 142*, 207-222. doi:https://doi.org/10.1016/j.rse.2013.12.002

UR, W. (n.d.). *https://bodemdata.nl/*. Retrieved from https://bodemdata.nl/

Van Breemen, N., & Buurman, P. (2002). *Soil Formation (2nd ed.).* Kluwer Academic Publishers. doi:https://doi.org/10.1007/0-306-48163-4

Van der Velde, R., Benninga, H.-J. F., Retsios, B., Vermunt, P. C., & Salama, M. S. (2023). Twelve years of profile soil moisture and temperature measurements in Twente, the Netherlands. *Earth System Science Data, 15*, 1889-1909. doi:https://doi.org/10.5194/essd-15-1889-2023

Vereecken, H., Huisman, J. A., Pachepsky, Y., Montzka, C., van der Kruk, J., Bogena, H., . . . Vanderborght, J. (2014). On the spatio-temporal dynamics of soil moisture at the field scale. *Journal of Hydrology.*, 76–96. doi:https://doi.org/10.1016/J.JHYDROL.2013.11.061

Verstraeten, W., Veroustraete, F., & Feyen, J. (2008). Assessment of evapotranspiration and soil moisture content across different scales of observation. *Sensors, 8*(1), 70-117. doi: https://doi.org/10.3390/s8010070

Walker, J., Houser, P., & Willgoose, G. (2004). Active microwave remote sensing for soil moisture measurement: a field evaluation using ERS-2. *Hydrologiical Processes, 18*(11), 1975-1997. doi:doi:10.1002/hyp.1343

Wang, C., Fu, B., Zhang, L., Xu, Z., Zhang, L., & Fu, B. (2019). Soil moisture-plant interactions: an ecohydrological. *Journal of Soils and Sediments., 19*, 1–9. doi:https://doi.org/10.1007/s11368-018-2167-0

Wang, L., & Qu, J. (2009). Satellite remote sensing applications for surface soil moisture monitoring:. *Frontiers of Earth Science in China, 3*(2), 237-247. doi:doi: 10.1007/s11707-009-0023-7

Wang, S., Mo, X., Liu, S., Lin, Z., Hu, S., & Suxia, L. (2016). Validation and Trend Analysis of ECV Soil Moisture Data on Cropland in North China Plain during 1981–2010. *International Journal of Applied Earth Observations and Geoinformation., 48*, 110-121. doi:https://doi.org/10.1016/j.jag.2015.10.010

Willmott, C. J., & Matsuura, K. (2005). Advantages of the mean absolute error (MAE) over the root mean square error (RMSE) in assessing average model performance. *Climate Research, 30*(1), 79-82. Retrieved from https://www.jstor.org/stable/24869236

Zhang, J., Yao, F., Yang, L., & Hao, C. (2015). Validating the Modified Perpendicular Drought Index in the North China Region Using In Situ Soil Moisture Measurement. *IEEE Geoscience and Remote Sensing Letters, 12*(3). doi:DOI:10.1109/LGRS.2014.2349957

Zhang, J., Zhou, Z., Yao, F., Yang, L., & Hao, C. (2015). Validating the Modified Perpendicular Drought Index in the North China Region Using In Situ Soil Moisture Measurement. *IEEE Geoscience and Remote Sensing Letters, 12*(3). doi:DOI: 10.1109/LGRS.2014.2349957